

POOL HEAT TRANSFER
IN A SIMULATED PWR PRESSURIZER

by

Shin-Won Kang

B.S., Mechanical Engineering
Seoul National University
(1979)

SUBMITTED IN PARTIAL FULFILLMENT
OF THE REQUIREMENTS OF THE
DEGREE OF

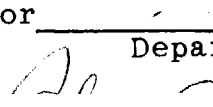
MASTER OF SCIENCE
IN MECHANICAL ENGINEERING

at the


MASSACHUSETTS INSTITUTE OF TECHNOLOGY
JANUARY, 1984

© Massachusetts Institute of Technology 1984

Signature of Author


Department of Mechanical Engineering
January, 1984

Certified by


Professor Peter Griffith
Thesis Supervisor

Accepted by

Professor Warren M. Rohsenow
Chairman, Departmental Committee on Graduate Students
Department of Mechanical Engineering

MASSACHUSETTS INSTITUTE
OF TECHNOLOGY

JUL 17 1984

LIBRARIES

Archives

POOL HEAT TRANSFER
IN A SIMULATED PWR PRESSURIZER

by

SHIN-WON KANG

Submitted to the Department of Mechanical Engineering
in January, 1984 in partial fulfillment of the
requirements for the Degree of Master of Science in
Mechanical Engineering

ABSTRACT

An experimental and analytical study of heat transfer at the steam/water interface in a simulated PWR pressurizer has been performed.

Experiments were carried out in a steady state in a small scale pressurizer at atmospheric pressure. Four different shaped sparger models were tested and compared. Water flow rates ranged from 1.7 to 9.35 gpm and water levels ranged from 0.75 to 9.0 in.

Experimental results for heat transfer coefficients at the steam/water interface are presented graphically for each sparger model. Three distinct ranges of water level are identified, in which, significantly different relations between heat transfer coefficient and water level exist. Stanton number scaling appears appropriate in normalized heat transfer and fluid mechanical phenomena. Correlations between Stanton number and reference water level in a pressurizer were established. A prediction of the pressure response during pressurizer insurge transients was made and successfully compared with experimental data.

Thesis Supervisor: Dr. Peter Griffith

Title: Professor of Mechanical Engineering

DEDICATION

This thesis is dedicated with infinite love and appreciation to my wonderful parents, grandmother, and wife.

ACKNOWLEDGEMENTS

I wish to express my deepest appreciation to Professor Peter Griffith whose kind guidance, patience, insight, and accessibility greatly encouraged me in many parts of the work carried out in this thesis.

I am also grateful to Mr. Joseph A. Caloggero and Mr. Fred Johnson for their continuous help in making the apparatus and to Ms. Eva Kish for typing this thesis.

I would also like to thank Dr. Sang-Nyung Kim, Mr. Mark T. Leonard, Dr. Jung-Hoon Chun, and Mr. Hamid R. Saedi for their helpful discussions.

Finally, I wish to express my gratitude to the Yankee Atomic Electric Co. and the Northeast Utilities Service Co. who sponsored this research.

TABLE OF CONTENTS

	Page
NOMENCLATURE.	13
CHAPTER 1. INTRODUCTION.	16
1.1 Introduction.	16
1.2 Objectives of the Investigation	17
CHAPTER 2. EXPERIMENTAL INVESTIGATION.	19
2.1 Description of Experimental Apparatus	19
2.2 Description of Sparger Models	25
2.3 Experimental Procedures	31
CHAPTER 3. ANALYTICAL MODEL.	33
3.1 Reduction of Data	33
3.2 Governing Equations in Turbulent Flows.	40
CHAPTER 4. EXPERIMENTAL RESULTS.	47
4.1 Flow Patterns for the TMI 2 Sparger Model	47
4.2 Variation of Heat Transfer Coefficient with Water Level	51
4.3 Stratification.	53
4.4 Variation of Heat Transfer Coefficient with Reynolds Number	54
4.5 Non-condensable Gases	54
4.5.1 Non-condensable Gases Study.	54
4.5.2 Effects of Non-condensable Gases on Interface Heat Transfer.	58

CHAPTER 5.	EXPERIMENTAL DATA ANALYSIS.	61
5.1	Variation of Stanton Number with Reference Water Level	61
5.2	Scaling Laws.	64
5.3	Composite Plot of Stanton Number versus Reference Water Level for each Sparger Geometry.	66
5.4	Prediction of Pressure Response during Pressurizer Insurge Transients.	68
CHAPTER 6.	CONCLUSIONS	72
REFERENCES.	74
APPENDIX A.	EXPERIMENTAL RESULTS FOR THE MILLSTONE 2 SPARGER MODEL.	75
A.1	Flow Patterns	75
A.2	Variation of Heat Transfer Coefficient with Water Level	78
A.3	Variation of Stanton Number with Reference Water Level	80
A.4	Variation of Heat Transfer Coefficient with Reynolds Number	81
APPENDIX B.	EXPERIMENTAL RESULTS FOR THE ROWE YANKEE SPARGER MODEL.	85
B.1	Flow Patterns	85
B.2	Variation of Heat Transfer Coefficient with Water Level	87
B.3	Variation of Stanton Number with Reference Water Level	90
B.4	Variation of Heat Transfer Coefficient with Reynolds Number	92

APPENDIX C.	EXPERIMENTAL RESULTS FOR THE MILLSTONE 3 SPARGER MODEL	94
C.1	Flow Patterns	94
C.2	Variation of Heat Transfer Coefficient with Water Level	97
C.3	Variation of Stanton Number with Reference Water Level	97
C.4	Variation of Heat Transfer Coefficient with Reynolds Number	99
APPENDIX D.	SCALING LAWS102
APPENDIX E.	EXPERIMENTAL RESULTS FOR THE ROUND BOTTOM TEST VESSEL.106
APPENDIX F.	EFFECTS OF DIFFERENT SUBCOOLING.110
APPENDIX G.	COMPARISON OF MEASURED OUTLET WATER TEMPERATURES FOR EACH THERMOCOUPLE LOCATION113
APPENDIX H.	CALIBRATION OF WATER FLOW METER.114
APPENDIX I.	DATA TABLE115
APPENDIX J.	DESCRIPTION OF A SCALED PRESSURIZER APPARATUS AND EXPERIMENTAL PROCEDURES.130
APPENDIX K.	DETAILS OF ACTUAL SPARGERS135
APPENDIX L.	DETAILS OF ACTUAL PRESSURIZER.139

LIST OF FIGURES

<u>FIGURE</u>		<u>PAGE</u>
1	SCHEMATIC DIAGRAM OF THE EXPERIMENTAL APPARATUS (ISOMETRIC VIEW)	20
2	SCHEMATIC DIAGRAM OF THE EXPERIMENTAL APPARATUS (SIDE VIEW)	21
3	SCHEMATIC DIAGRAM OF PRESSURIZER TEST VESSELS	22
4	SCHEMATIC DIAGRAM OF THERMOCOUPLE ARRANGEMENT	24
5	TMI 2 SPARGER MODEL	26
6	MILLSTONE 2 SPARGER MODEL	27
7	ROWE YANKEE SPARGER MODEL	28
8	MILLSTONE 3 SPARGER MODEL	29
9	CONTROL VOLUME MODELING CONFIGURATION OF THE EXPERIMENTAL APPARATUS.	34
10	TEMPERATURE & DENSITY PROFILE IN BULK WATER REGION.	38
11	FLOW PATTERNS FOR TMI 2 SPARGER MODEL (REGION 1)	49
12	FLOW PATTERNS FOR TMI 2 SPARGER MODEL (REGIONS 2 & 3)	50
13	VARIATION OF HEAT TRANSFER COEFFICIENT WITH WATER LEVEL AND WATER FLOW RATE (TMI 2 SPARGER MODEL).	52
14	VARIATION OF HEAT TRANSFER COEFFICIENT WITH REYNOLDS NUMBER (TMI 2 SPARGER MODEL)	55
15	CONFIGURATIONS OF NON-CONDENSABLE GAS AT THE INTERFACE	57
16	DEGRADATION OF HEAT TRANSFER COEFFICIENT WITH NON-CONDENSABLE GAS	60
17	VARIATION OF STANTON NUMBER WITH REFERENCE WATER LEVEL AND WATER FLOW RATE (TMI 2 SPARGER MODEL)	63

18	SIMPLIFIED St vs. L/Z DIAGRAM (TMI 2 SPARGER MODEL)	65
19	COMPOSITE PLOT OF St vs. L/Z FOR EACH SPARGER GEOMETRY.	67
20	PREDICTION AND EXPERIMENTAL DATA OF PRESSURE RESPONSE DURING INSURGE TRANSIENT	69
21	PRESSURE RESPONSE OF A SCALED PRESSURIZER TO AN EMPTY TANK INSURGE TRANSIENT.	70
22	MEASURED INSURGE FLOW RATE FOR AN EMPTY TANK INSURGE TRANSIENT	71
A.1	FLOW PATTERNS FOR MILLSTONE 2 SPARGER MODEL (REGION 1).	76
A.2	FLOW PATTERNS FOR MILLSTONE 2 SPARGER MODEL (REGIONS 2 & 3)	77
A.3	VARIATION OF HEAT TRANSFER COEFFICIENT WITH WATER LEVEL AND WATER FLOW RATE (MILLSTONE 2 SPARGER MODEL).	79
A.4	VARIATION OF STANTON NUMBER WITH REFERENCE WATER LEVEL AND WATER FLOW RATE (MILLSTONE 2 SPARGER MODEL).	82
A.5	VARIATION OF HEAT TRANSFER COEFFICIENT WITH REYNOLDS NUMBER (MILLSTONE 2 SPARGER MODEL)	84
B.1	FLOW PATTERNS FOR ROWE YANKEE SPARGER MODEL (REGION 1).	86
B.2	FLOW PATTERNS FOR ROWE YANKEE SPARGER MODEL (REGIONS 2 & 3)	88
B.3	VARIATION OF HEAT TRANSFER COEFFICIENT WITH WATER LEVEL AND WATER FLOW RATE (ROWE YANKEE SPARGER MODEL)	89
B.4	VARIATION OF STANTON NUMBER WITH REFERENCE WATER LEVEL AND WATER FLOW RATE (ROWE YANKEE SPARGER MODEL).	91
B.5	VARIATION OF HEAT TRANSFER COEFFICIENT WITH REYNOLDS NUMBER (ROWE YANKEE SPARGER MODEL)	93
C.1	FLOW PATTERNS FOR MILLSTONE 3 SPARGER MODEL (REGION 1).	95

C.2	FLOW PATTERNS FOR MILLSTONE 3 SPARGER MODEL (REGION 2).	96
C.3	VARIATION OF HEAT TRANSFER COEFFICIENT WITH WATER LEVEL AND WATER FLOW RATE (MILLSTONE 3 SPARGER MODEL).	98
C.4	VARIATION OF STANTON NUMBER WITH REFERENCE WATER LEVEL AND WATER FLOW RATE (MILLSTONE 3 SPARGER MODEL).100
C.5	VARIATION OF HEAT TRANSFER COEFFICIENT WITH REYNOLDS NUMBER (MILLSTONE 3 SPARGER MODEL)101
D.1	SIMPLIFIED St vs. L/Z DIAGRAM (MILLSTONE 2 SPARGER MODEL).103
D.2	SIMPLIFIED St vs. L/Z DIAGRAM (ROWE YANKEE SPARGER MODEL).104
D.3	SIMPLIFIED St vs. L/Z DIAGRAM (MILLSTONE 3 SPARGER MODEL).105
E.1	FLOW PATTERNS OF WATER JETS FOR DIFFERENT SHAPED VESSEL BOTTOMS107
E.2	VARIATION OF HEAT TRANSFER COEFFICIENT WITH VESSEL BOTTOM GEOMETRY.108
F.1	VARIATION OF HEAT TRANSFER COEFFICIENT WITH INLET WATER SUBCOOLING.112
G.1	CIRCUMFERENTIAL LOCATIONS OF THERMOCOUPLES. . .	.113
H.1	CALIBRATION OF WATER FLOW METER114
J.1	SCHEMATIC DIAGRAM OF A SCALED PRESSURIZER APPARATUS131
J.2	SCHEMATIC DIAGRAM OF A SCALED PRESSURIZER VESSEL (MIT TEST VESSEL).132
K.1	DETAILS OF MILLSTONE 2 SPARGER.135
K.2(a)	DETAILS OF ROWE YANKEE SPARGER (SURGE CHAMBER)136
K.2(b)	DETAILS OF ROWE YANKEE SPARGER (SURGE LINE).137
K.3	DETAILS OF MILLSTONE 3 SPARGER.138

L.1 DETAILS OF WESTINGHOUSE PRESSURIZER139
L.2 DETAILS OF WESTINGHOUSE PRESSURIZER140
L.3 DETAILS OF MILLSTONE 2 PRESSURIZER.141

LIST OF TABLES

<u>TABLE</u>	<u>PAGE</u>
I CORRELATION OF STANTON NUMBER AS A FUNCTION OF REFERENCE WATER LEVEL (TMI 2 SPARGER MODEL)	65
II CORRELATION OF STANTON NUMBER AS A FUNCTION OF REFERENCE WATER LEVEL (MILLSTONE 2 SPARGER MODEL)103
III CORRELATION OF STANTON NUMBER AS A FUNCTION OF REFERENCE WATER LEVEL (ROWE YANKEE SPARGER MODEL)104
IV CORRELATION OF STANTON NUMBER AS A FUNCTION OF REFERENCE WATER LEVEL (MILLSTONE 3 SPARGER MODEL)105
V HEAT TRANSFER COEFFICIENT VS. WATER LEVEL AND WATER FLOW RATE (TMI 2 SPARGER MODEL)116
VI STANTON NUMBER VS. REFERENCE WATER LEVEL AND WATER FLOW RATE (TMI 2 SPARGER MODEL)118
VII HEAT TRANSFER COEFFICIENT VS. WATER LEVEL AND WATER FLOW RATE (MILLSTONE 2 SPARGER MODEL)120
VIII STANTON NUMBER VS. REFERENCE WATER LEVEL AND WATER FLOW RATE (MILLSTONE 2 SPARGER MODEL)121
IX HEAT TRANSFER COEFFICIENT VS. WATER LEVEL AND WATER FLOW RATE (ROWE YANKEE SPARGER MODEL)122
X STANTON NUMBER VS. REFERENCE WATER LEVEL AND WATER FLOW RATE (ROWE YANKEE SPARGER MODEL)123
XI HEAT TRANSFER COEFFICIENT VS. WATER LEVEL AND WATER FLOW RATE (MILLSTONE 3 SPARGER MODEL)124
XII STANTON NUMBER VS. REFERENCE WATER LEVEL AND WATER FLOW RATE (MILLSTONE 3 SPARGER MODEL)125
XIII HEAT TRANSFER COEFFICIENTS FOR ROUND AND FLAT BOTTOM VESSELS (TMI 2 SPARGER MODEL)126
XIV HEAT TRANSFER COEFFICIENTS FOR DIFFERENT INLET WATER SUBCOOLING (TMI 2 SPARGER MODEL)127
XV CIRCUMFERENTIAL VARIATION OF OUTLET WATER TEMPERATURES129

NOMENCLATURE

Symbol

A	Condensation area, Eq. 15 & 17
A	Area uniquely defined for each sparger geometry
c_p	Specific heat at constant pressure
D	Diameter of the model of the TMI 2 sparger
d	Distance between interface and blow-down pipe
E	Energy
f	Friction factor
G	Mass velocity ($G = \dot{m}/A = \rho V$)
g	Gravitational acceleration
h	Enthalpy, Eq. 4 & 5
h	Heat transfer coefficient
h_{NC}	Non-condensable gas heat transfer coefficient
L	Water level
L/Z	Reference water level
\dot{m}	Mass flow rate
m	Variable slope of St curve
P	Pressure
\dot{Q}	Rate of heat transfer
Re	Reynolds number
R_f	Flux Richardson number
R_g	Gradient Richardson number

R_i	Thermal resistance
s_{ij}	Strain rate tensor
St	Stanton number
T	Temperature
T_o	Mean temperature of fluid
T^*	Temperature difference between actual temperature and mean temperature of fluid
ΔT	Overall temperature difference, Eq. 13
t	Time
u_i, u_j	Velocity tensor
U_i, U_j	Velocity tensor
V	Velocity, Eq. 30
\dot{W}	Work
x_i, x_j	Space coordinate tensor
Z	Elevation, Eq. 4 & 5
Z	Sparger height

Greek Letters

α	Thermal diffusivity ($\alpha = k/\rho c_p$)
δ_{ij}	Kronecker delta
μ	Dynamic viscosity
ν	Kinematic viscosity ($\nu = \mu/\rho$)
ρ	Density of fluid
σ_{ij}	Stress tensor
ϕ	Velocity, Eq. 4 & 5

Subscripts

i	Inlet condition
inter	Interface
NC	Non-condensable gas
o	Outlet condition
s	Steam
w	Water
∞	Bulk condition

Superscripts

-	Bar denotes the average value
\sim	Tilde denotes the instantaneous value at (x_i, t)
'	Prime denotes the fluctuating value

CHAPTER 1
INTRODUCTION

1.1 Introduction

The role of the pressurizer in a Pressurized Water Reactor (PWR) is to control the Reactor Coolant System (RCS) pressure during steady-state operation and to limit pressure changes during transients. The pressurizer is a vertical cylindrical vessel connected to the RCS by a single line from its bottom head to hot leg piping, and by a spray line from cold leg piping to the pressurizer top head.

The pressurizer contains steam and water maintained at saturated conditions at 2250 psia by electric immersion heaters located in the lower liquid section of the vessel and a cool water spray located in the upper vapor section. Pressurizer insurges caused by the expansion of the reactor coolant increase the pressurizer pressure. The pressure increase is limited by cool water spray, which condenses some of the steam in the pressurizer. Pressurizer outsurges, caused by contraction of the reactor coolant, decrease the pressurizer pressure. The electric heaters are actuated to restore normal operating pressure by generating steam. Spray flow and the electric heaters are automatically controlled by a pressurizer controller during normal operation.

1.2 Objectives of the Investigation

Transients in the PWR pressurizer are caused by abnormal operating conditions or accidents, such as, a loss-of-coolant accident (LOCA), and events which lead to a concern for pressurized thermal shock (PTS), such as, a steam generator tube rupture (SGTR). The pressurizer response to PWR transients plays an important role in determining the pressure history of the RCS. Recent studies have been performed by Saedi [1] and Kim [2] at MIT to predict the pressurizer transient response during accident conditions. Their experimental results show very large initial reductions in pressure during insurge transients which are initiated from low water levels in the MIT test vessel at low pressure. They concluded, qualitatively, that significant interface heat transfer over a small range of low liquid levels was the cause of the large pressure reduction.

The purpose of this investigation is to experimentally determine the magnitude of heat transfer coefficients at the steam/water interface and establish correlations between Stanton number and reference water level in the pressurizer. Flow patterns of the dispersed insurge water jets for four different shaped sparger models will be observed. Since the presence of a non-condensable gas at the steam/water

interface significantly affects the interface heat transfer in the pressurizer test vessel, these effects will be also investigated.

CHAPTER 2
EXPERIMENTAL INVESTIGATION

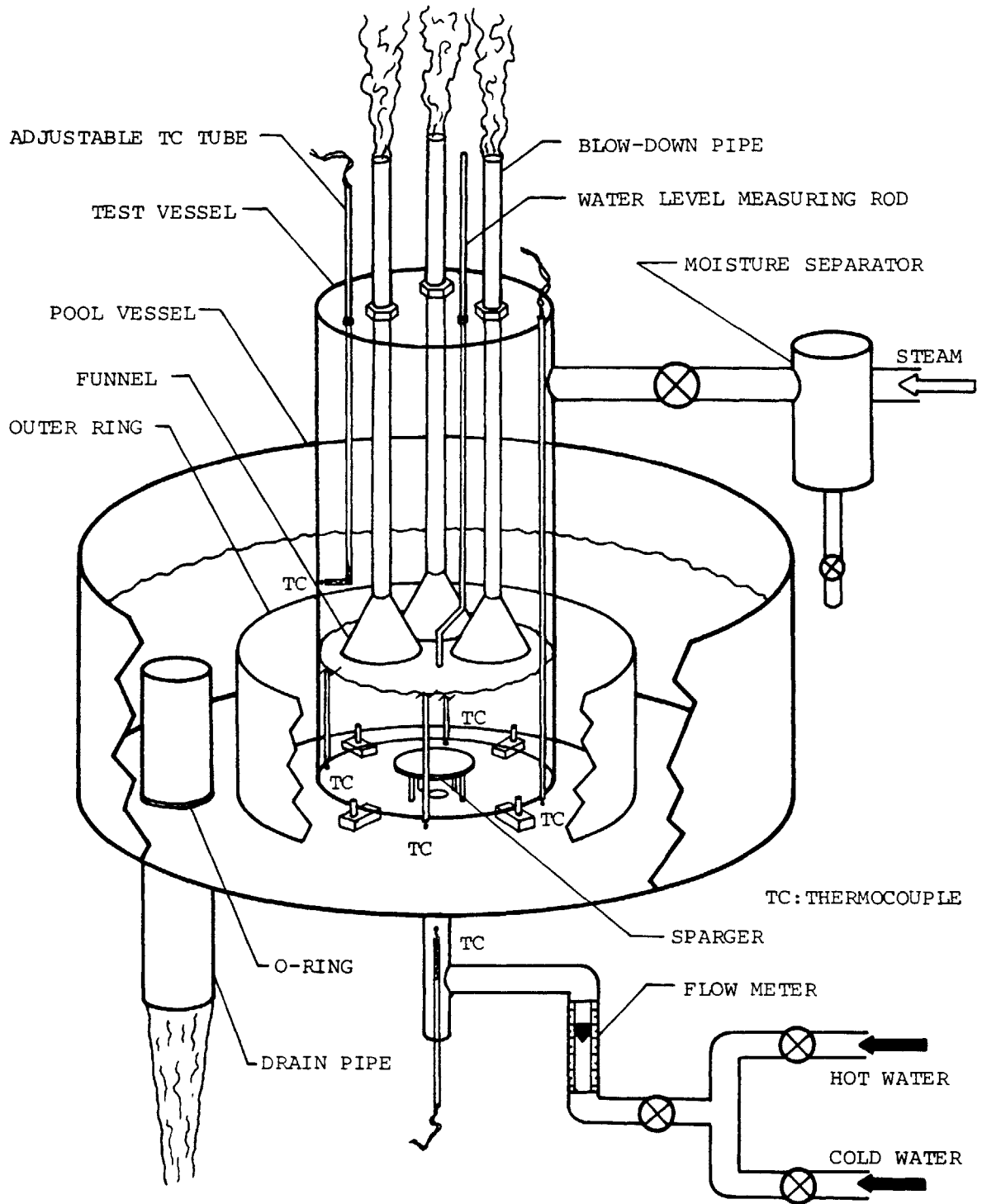
2.1 Description of Experimental Apparatus

The experimental apparatus, schematically shown in Fig. 1 and Fig. 2, consists of the pool vessel, the pressurizer test vessel, moisture separator, blow-down pipes, outer ring, drain pipe, and sparger.

The pool vessel is a cylindrical steel vessel, 22-1/2 in. ID and 9-1/2 in. in height. It was connected to the 1.0 in. ID (or 0.716 in. ID) water pipe.

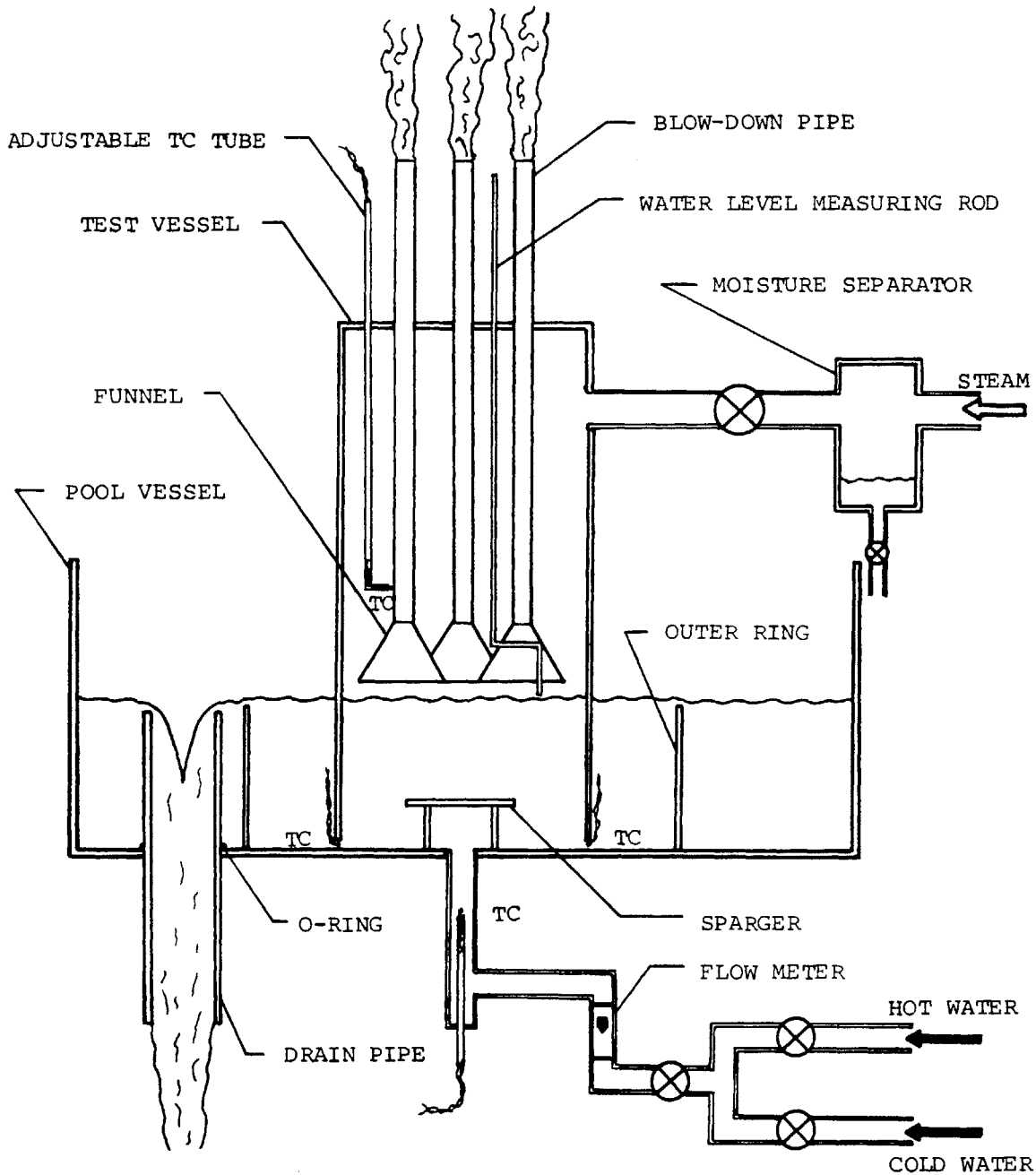
Two simulated pressurizer test vessels were made to have different shaped bottoms, one flat, the other hemispherical (Fig. 3). Both were made from a plexi-glass cylinder, 8-1/4 in. ID, 17.0 in. high, and 1/4 in. thick. As shown in Appendix L, the actual pressurizer has a hemispherical bottom. The hemispherical bottom vessel was designed to model the geometry of the actual pressurizer. The hemispherical bottom is made of pyrex-glass which has 4-3/8 in. radius of curvature and 3/16 in. thickness. The upper OD of the hemisphere-shaped bottom part is 8.0 in., the lower OD, 4.0 in., and the height, 3.0 in. The test vessel is supported by four legs which are made of 1/2" x 1" x 1/4" plexi-glass blocks.

The upper plate of the test vessel supports three blow-down pipes, a water level measuring rod, and an



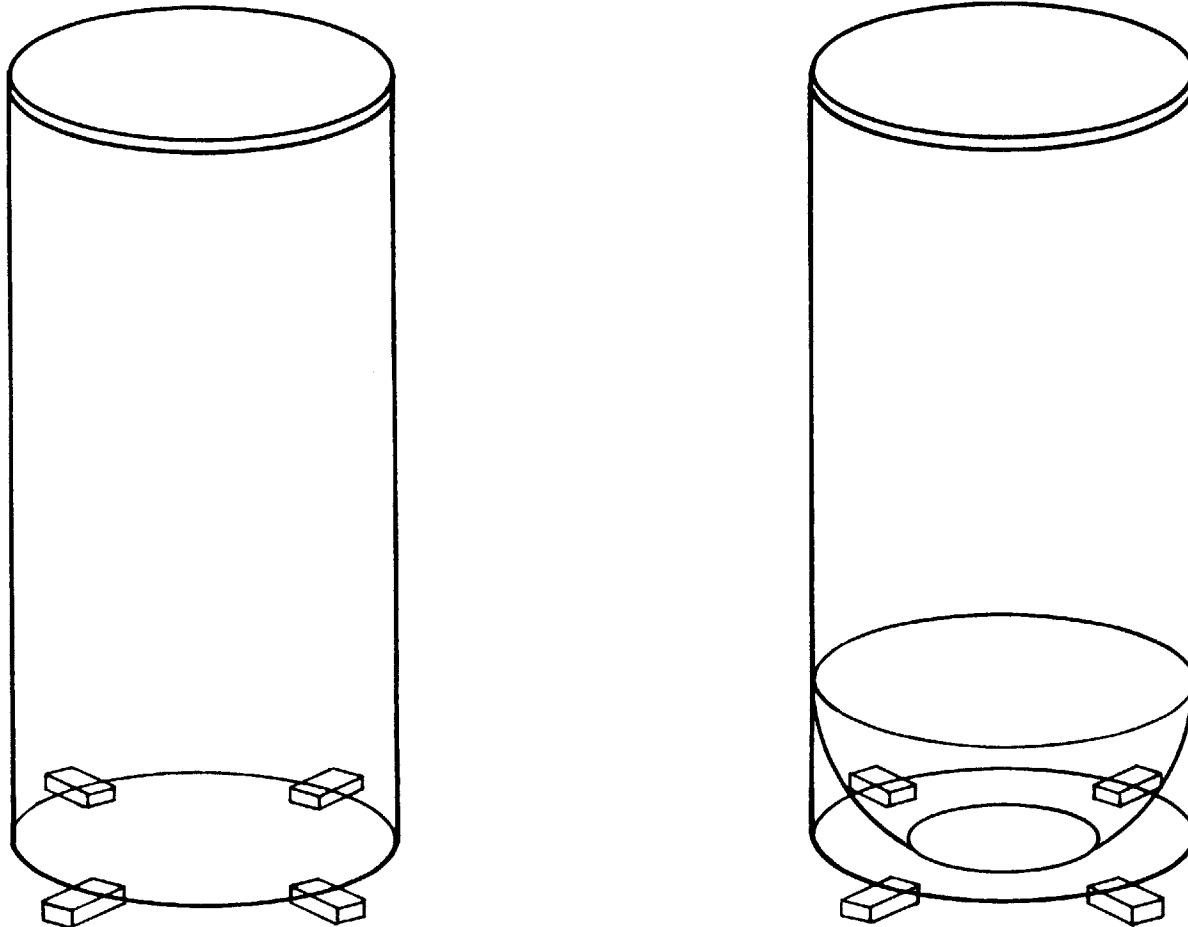
SCHEMATIC DIAGRAM OF THE EXPERIMENTAL APPARATUS
(ISOMETRIC VIEW)

FIG. 1



SCHEMATIC DIAGRAM OF THE EXPERIMENTAL APPARATUS
(SIDE VIEW)

FIG. 2



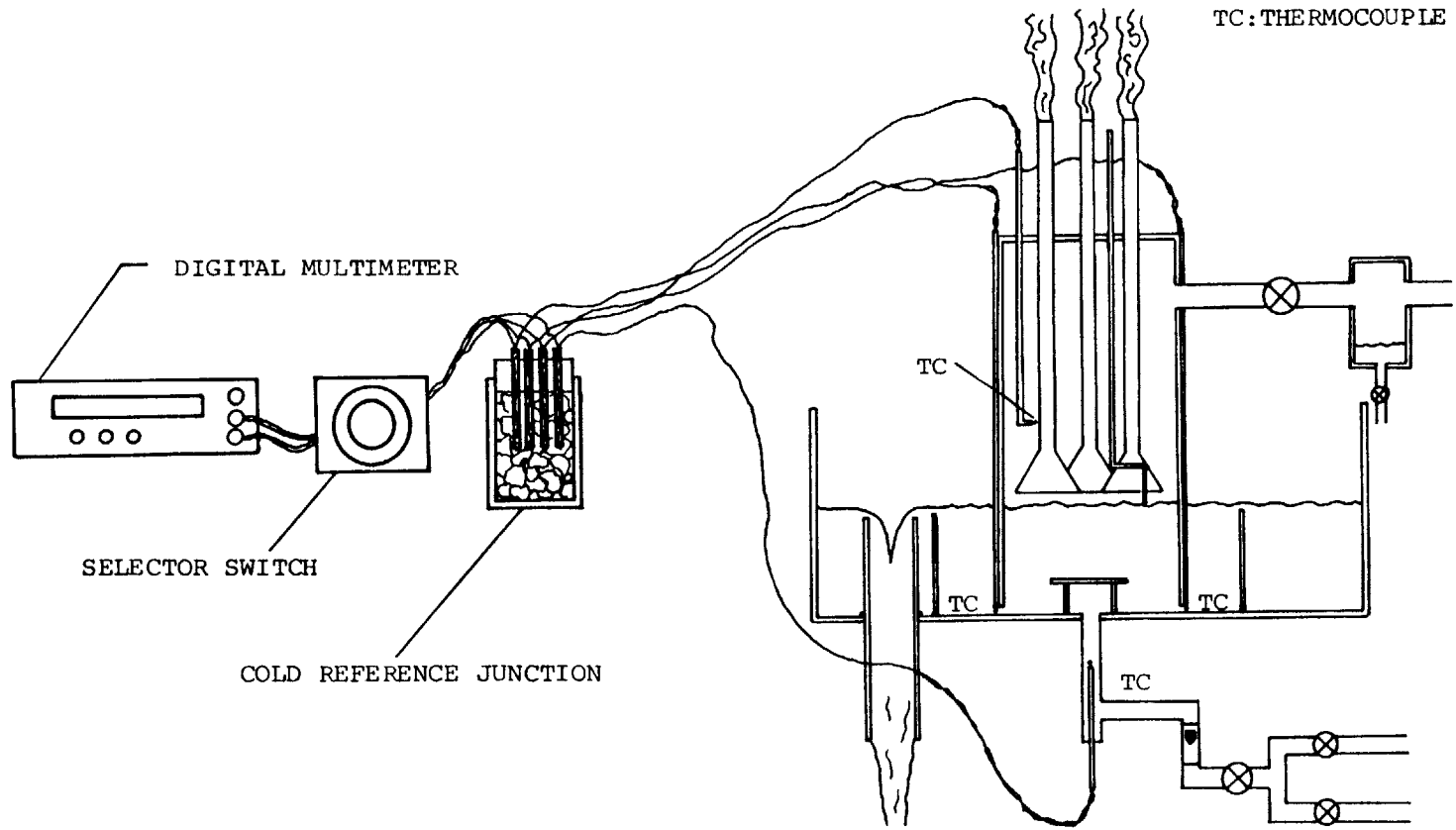
SCHEMATIC DIAGRAM OF PRESSURIZER TEST VESSELS

FIG. 3

adjustable thermocouple tube. The water level measuring rod was designed to move and measure the water level in the vertical and azimuthal directions. Scales were marked on the upper part of the measuring rod.

As shown in Fig. 1, four thermocouple tubes were fixed around the test vessel wall every 90 degrees. The thermocouples were made of 24 gage copper-constantan wire. Thermocouple beads were located in the center of outlet gaps of the test vessel to measure the outlet water temperature. These four thermocouple wires were connected in series to obtain the average outlet water temperature. One additional thermocouple was placed 5.0 in. below the pool vessel bottom in the inlet water pipe to measure the inlet water temperature. An adjustable thermocouple tube was designed to measure the steam temperature in the vertical and azimuthal directions. This thermocouple wire is inserted through a 3/32 in. ID brass tube. As shown in Fig. 4, all thermocouple wires were connected to cold reference junctions, which were in an ice bath, and to a selector switch. A digital multimeter (HP 3465 B) was used to measure the output voltages. In order to measure the inlet water flow rate, the flow meter whose maximum capacity is 11.0 gpm was equipped in the inlet water pipe.

Live steam was supplied to the test vessel through a 1-1/4 in. ID steam pipe which was insulated with a fiberglass pipe covering, 1/2 in. thick. A moisture



SCHEMATIC DIAGRAM OF THERMOCOUPLE ARRANGEMENT

FIG. 4

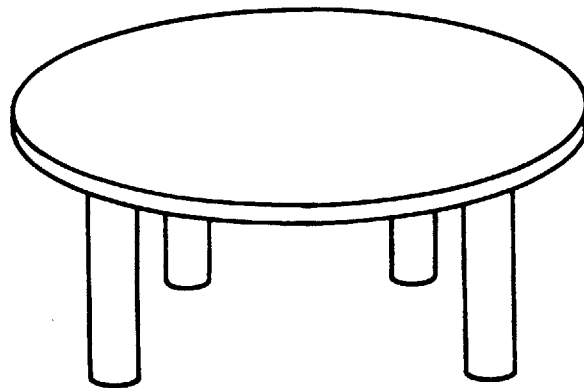
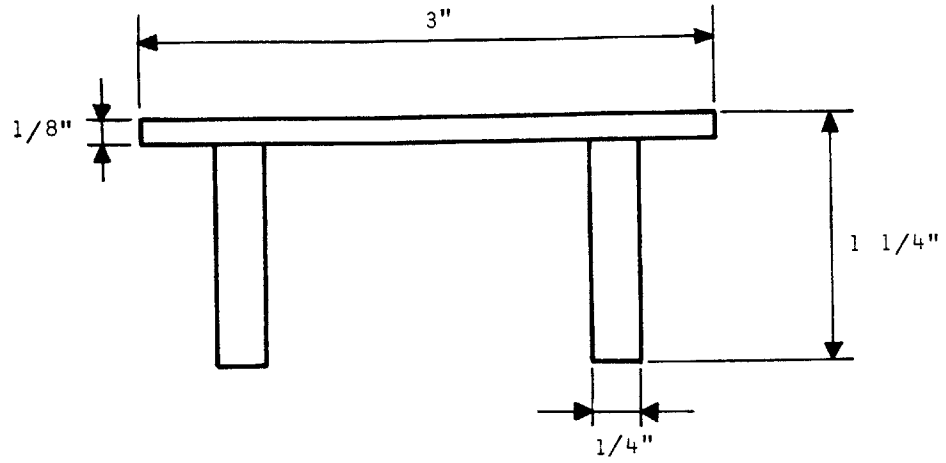
separator, located 25.0 in. away from the test vessel, was built in the steam pipe in order to supply dry steam to the test vessel. It was made of a cylindrical steel tank, 7.0 in. OD, 9.0 in. high, 3/8 in. thick. Sixteen outer rings, each of a different height over the range from 1/2 in. to 8-1/2 in., were made of a cylindrical tin plate, 12.0 in. ID and 0.023 in. thick. The function of the outer ring (Fig. 1) is to isolate the interface motion inside the test vessel from that outside the test vessel. It also prevents outlet water flowing back into the test vessel.

The function of the blow-down pipe is to remove excess steam and non-condensable gases from the interface. The blow-down pipe (Fig. 1) consists of a copper tube, 1/2 in. ID and 20.0 in. in height, and a funnel, 3-1/2 in. maximum ID and 2-1/2 in. in height.

By varying the height of the drain pipe, the water level in the test vessel could be adjusted. The outlet water was leaving the pool vessel through the drain pipe. This drain pipe was made of a copper tube, 1-3/4 in. ID, 11.0 in. in height, and 1/16 in. thick. The gap between the drain pipe and the pool vessel was sealed by two 1-3/4 in. ID Buna-N O-rings.

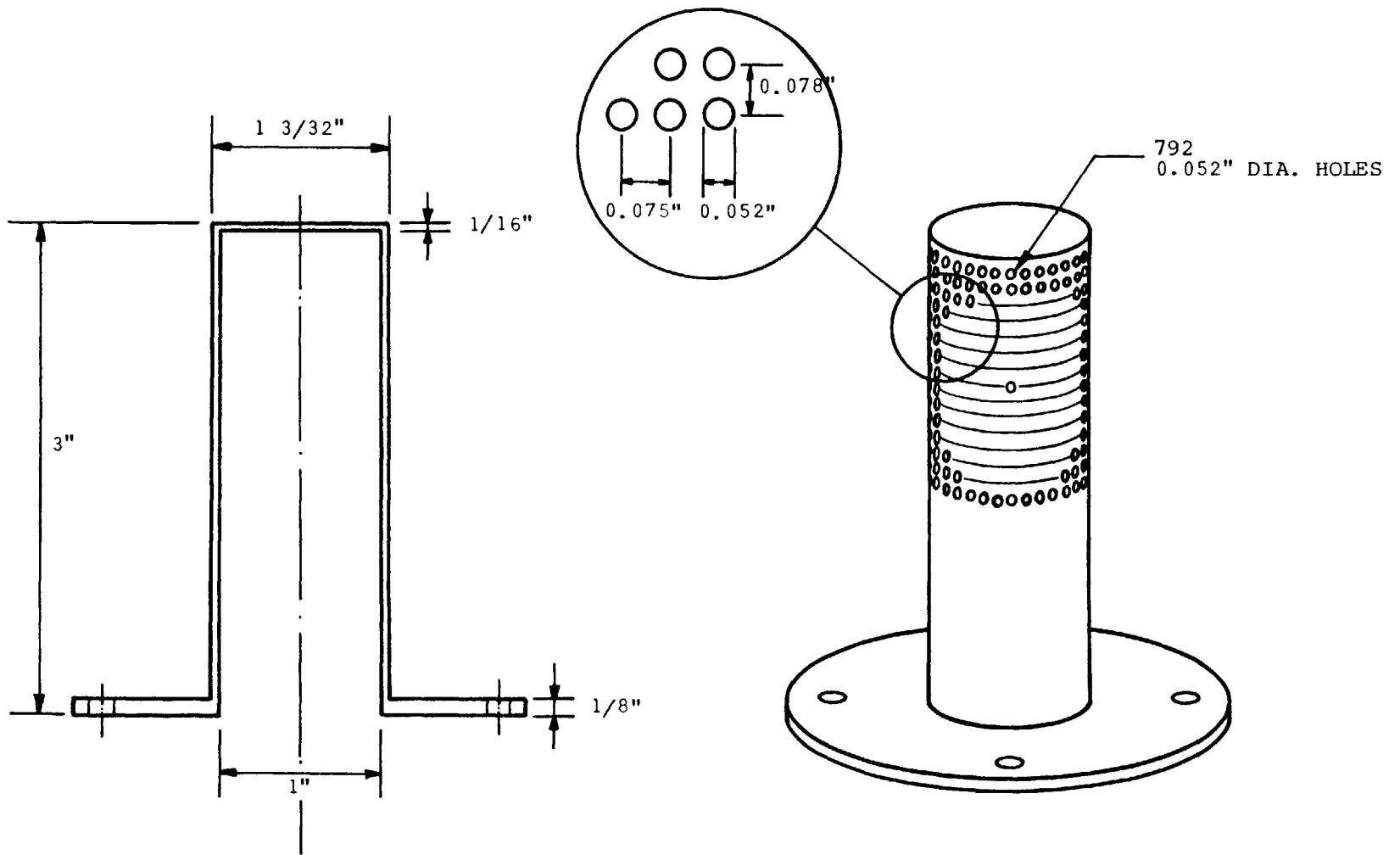
2.2 Description of Sparger Models

Four different shaped sparger models, used in the experiments, are shown in Fig. 5, 6, 7, and 8. Fig. 5 shows



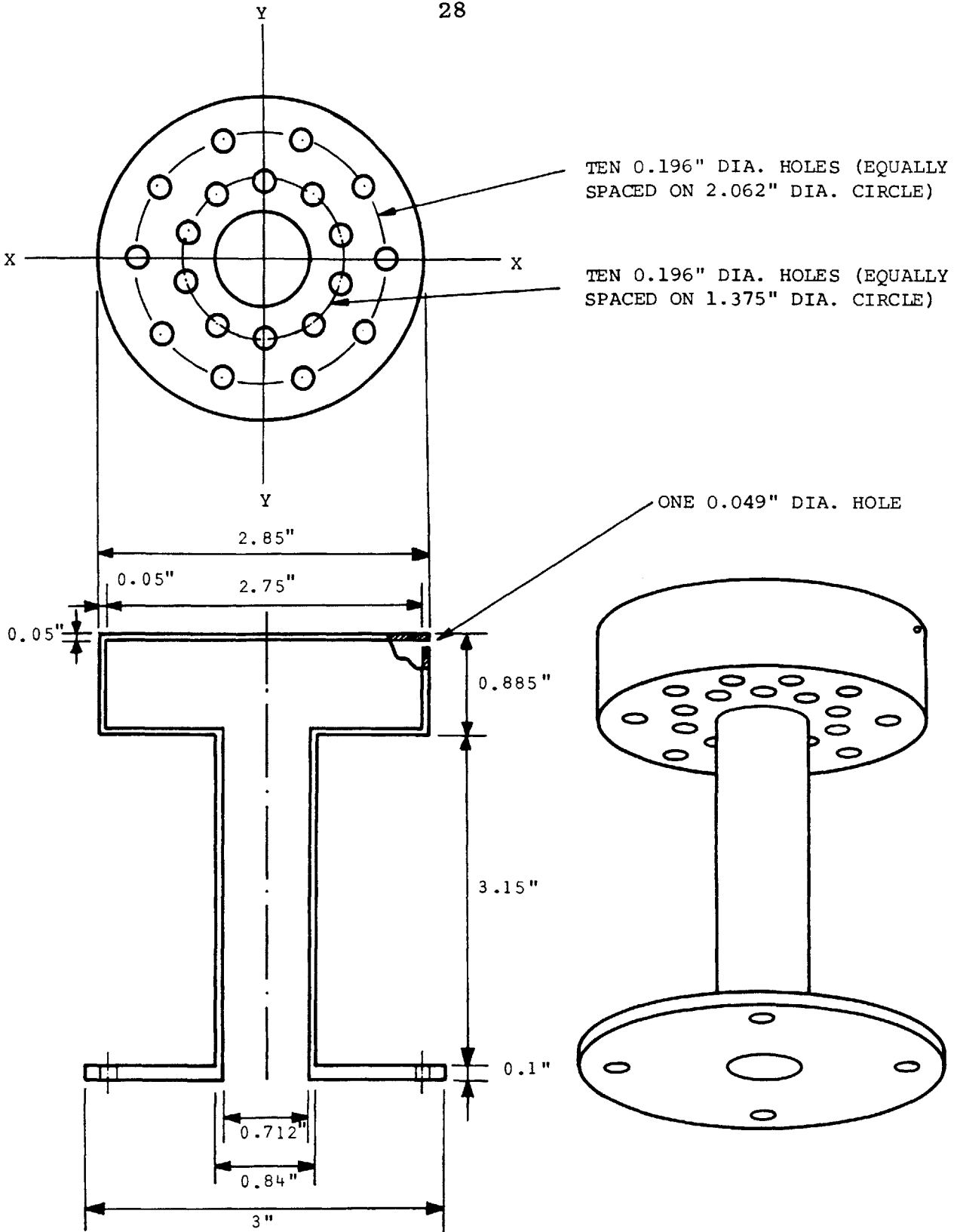
TMI 2 SPARGER MODEL

FIG. 5



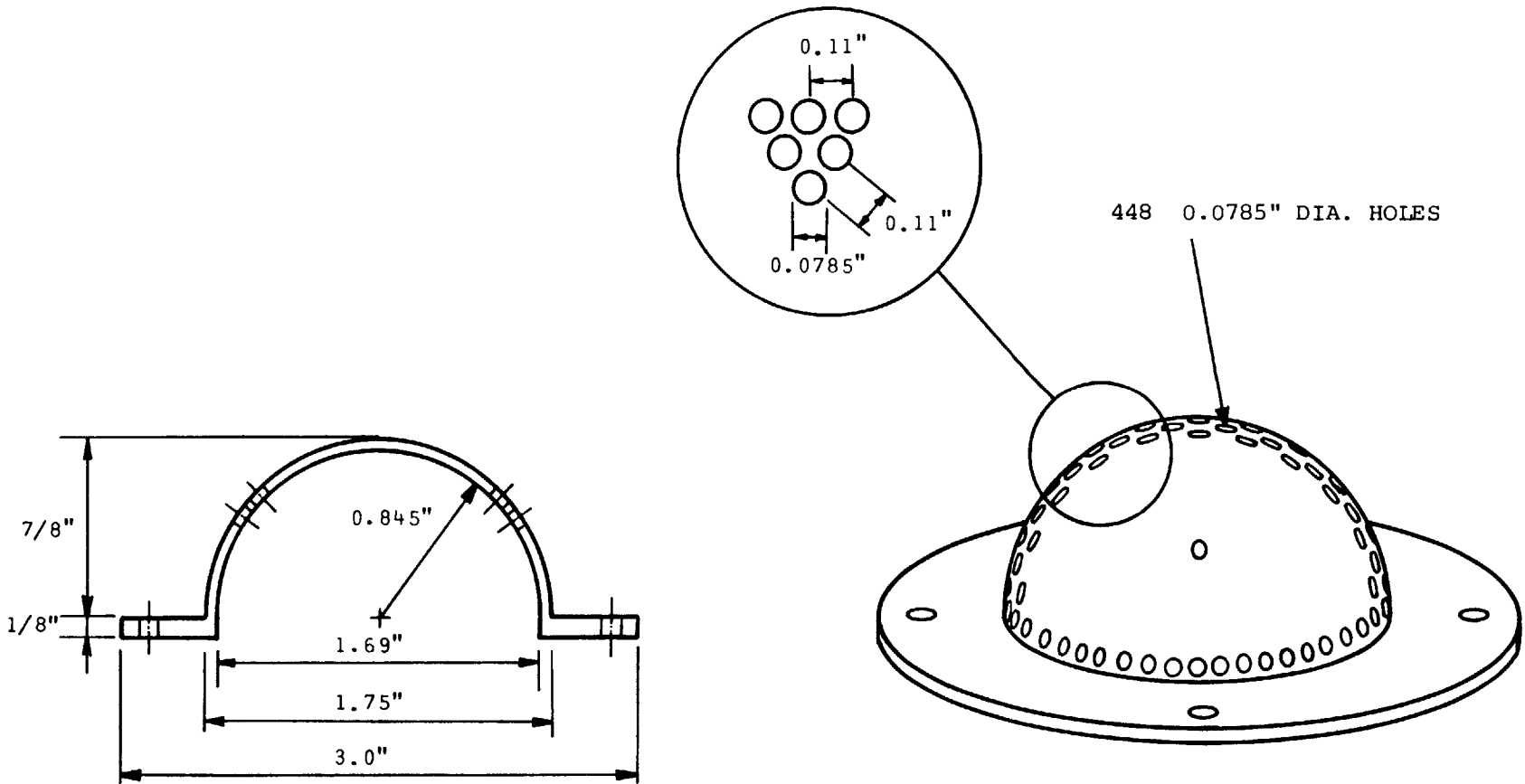
MILLSTONE 2 SPARGER MODEL

FIG. 6



ROWE YANKEE SPARGER MODEL

FIG. 7



MILLSTONE 3 SPARGER MODEL

FIG. 8

a TMI 2 sparger design which was the primary geometry during the experiments. This sparger model has the same shape and dimension as the one in Kim's [2] apparatus. It consists of an aluminum disk, 3.0 in. diameter and 1/8 in. thick, and four aluminum tubes, 1/4 in. OD and 1-1/8 in. in height, and fixed to the pool vessel bottom.

Fig. 6 shows the model of the Millstone 2 sparger (Northeast Utilities Service Co.). It was made from a brass tube, 1.0 in. ID, 1-3/32 in. OD, and 3.0 in. high. Seven hundred and ninety-two 0.052 in. ID holes were drilled around the upper part of the sparger model. In order to filter small particles from the inlet water, a brass wire cloth (1000 mesh) was placed between the sparger and the inlet water pipe.

The model of the Rowe Yankee sparger (Yankee Atomic Electric Co.) is shown in Fig. 7. It consists of a brass tube, 0.712 in. ID, 0.84 in. OD, and 3.25 in. high, and a cylindrical brass cap, 2.75 in. ID, 2.85 in. OD, and 0.885 in. in height. Twenty holes were drilled through the under-side of the cylindrical cap. Ten 0.196 in. diameter holes, which are equally spaced on 2.062 in. diameter circle, straddle the X-X axis, and ten equally spaced 0.196 in. diameter holes on 1.375 in. diameter circle, straddle the Y-Y axis (Fig. 7). In addition, one 0.049 in. diameter hole was drilled through the top cap. This sparger model was connected to the 0.712 in. ID inlet water pipe.

Fig. 8 shows the model of the Millstone 3 sparger (Northeast Utilities Service Co.). It was made from a copper hemispherical cap, 1.69 in. ID and 1.75 in. OD. Four hundred and forty-eight 0.0785 in. ID holes were drilled through the surface of the sparger model. Drawings of the actual spargers are shown in Appendix K.

2.3 Experimental Procedures

The experiments were conducted by the following procedures:

- i) Open the hot and cold water valves and adjust them to obtain the desired inlet water temperature. The inlet water flow rate is monitored by the flow meter.
- ii) Adjust the height of the drain pipe for the desired water level, and check the water level by the measuring rod. Select the outer ring whose height is $1/4$ to $1/2$ in. less than the desired water level, and place it around the test vessel.
- iii) Adjust the height of the blow-down pipe to maintain a distance of $1/4$ to $3/8$ in. between the interface and the bottom of the funnel.
- iv) Open the steam valve slowly while checking whether excess steam is being properly discharged to atmosphere through blow-down pipes. By moving the thermocouple rod in the azimuthal and

vertical directions, check the steam temperature in the test vessel. If the steam temperature at the interface is lower than the inlet steam temperature, open the steam valve slowly until the interface steam temperature reaches the inlet steam temperature. However, the steam pressure in the test vessel should not significantly exceed atmospheric. This can be detected by comparing the inside and outside water levels.

- v) Once a steady state is established, fix the adjustable thermocouple tube 1/4 in. above the interface, and read the inlet, outlet water temperatures and the interface steam temperature. During runs, the outlet water temperature should be read and recorded every few seconds.
- vi) Repeat this procedure 4-5 times for the same condition.
- vii) Obtain the average temperatures and calculate heat transfer coefficient for each run by using Eq. 17.
- viii) Obtain the average heat transfer coefficient for the same water level and water flow rate.

CHAPTER 3
ANALYTICAL MODEL

The heat transfer coefficient at the steam/water interface is determined from the conservation equations in Sect. 3.1. A dimensionless heat transfer coefficient (Stanton number) and a stratification parameter (Richardson number) are derived from the governing equations in turbulent flows in Sect. 3.2.

3.1 Reduction of Data

The interface heat transfer coefficient is determined from the governing equations, described below.

The control volumes (C.V.) for the steam region and the bulk water region are defined in Fig. 9.

The equations of mass conservation are expressed as

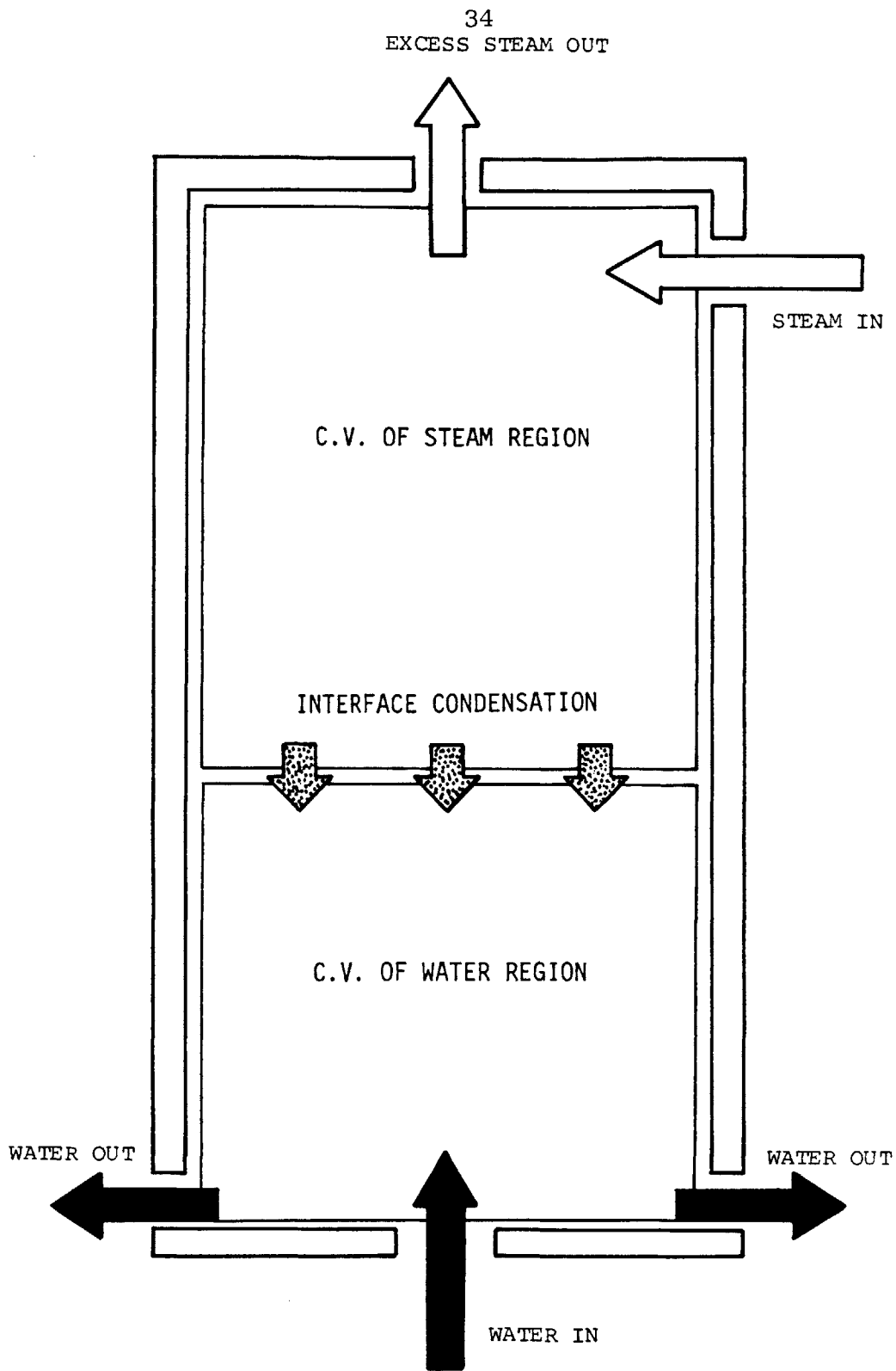
$$(\dot{m}_w)_{\text{inter}} = (\dot{m}_s)_{\text{inter}} \quad (1)$$

For the steam region,

$$(\dot{m}_s)_i = (\dot{m}_s)_o + (\dot{m}_s)_{\text{inter}} \quad (2)$$

For the water region,

$$(\dot{m}_w)_i + (\dot{m}_w)_{\text{inter}} = (\dot{m}_w)_o \quad (3)$$



CONTROL VOLUME MODELING CONFIGURATION
OF THE EXPERIMENTAL APPARATUS

FIG. 9

Here, \dot{m} denotes mass flow rate, and subscripts s, w, i, o, and inter denote the steam region, water region, flow into C.V., flow out of C.V., and interface, respectively.

The general equations of energy conservation are expressed as

For the steam region,

$$\begin{aligned} \frac{dE_s}{dt} = & (\dot{m}_s)_i \left[(h_s)_i + \frac{(\phi_s)_i^2}{2} + gZ_1 \right] - (\dot{m}_s)_o \left[(h_s)_o \right. \\ & \left. + \frac{(\phi_s)_o^2}{2} + gZ_2 \right] + (\dot{m}_s)_{inter} \left[(h_s)_{inter} + \right. \\ & \left. \frac{(\phi_s)_{inter}^2}{2} + gZ_3 \right] - (\dot{Q}_s)_{loss} + \dot{W}_s \quad (4) \end{aligned}$$

For the water region,

$$\begin{aligned} \frac{dE_w}{dt} = & (\dot{m}_w)_i \left[(h_w)_i + \frac{(\phi_w)_i^2}{2} + gZ_4 \right] - (\dot{m}_w)_o \left[(h_w)_o \right. \\ & \left. + \frac{(\phi_w)_o^2}{2} + gZ_5 \right] + (\dot{m}_w)_{inter} \left[(h_w)_{inter} + \right. \\ & \left. \frac{(\phi_w)_{inter}^2}{2} + gZ_6 \right] - (\dot{Q}_w)_{loss} + \dot{W}_w \quad (5) \end{aligned}$$

In Eq. 4 and Eq. 5, it is assumed that

- i) Heat loss through the test vessel wall and the pool vessel bottom can be neglected.
- ii) The steam condensation rate, $(\dot{m}_s)_{inter}$, is much smaller than the inlet water flow rate, $(\dot{m}_w)_i$. Hence, the steam condensation rate, $(\dot{m}_s)_{inter}$, can be neglected.
- iii) The kinetic energy of water and steam can be neglected.
- iv) The gravity effect can be neglected.

Since the system is in steady-state and there is no work, Eq. 3, Eq. 4, and Eq. 5 yield as follows:

$$(\dot{m}_w)_i = (\dot{m}_w)_o \quad (6)$$

$$0 = (\dot{m}_s)_i (h_s)_i - (\dot{m}_s)_o (h_s)_o + (\dot{m}_s)_{inter} (h_s)_{inter} \quad (7)$$

and

$$0 = (\dot{m}_w)_i (h_w)_i - (\dot{m}_w)_o (h_w)_o + (\dot{m}_w)_{inter} (h_w)_{inter} \quad (8)$$

From Eq. 7 and Eq. 8, the rate of interface heat transfer, \dot{Q}_{inter} , is expressed as

$$\begin{aligned} \dot{Q}_{inter} &= (\dot{m}_s)_{inter} (h_s)_{inter} \\ &= (\dot{m}_s)_o (h_s)_o - (\dot{m}_s)_i (h_s)_i \end{aligned} \quad (9)$$

$$\begin{aligned}
 \text{or} \quad \dot{Q}_{\text{inter}} &= (\dot{m}_w)_{\text{inter}} (h_w)_{\text{inter}} \\
 &= (\dot{m}_w)_o (h_w)_o - (\dot{m}_w)_i (h_w)_i \quad (10)
 \end{aligned}$$

Here, the enthalpy of water, h_w , can be expressed as

$$h_w = c_p T_w \quad (11)$$

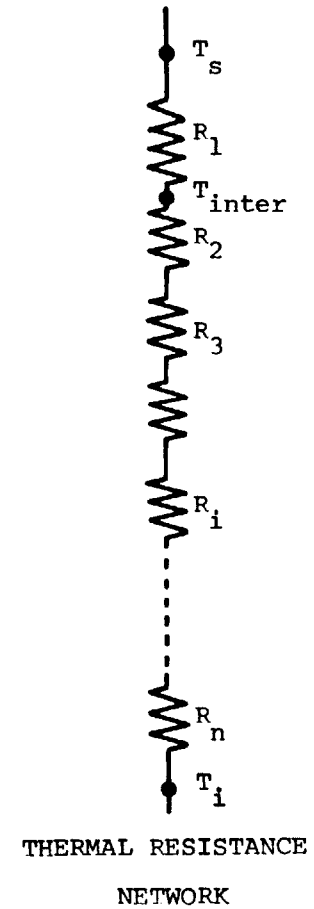
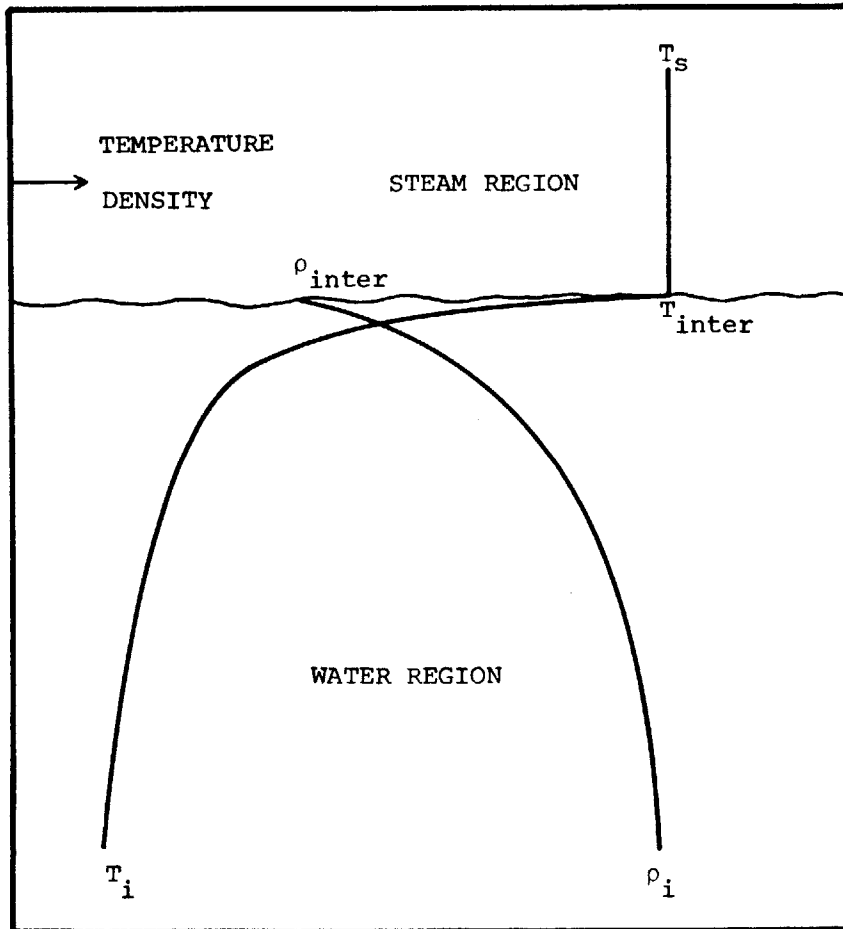
Therefore, from Eq. 10 and Eq. 11, the rate of interface heat transfer, \dot{Q}_{inter} , can be obtained as

$$\dot{Q}_{\text{inter}} = c_p (\dot{m}_w)_i \left[(T_w)_o - (T_w)_i \right] \quad (12)$$

where $(T_w)_i$ denotes the inlet water temperature, and $(T_w)_o$ denotes the outlet water temperature.

As shown in Fig. 10, the heat transfer process between steam and water region may be represented by a thermal resistance network. Thermal resistances corresponding to the steam region, the bulk water region are defined R_1 , R_2 , R_3 , etc. The overall heat transfer, \dot{Q}_{overall} , is calculated as the ratio of the overall temperature difference, ΔT , to the sum of thermal resistances.

$$\dot{Q}_{\text{overall}} = \frac{\Delta T}{\sum_i R_i} \quad (13)$$



TEMPERATURE & DENSITY PROFILE IN BULK WATER REGION

FIG. 10

The overall heat transfer coefficient, h_{overall} , is expressed as follows:

$$h_{\text{overall}} = \frac{1}{A \sum_i R_i} \quad (14)$$

Hence, the rate of interface heat transfer, \dot{Q}_{inter} , is represented by

$$\dot{Q}_{\text{inter}} = h_{\text{overall}} A \Delta T \quad (15)$$

Here, A denotes the condensation area. The overall temperature difference, ΔT , is defined as

$$\Delta T = T_s - (T_w)_i \quad (16)$$

where T_s denotes the steam temperature.

Hence, from Eq. 12, Eq. 15, and Eq. 16, the heat transfer coefficient at the interface is obtained as follows:

$$h = c_p \frac{(\dot{m}_w)_i \left[(T_w)_o - (T_w)_i \right]}{A \left[T_s - (T_w)_i \right]} \quad (17)$$

In all experiments, the condensation area A is defined by the cross-sectional area of the pressurizer test vessel.

3.2 Governing Equations in Turbulent Flows

In turbulence, the instantaneous quantities such as velocities, temperature, pressure, etc. can be expressed as

$$\left\{ \begin{array}{l} \tilde{u}_i = \bar{U}_i + u'_i \\ \tilde{T} = \bar{T} + T' \\ \tilde{p} = \bar{p} + p' \end{array} \right. \quad (18)$$

Here, a tilde denotes the instantaneous value at (x_i, t) and a bar denotes the temporal average value and a prime denotes the fluctuating quantity.

Since mass, momentum, and energy should be conserved in turbulent as well as in laminar flow, the conservation equations hold equally for turbulent flow, if the quantities in these equations are interpreted as the instantaneous quantities of the turbulent field.

The equation of mass conservation of an incompressible fluid is

$$\frac{\partial \tilde{u}_i}{\partial x_i} = 0 \quad (19)$$

Taking the time average of Eq. 19 yields

$$\frac{\partial \bar{U}_i}{\partial x_i} = 0 \quad (20)$$

The equations of motion of an incompressible fluid are

$$\frac{\partial \tilde{u}_i}{\partial t} + \tilde{u}_j \frac{\partial \tilde{u}_i}{\partial x_j} = \frac{1}{\rho} \frac{\partial}{\partial x_j} \tilde{\sigma}_{ij} \quad (21)$$

$$\text{and} \quad \frac{\partial \tilde{u}_i}{\partial x_i} = 0 \quad (22)$$

Here, $\tilde{\sigma}_{ij}$ denotes the stress tensor. If the fluid is Newtonian, the stress tensor $\tilde{\sigma}_{ij}$ is given by

$$\tilde{\sigma}_{ij} = -\tilde{P} \delta_{ij} + 2\mu \tilde{s}_{ij} \quad (23)$$

In Eq. 23, δ_{ij} is the Kronecker delta, \tilde{P} is the hydrodynamic pressure and μ is the dynamic viscosity (which will be assumed to be constant). The rate of strain \tilde{s}_{ij} is defined by

$$\tilde{s}_{ij} = \frac{1}{2} \left(\frac{\partial \tilde{u}_i}{\partial x_j} + \frac{\partial \tilde{u}_j}{\partial x_i} \right) \quad (24)$$

From Eq. 21, Eq. 22, and Eq. 23, the Navier-Stokes equations are obtained as follows:

$$\frac{\partial \tilde{u}_i}{\partial t} + \tilde{u}_i \frac{\partial \tilde{u}_i}{\partial x_j} = -\frac{1}{\rho} \frac{\partial \tilde{P}}{\partial x_i} + \nu \frac{\partial^2 \tilde{u}_i}{\partial x_j^2} \quad (25)$$

Taking the time average of Eq. 25 yields

$$\bar{U}_j \frac{\partial \bar{U}_i}{\partial x_j} + \overline{u'_j \frac{\partial u'_i}{\partial x_j}} = \frac{1}{\rho} \frac{\partial}{\partial x_j} \left[-\bar{P} \delta_{ij} + \mu \left(\frac{\partial \bar{U}_i}{\partial x_j} + \frac{\partial \bar{U}_j}{\partial x_i} \right) \right] \quad (26)$$

or

$$\bar{U}_j \frac{\partial \bar{U}_i}{\partial x_j} = \frac{1}{\rho} \frac{\partial}{\partial x_j} \left[-\bar{P} \delta_{ij} + \mu \left(\frac{\partial \bar{U}_i}{\partial x_j} + \frac{\partial \bar{U}_j}{\partial x_i} \right) - \overline{\rho u'_i u'_j} \right] \quad (27)$$

These two equations are called the Reynolds momentum equations, and $-\overline{\rho u'_i u'_j}$ term is called Reynolds stress tensor.

The equation governing heat transfer in turbulent flow of a constant-density fluid can be derived as follows:

$$\frac{\partial \tilde{T}}{\partial t} + \tilde{u}_j \frac{\partial \tilde{T}}{\partial x_j} = \alpha \frac{\partial^2 \tilde{T}}{\partial x_j^2} \quad (28)$$

Here, it is assumed that gravity-induced density stratification may be neglected. When all terms of Eq. 28 have been averaged, some arrangement yields that following equations:

$$\bar{U}_j \frac{\partial \bar{T}}{\partial x_j} = \frac{\partial}{\partial x_j} \left(\alpha \frac{\partial \bar{T}}{\partial x_j} - \overline{u'_j T'} \right) \quad (29)$$

Here, the turbulent flux is defined as $-\rho c_p \overline{u'_j T'}$. By the Reynolds analogy [3], correlations between heat transfer coefficients h and friction factor f are obtained as follows:

$$\frac{h}{\rho c_p V} = \frac{f}{2} \quad (30)$$

The above dimensionless parameter is known as Stanton number. It is an alternative means of expressing the heat transfer coefficient, and physically represents the ratio of the total heat transferred from a surface to that transported at the surface by convection.

The equation governing the mean kinetic energy $\frac{1}{2} \overline{u'_i u'_i}$ of the turbulent velocity fluctuations is obtained by multiplying the Navier-Stokes equations Eq. 25 by \tilde{u}_i , and taking the time average of all terms as follows:

$$\begin{aligned} \bar{U}_j \frac{\partial}{\partial x_j} \left(\frac{1}{2} \overline{u'_i u'_i} \right) &= - \frac{\partial}{\partial x_j} \left(\frac{1}{\rho} \overline{u'_j P'} + \frac{1}{2} \overline{u'_i u'_i u'_j} \right. \\ &\quad \left. - 2 \nu \overline{u'_i s_{ij}} \right) - \frac{1}{2} \overline{u'_i u'_j} \left(\frac{\partial \bar{U}_i}{\partial x_j} + \frac{\partial \bar{U}_j}{\partial x_i} \right) - 2 \nu \overline{s_{ij} s_{ij}} \end{aligned} \quad (31)$$

The quantity s_{ij} is the fluctuating rate of strain, defined by

$$s_{ij} \equiv \frac{1}{2} \left(\frac{\partial u'_i}{\partial x_j} + \frac{\partial u'_j}{\partial x_i} \right) \quad (32)$$

If temperature can contribute to the generation of velocity fluctuations, a fluctuating body force term should be added on the right hand side of Eq. 31, that is, temperature fluctuations cause density fluctuations in a fluid at constant pressure, and the density fluctuations cause a fluctuating body force $g_j \rho' / \bar{\rho}$. Here, g_j is the vector acceleration of gravity, ρ' is the density fluctuation, and $\bar{\rho}$ is the mean density. In the Boussinesq approximation, the fluctuating body force can be expressed as $-g_j T^* / T_0$, where T_0 is the mean temperature of fluid and T^* is the difference between the actual temperature and T_0 .

In a flow in which the only nonzero components of \bar{U}_i and g_i are $\bar{U}_1 = \bar{U}_1(x_3)$ and $g_3 = -g$ (where the x_3 direction is vertically upwards), the equations for $\frac{1}{2} \overline{u'_i u'_i}$ and $\overline{(T')^2}$ can be drawn from Eq. 31 as follows [4]:

$$\begin{aligned} \overline{u'_1 u'_3} \frac{\partial \bar{U}_1}{\partial x_3} &= - \frac{\partial}{\partial x_3} \left(\frac{1}{\rho} \overline{p' u'_3} + \frac{1}{2} \overline{u'_i u'_i u'_3} \right) \\ &\quad - \nu \overline{\frac{\partial u'_i}{\partial x_j} \frac{\partial u'_i}{\partial x_j}} + \frac{g}{T_0} \overline{u'_3 T'} \end{aligned} \quad (33)$$

Here, the parameter governing Eq. 33 can be expressed as the ratio of buoyant production to stress production of turbulent kinetic energy. This parameter is called the flux Richardson number, R_f , defined as

$$R_f \equiv \frac{g}{T_0} \frac{\overline{u'_3 T'}}{\overline{u'_1 u'_3} (\partial \bar{U}_1 / \partial x_3)} \quad (34)$$

where $\overline{u'_3 T'}$ is an eddy conductivity, and $\partial \bar{U}_1 / \partial x_3$ is an eddy viscosity.

$$\overline{u'_3 T'} \equiv -\alpha (\partial \bar{T}^* / \partial x_3) \quad (35)$$

$$\overline{u'_1 u'_3} \equiv -\nu (\partial \bar{U}_1 / \partial x_3) \quad (36)$$

From Eq. 34, Eq. 35, and Eq. 36, the flux Richardson number, R_f , is also expressed as

$$R_f \equiv \frac{\alpha}{\nu} \frac{g}{T_0} \frac{\partial \bar{T}^* / \partial x_3}{(\partial \bar{U}_1 / \partial x_3)^2} \quad (37)$$

The gradient Richardson number, R_g , is defined as

$$R_g \equiv \frac{g}{T_0} \frac{\partial \bar{T}^* / \partial x_3}{(\partial \bar{U}_1 / \partial x_3)^2} \quad (38)$$

$$\text{or } R_g \equiv - \frac{g \left(\partial \rho / \partial x_3 \right)}{\rho \left(\partial \bar{U}_1 / \partial x_3 \right)^2} \quad (39)$$

where ρ is the fluid density. These two dimensionless parameters are used to describe the buoyancy effects in the stratified fluid.

CHAPTER 4

EXPERIMENTAL RESULTS

Experiments were performed with four different shaped sparger models described in Sect. 2.2. The results for the TMI 2 sparger model, including flow patterns, heat transfer coefficient versus water level, and heat transfer coefficient versus Reynolds number in the inlet water pipe, are described in Sect. 4.1 to Sect. 4.4, and those for the other sparger models are in Appendix A, B, and C. The results show a similar overall trend for each sparger model, despite the dramatically different sparger geometries, and the results of the TMI 2 sparger model are discussed as an example for all cases.

The experimental results for the effects of a non-condensable gas on interface heat transfer are discussed in Sect. 4.5. The results for the round bottom test vessel, which are described in Appendix E, also show a similar trend to those for the flat bottom test vessel. Finally, the experimental results for different inlet water temperatures are discussed in Appendix F.

4.1 Flow Patterns for the TMI 2 Sparger Model

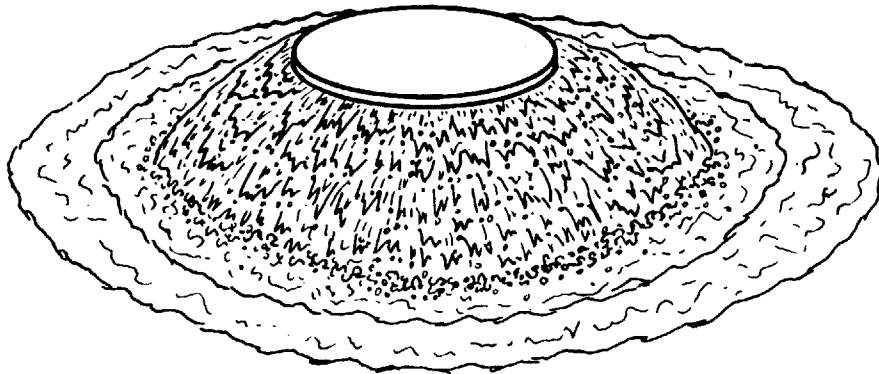
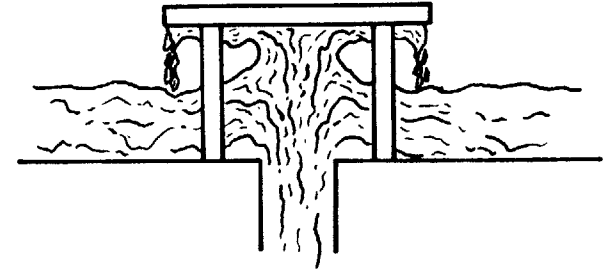
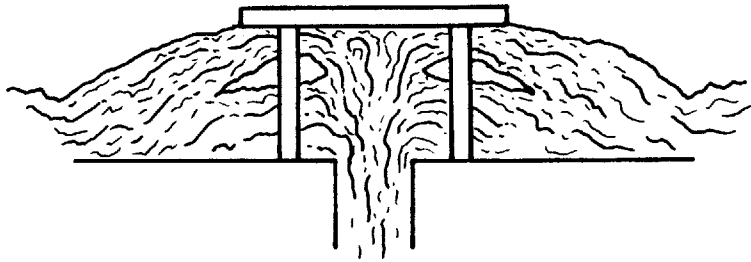
The model of the TMI 2 sparger was connected to the inlet water pipe (1.0 in. ID), and the flat bottom test vessel was used. The inlet water flow rate was varied from

2.2 gpm to 9.35 gpm and the water level ranged from 0.75 in. to 7.75 in. The inlet water temperature was maintained at a temperature of 75.0° F.

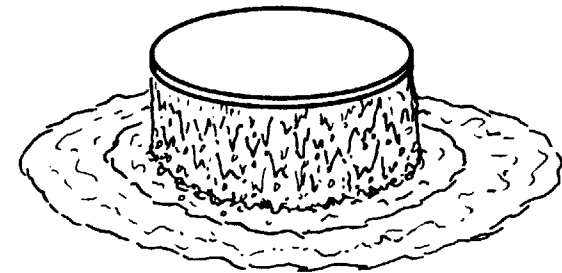
Fig. 11 shows two different observed flow patterns for the baffled water jets, when the water level is below the sparger height. For flow rates greater than 6.6 gpm, the water jets spreaded as shown in Fig. 11(a). However, for flow rates less than 5.5 gpm, due to the lower momentum of water jets, water dripped from around the edge of the sparger disk as shown in Fig. 11(b). Water levels less than the sparger height are defined as Region 1.

As shown in Fig. 12(a), when the water level was slightly greater than the sparger height, a hydraulic jump was observed around the edge of the sparger disk. The height of the hydraulic jump tended to increase with increasing water flow rate. As the water level reached around 2.0 in., the hydraulic jump disappeared suddenly and interface motion ceased. This transitional water level seems not to change for various water flow rates.

The region of water levels between the sparger height and the transitional water level is defined as Region 2. Liquid levels above the transitional level are defined as Region 3. As shown in Fig. 12(b), in Region 3, baffled water jets did not reach the interface and no interface motion was observed.



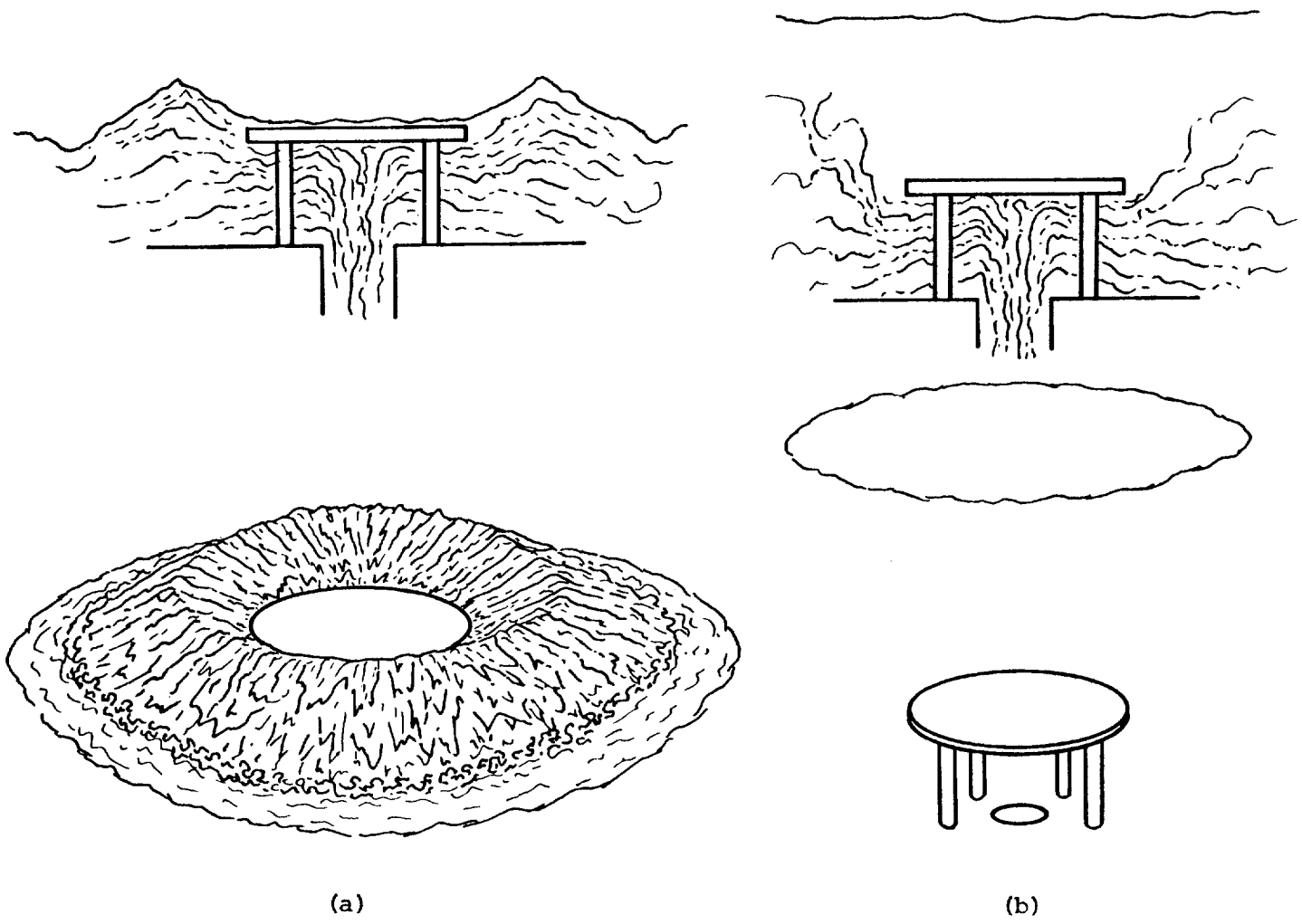
(a)



(b)

FLOW PATTERNS FOR TMI 2 SPARGER MODEL (REGION 1)

FIG. 11



FLOW PATTERNS FOR TMI 2 SPARGER MODEL (REGIONS 2 & 3)

FIG. 12

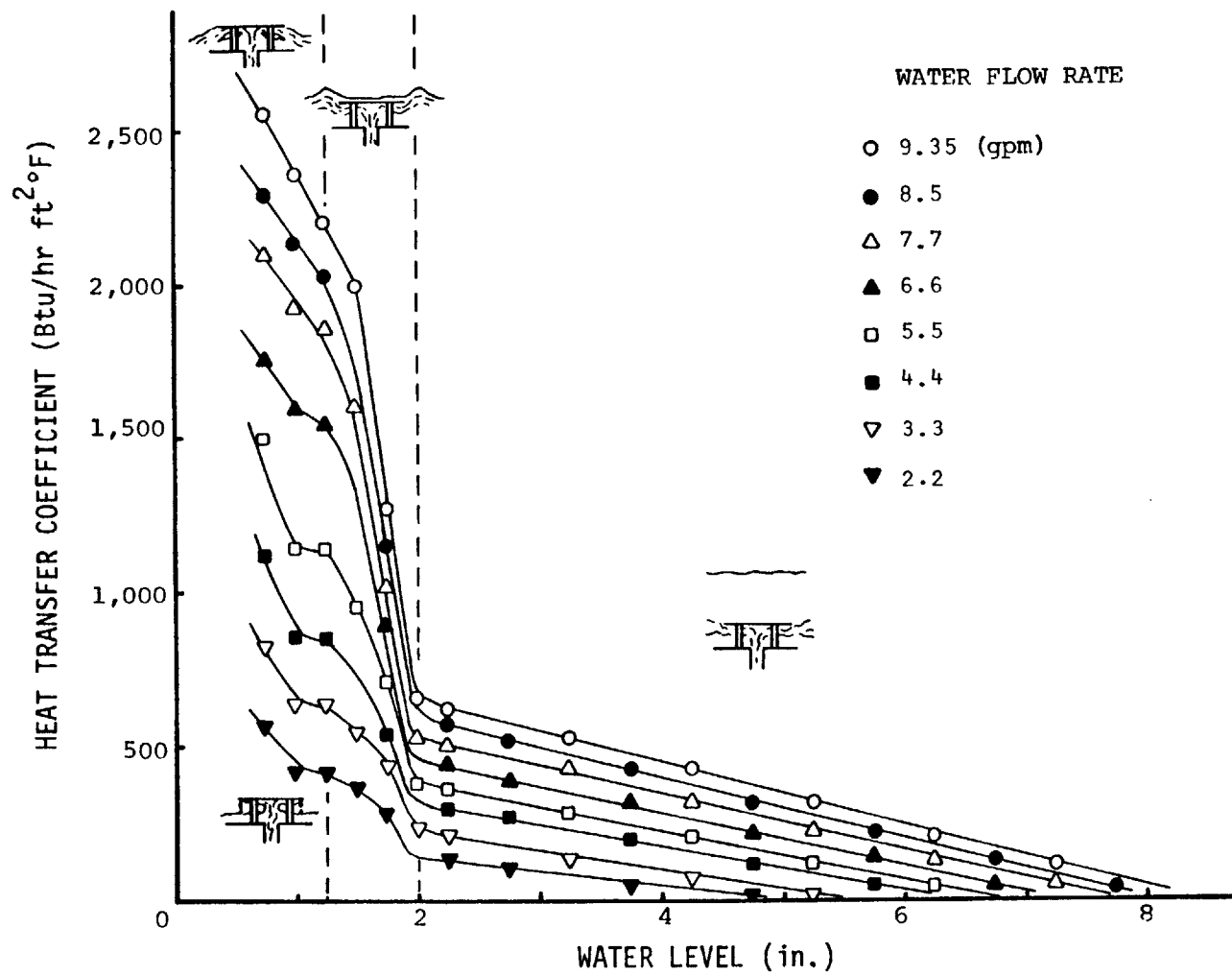
4.2 Variation of Heat Transfer Coefficient with Water Level

The variation of heat transfer coefficient (h) with water level (L) and water flow rate is shown in Fig. 13. As mentioned in Sect. 4.1, in Region 1, the interface is severely agitated, and therefore, the condensation area seems to be much larger than that of Regions 2 or 3. Hence, as shown in Fig. 13, the heat transfer coefficients in Region 1 are higher than those in Regions 2 and 3.

In Region 1, the heat transfer coefficients for flow rates greater than 6.6 gpm seem to decrease almost linearly with increasing water level. However, for flow rates over the range of 2.2 gpm to 5.5 gpm, h decreases up to 1.0 in. water level, and then remains unaltered between 1.0 in. and 1-1/4 in. water level.

In Region 2, h appears to decrease drastically with increasing water level. The slopes of the curve in Fig. 13 are much steeper in Region 2 than in Regions 1 or 3.

In Region 3, h decreases linearly, and then approaches zero asymptotically with increasing water level. The water level, where h approaches zero, appears to increase with increasing water flow rate, for example, it is around 5.0-6.0 in. for 2.2 gpm and 7.0-8.0 in. for 5.5 gpm. This can be explained by examining the conditions for stable stratification of the bulk water region. Details of stratification are described in Sect. 4.3.



VARIATION OF HEAT TRANSFER COEFFICIENT WITH WATER LEVEL AND WATER FLOW RATE (TMI 2 SPARGER MODEL)

FIG. 13

4.3 Stratification

When the water level in the test vessel becomes higher than 4.0-5.0 in., stable stratification of the bulk water is observed. As mentioned in Sect. 3.2, whether the turbulence of water jets is affected by the stratification of the bulk water is indicated by a stratification parameter, known as the Richardson number. [5] Positive Richardson numbers correspond to a stable stratification, negative Richardson numbers to an unstable stratification, and zero Richardson numbers to a homogeneous fluid.

In stable stratification, as shown in Fig. 10, the fluid density increases with depth. A turbulent water jet, pointed vertically upward from the bottom of a fluid in stable stratification, must do work against negative buoyancy forces, which produces a loss of turbulent energy in addition to viscous dissipation. As water level increases, the Richardson number tends to increase, and the turbulent water jets tends to be more suppressed by negative buoyancy forces. Consequently, the inlet water jets would hardly mix with adjacent water layer, and therefore, the heat transfer mechanism between the steam region and the bulk water region is primarily conduction. Hence, the interface heat transfer rate tends to approach zero with increasing water level.

4.4 Variation of Heat Transfer Coefficient with Reynolds Number

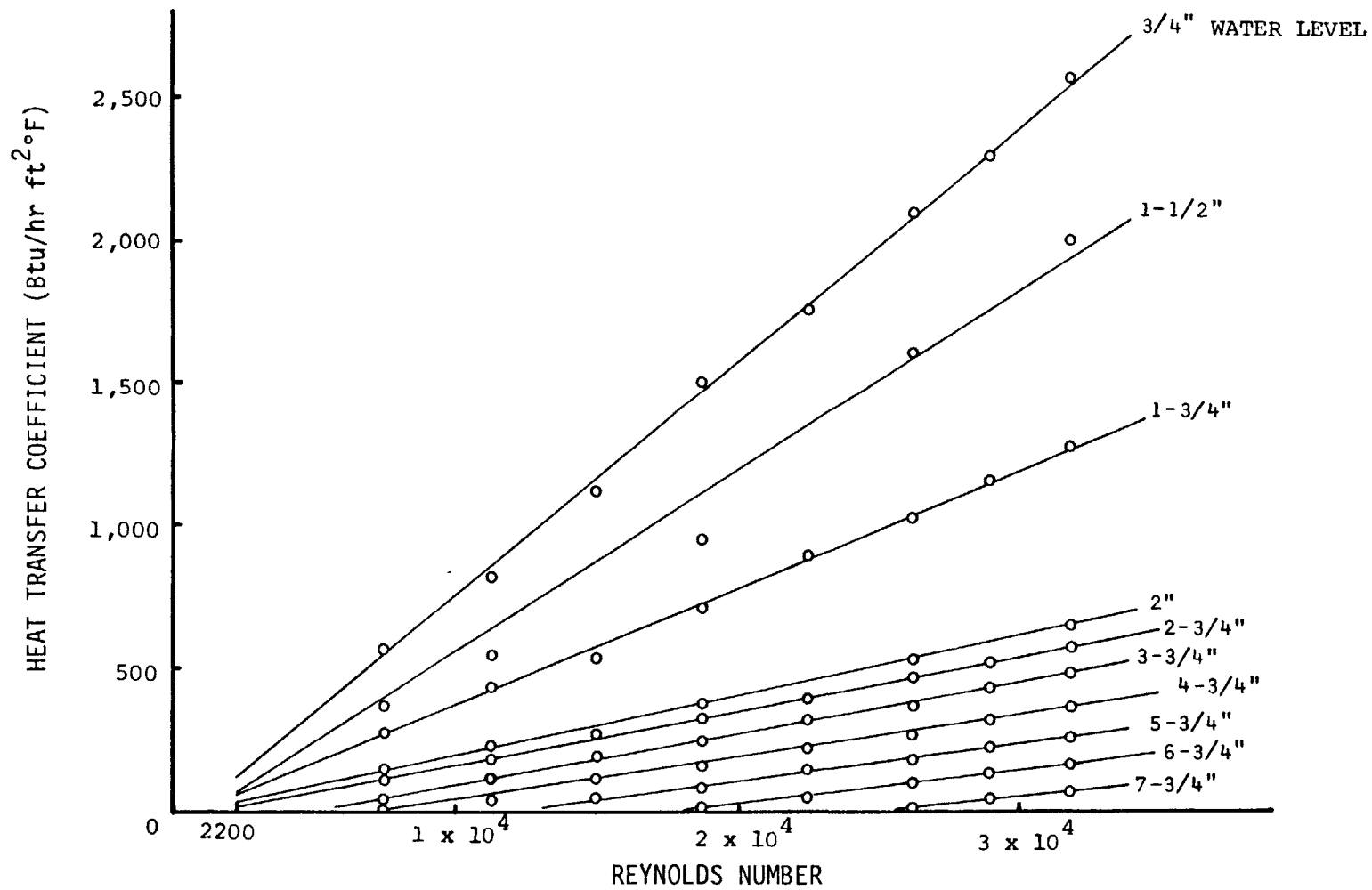
The variation of heat transfer coefficient (h) with the Reynolds number (Re) in the inlet water pipe is shown in Fig. 14. A linear increase in the heat transfer coefficients with increasing Reynolds number is observed in Regions 2 and 3. Despite the data scatter, the heat transfer coefficient in Region 1 also increases linearly with increasing Reynolds number. The slope of the h curves in Fig. 14 is equal to Stanton number, if heat transfer coefficient is plotted versus Gc_p , where G denotes the mass velocity of water jets in the inlet water pipe, and c_p denotes the specific heat of the inlet water.

Based upon these results, it is concluded that the heat transfer coefficient at the steam/water interface is proportional to the first power of the velocity of the turbulent water jets in the inlet water pipe.

4.5 Non-condensable Gases

4.5.1 Non-condensable Gases Study

The presence of non-condensable (N.C.) gases in the condensing vapor has a significant influence on the resistance to heat transfer at the interface. Leonard [6] showed that the effects of non-condensable gases on insurge transients in the MIT test vessel at low pressure are profound.



VARIATION OF HEAT TRANSFER COEFFICIENT WITH REYNOLDS NUMBER
(TMI 2 SPARGER MODEL)

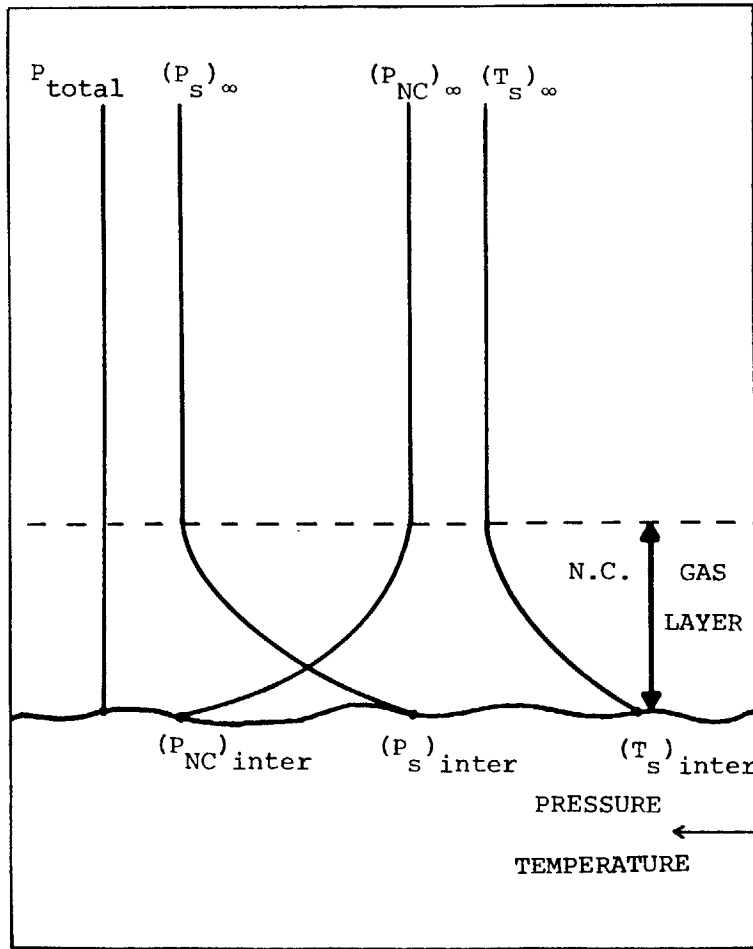
FIG. 14

Fig. 15(a) shows the variation of steam temperature at the interface and the pressure gradients for non-condensable gases and steam. The partial pressure of non-condensable gases at the interface increases above that in the bulk of the mixture, producing a driving force for gas diffusion away from the interface. [7] Since the total pressure P_{total} remains constant, the following equation can be obtained

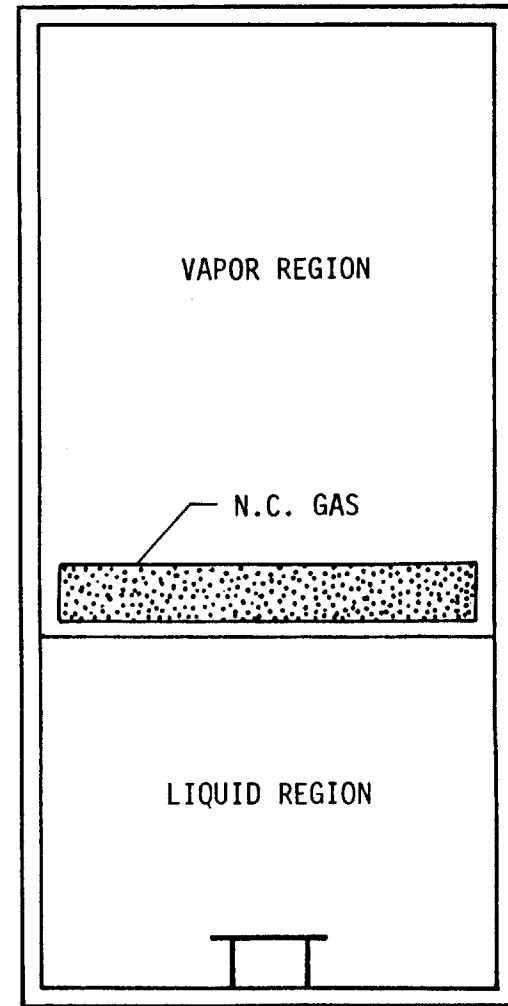
$$\begin{aligned} P_{total} &= (P_s)_{inter} + (P_{NC})_{inter} \\ &= (P_s)_{\infty} + (P_{NC})_{\infty} \end{aligned} \quad (40)$$

Here, subscripts s, NC, inter, and ∞ denote steam, non-condensable gas, interface, and bulk conditions, respectively. Since, the steam temperature at the interface, $(T_s)_{inter}$, corresponds to the saturation temperature equivalent to the partial pressure of steam at the interface, $(P_s)_{inter}$, the presence of non-condensable gases at the interface can be detected by comparing $(T_s)_{inter}$ with $(T_s)_{\infty}$.

As shown in Fig. 15(b), non-condensable gases with the molecular weight heavier than 18.0 accumulate at the interface and reduce the interface heat transfer rate drastically.



(a)



(b)

CONFIGURATIONS OF NON-CONDENSABLE GAS AT THE INTERFACE

FIG. 15

$$\frac{1}{h_{\text{overall}}} = \frac{1}{h_{\text{inter}}} + \frac{1}{h_{\text{NC}}} \quad (41)$$

Eq. 41 gives the overall heat transfer coefficient (h_{overall}) for the condensation in the presence of non-condensable gases.

4.5.2 Effects of Non-condensable Gases on Interface Heat Transfer

During the experiments, non-condensable (N.C.) gases were carried with the steam and accumulated at the interface in the test vessel. This resulted in a drastic decrease in the interface heat transfer rate. Hence, N.C. gases should be removed by blow-down pipes.

When two 1/4 in. ID blow-down pipes were used, it was found that these pipes were too small to discharge N.C. gases sufficiently, and the data for determining the interface heat transfer coefficient turned out not to be useful. Hence, they were replaced by three 1/2 in. ID blow-down pipes with the funnels (Fig. 1 & 2). With these three blow-down pipes, N.C. gases could be removed properly and the results appeared appropriate.

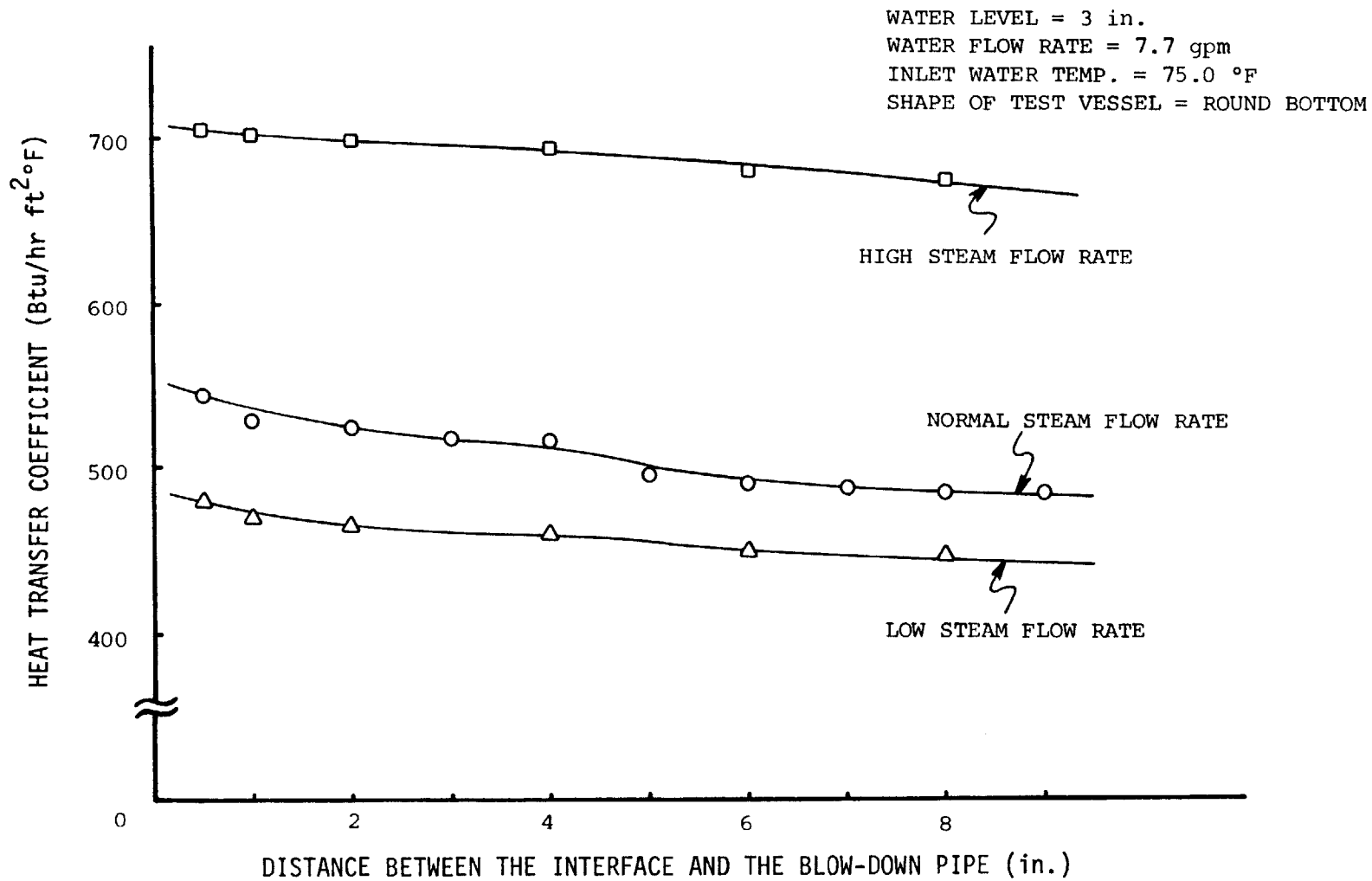
In order to evaluate the effects of N.C. gases at the interface, the axial position of the blow-down pipes was varied for some of the experiments. A constant water level of 3.0 in., water flow rate of 7.7 gpm, and inlet water temperature of 75.0° F was maintained. The steam flow rate was varied to change the momentum of steam at the interface.

The distance between the interface and the bottom of the blow-down pipe was varied from 1/2 in. to 9.0 in.

Fig. 16 shows the variation of the interface heat transfer coefficient (h) with the steam flow rate and the distance between the interface and the blow-down pipe (d). For the normal steam flow rate, as the distance increases, the heat transfer coefficient decreases gradually. This means that some amount of N.C. gases accumulate at the interface, as the distance increases. For the higher steam flow rate, due to the high momentum of steam, the interface was agitated by the steam, and N.C. gases were thoroughly mixed in the steam region. Therefore, h is higher than that for normal steam flow rate, and h slightly decreases with increasing distance. For the lower steam flow rate, due to the insufficient steam supply, h is lower than that for the normal steam flow rate.

Based upon these experimental results, the following conclusions are drawn:

- i) The effects of N.C. gases at the interface on the interface heat transfer rate are significant.
- ii) N.C. gases at the interface should be discharged sufficiently to get the accurate value of the interface heat transfer coefficient.



DEGRADATION OF HEAT TRANSFER COEFFICIENT WITH NON-CONDENSABLE GAS

FIG. 16

CHAPTER 5
EXPERIMENTAL DATA ANALYSIS

The measured interface heat transfer coefficient and the water level are non-dimensionalized as a Stanton number and a reference water level, respectively. The variation of Stanton number (St) with reference water level (L/Z) is obtained, and overall trends of the St curve are described in Sect. 5.1. Correlations between Stanton number and reference water level are established in Sect. 5.2. Based upon the St vs. L/Z diagram of each of the sparger models, a composite plot of the St curve for each sparger geometry is obtained in Sect. 5.3.

Finally, the prediction of the pressure response during pressurizer insurge transients is made and compared with Kim's [2] experimental data.

5.1 Variation of Stanton Number with Reference Water Level

As mentioned in Sect. 3.2, the heat transfer coefficient (h) can be non-dimensionalized as a Stanton number (St).

$$St = \frac{h}{G c_p} \quad (42)$$

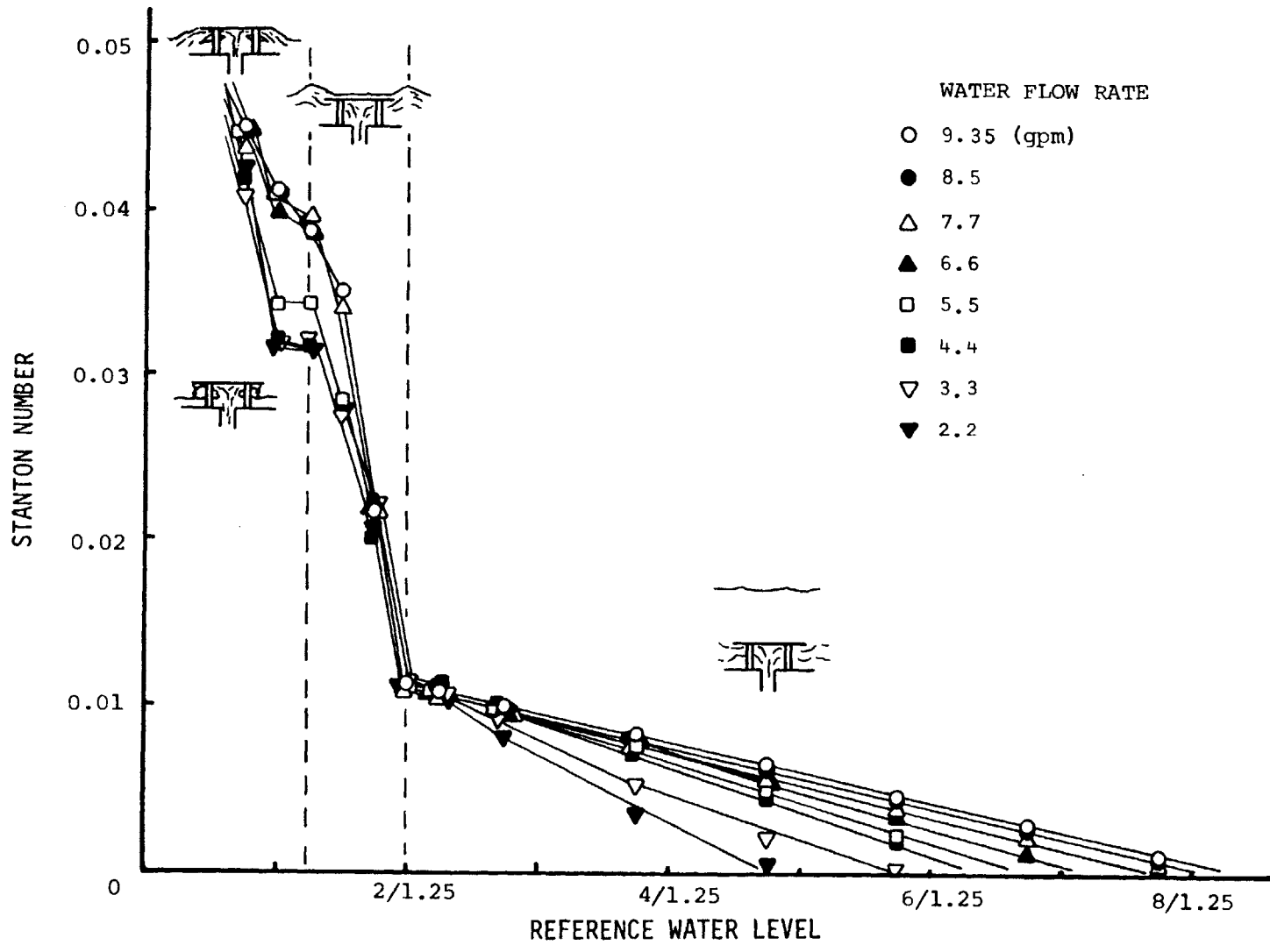
Here, mass velocity, G, is obtained as follows:

$$G = \frac{\dot{m}}{A} \quad (43)$$

where \dot{m} denotes the inlet water flow rate, and A is an area uniquely defined for a particular sparger geometry. For the TMI 2 sparger model, the water jets flow out through the sparger area (A) defined by πDZ . Here, D denotes the diameter of the sparger disk, and Z denotes the sparger height.

The water level (L) is non-dimensionalized as a reference water level (L/Z), where L denotes the water level and Z denotes the sparger height. A Stanton number versus reference water level diagram is obtained from the heat transfer coefficient versus water level data.

Fig. 17 shows the variation of Stanton number (St) with reference water level (L/Z) for water flow rates over the range of 2.2 gpm to 9.35 gpm. As discussed in Sect. 4.1, in Region 1, due to two different flow patterns of water jets, two groups of the St curve are observed. The upper group of the St curve corresponds to water flow rates greater than 6.6 gpm, and the lower one corresponds to water flow rates less than 5.5 gpm. In Region 2, the St curves coincide well. In Region 3, the St curves also coincide to some extent. However, as the reference water level becomes large, the St curves for the lower flow rates begin to deviate from the main St curve, and finally, approach zero.



VARIATION OF STANTON NUMBER WITH REFERENCE WATER LEVEL AND WATER FLOW RATE (TMI 2 SPARGER MODEL)

FIG. 17

For the same reference water level, due to the change in water jet velocity, the Richardson number for the higher flow rates is lower than that for the lower flow rates. Hence, the Stanton number for the higher flow rates is higher than that for the lower flow rates. Therefore, it is natural that each St curve can not coincide with increasing water level. In addition, the reference water level, where the Stanton number approaches zero, increases with increasing water flow rate.

5.2 Scaling Laws

As shown in Fig. 17, the Stanton number (St) is dependent upon the reference water level (L/Z) and the geometry of the sparger and the test vessel. Based Upon the St vs. L/Z diagram (Fig. 17), the simplified St vs. L/Z diagram is obtained as Fig. 18. Despite the slightly different St curves in Region 1 in Fig. 17, these curves are collectively considered as one straight line. The deviation of the St curves in Region 3, due to the stable stratification, is bounded by the two St curves shown in Fig. 18.

In Table I, an empirical fit for the Stanton numbers for the three regions are expressed as a function of the reference water level. The deviation of the St curves in Region 3 for flow rates over the range of 2.2 gpm to 9.35 gpm is modelled by a variable slope, m. In addition,

TABLE I

CORRELATION OF STANTON NUMBER AS A FUNCTION OF
REFERENCE WATER LEVEL (TMI 2 SPARGER MODEL)

Region 1 $(0 < \frac{L}{Z} \leq 1.0)$

$$St = St(\frac{L}{Z}) = -0.015 \frac{L}{Z} + 0.053$$

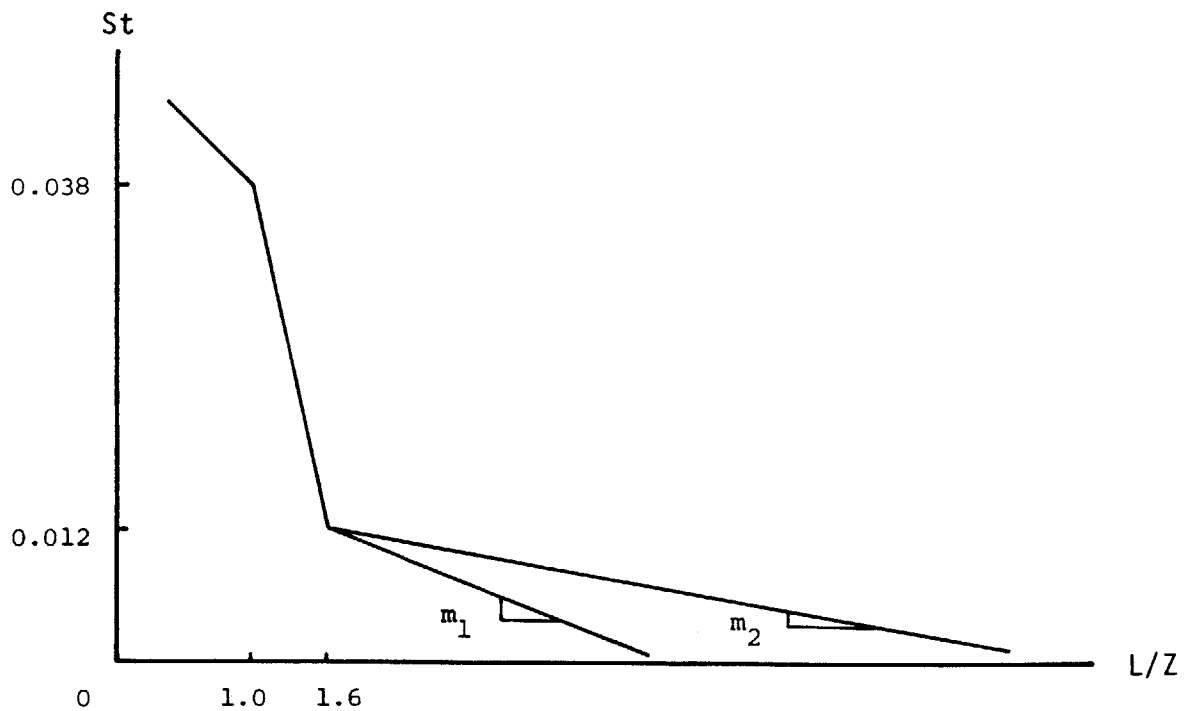
Region 2 $(1.0 \leq \frac{L}{Z} \leq 1.6)$

$$St = St(\frac{L}{Z}) = -0.044 \frac{L}{Z} + 0.082$$

Region 3 $(\frac{L}{Z} \geq 1.6)$

$$St = St(\frac{L}{Z}) = m(\frac{L}{Z} - 1.6) + 0.0115$$

$$\text{where } -0.0048 \leq m \leq -0.0022$$



SIMPLIFIED St vs. L/Z DIAGRAM (TMI 2 SPARGER MODEL)

FIG. 18

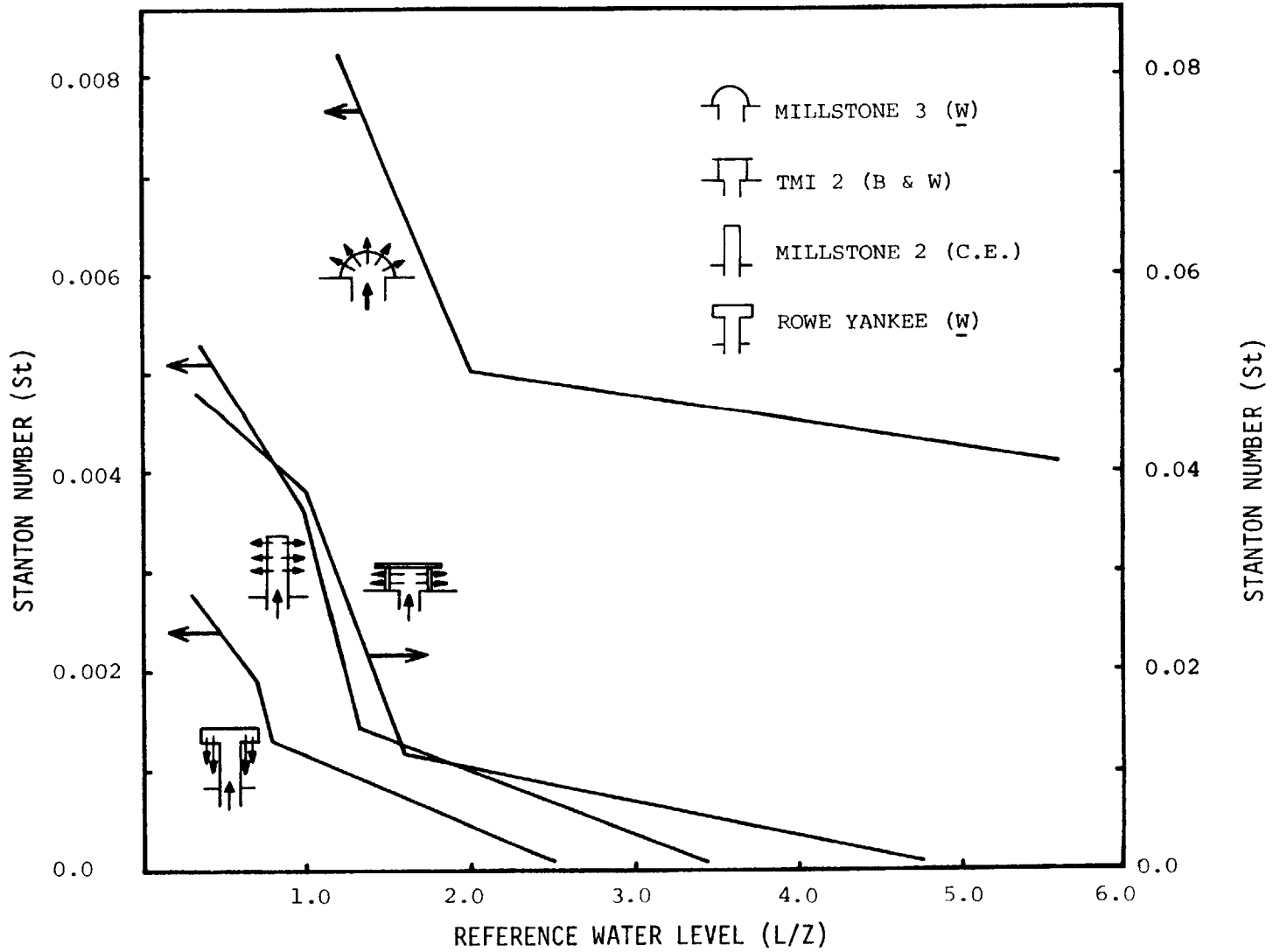
scaling laws for the other sparger models are described in Appendix D.

5.3 Composite Plot of Stanton Number versus Reference Water Level for Each Sparger Geometry

Based upon the simplified St vs. L/Z diagrams of each of the sparger models, the composite plot of Stanton number (St) versus reference water level (L/Z) for each sparger geometry is shown in Fig. 19.

These overall results indicate the following trends:

- i) The general trend of each of the sparger models is similar, despite significant differences in geometry.
- ii) The magnitude of the interface heat transfer coefficient (expressed in terms of the Stanton number, St) is a varying function of liquid level in three distinct and defineable regions.
- iii) For the sparger model which has the horizontal or downward direction of the injected water jets, the slope of the St curve in Region 2 is the steepest of the three regions. On the other hand, for the sparger model which has the upward injected water jets, the slope of the St curve in Region 2 is almost zero.



COMPOSITE PLOT OF ST VS. L/Z FOR EACH SPARGER GEOMETRY

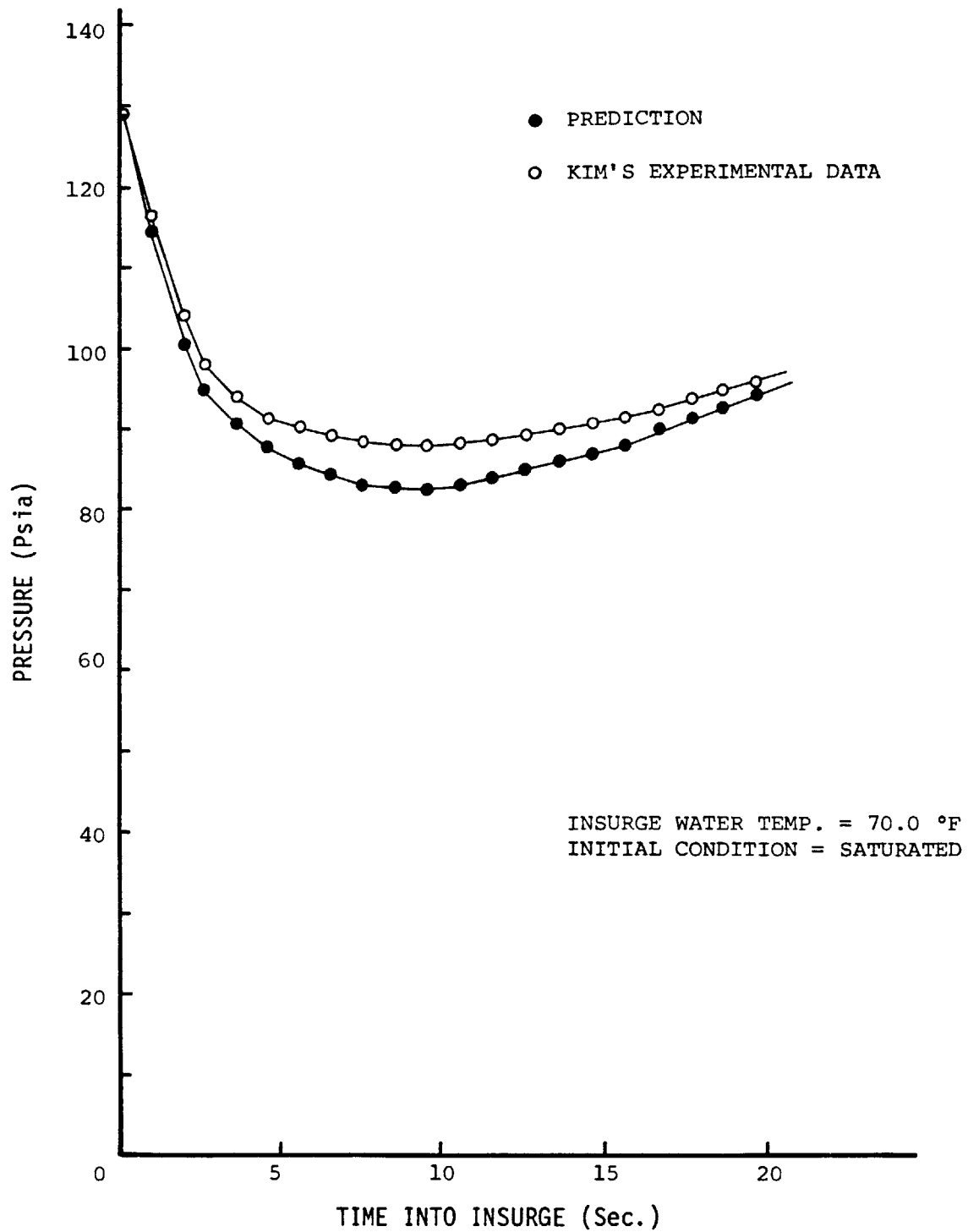
FIG. 19

5.4 Prediction of Pressure Response during Pressurizer

Insurge Transients

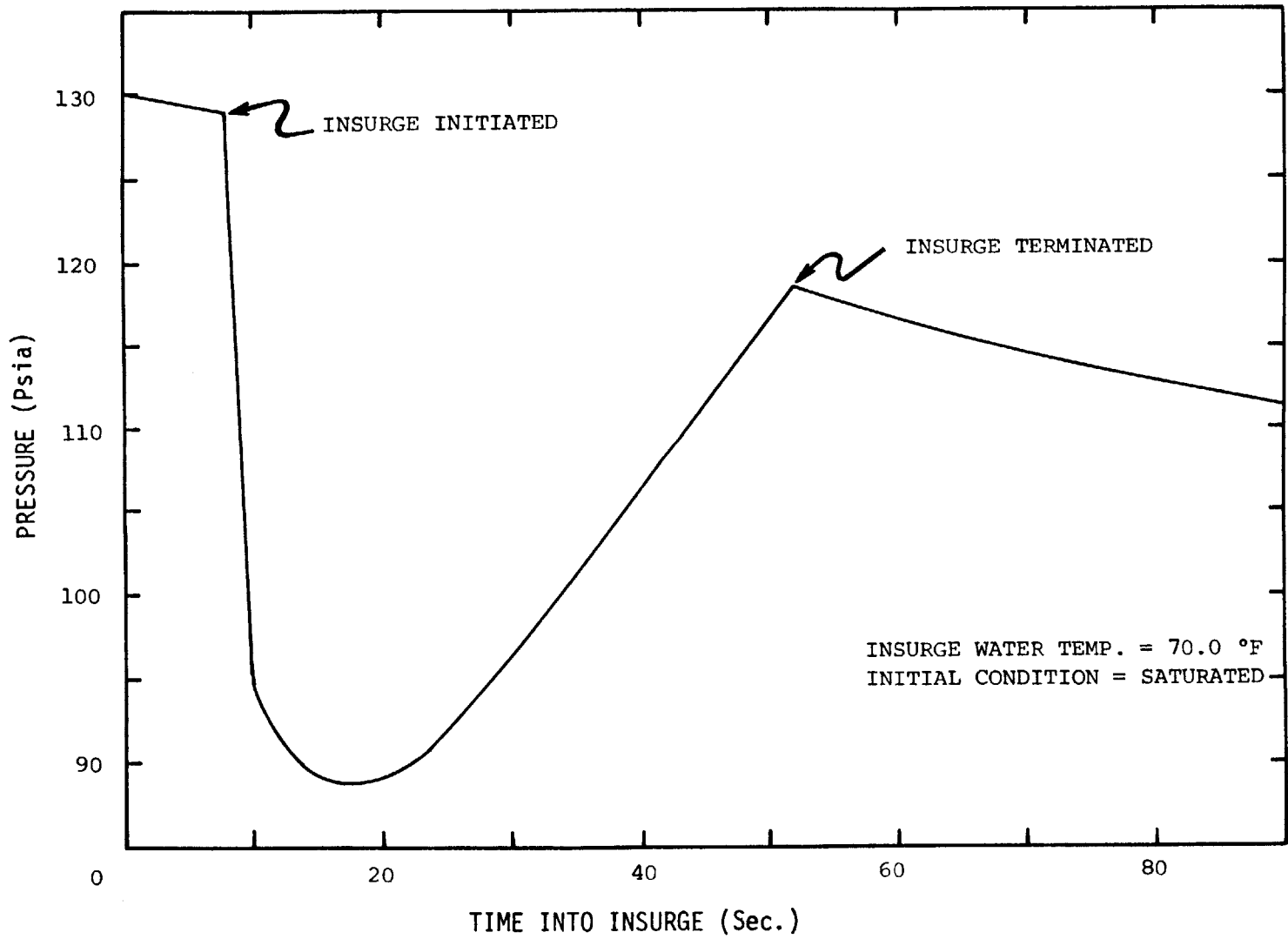
Based upon the experimentally determined heat transfer coefficients at the interface, the pressure response during pressurizer insurge transients was predicted and compared with Kim's [2] experimental data.

Fig. 20, 21, and 22 show Kim's data for an empty tank insurge. A prediction of the pressure response during first 20.0 seconds of this transients, using the interface heat transfer model given in Sect. 4.2, is shown in Fig. 20. The prediction is in good agreement with the experimental data. Details of Kim's experimental apparatus and procedures are described in Appendix J.



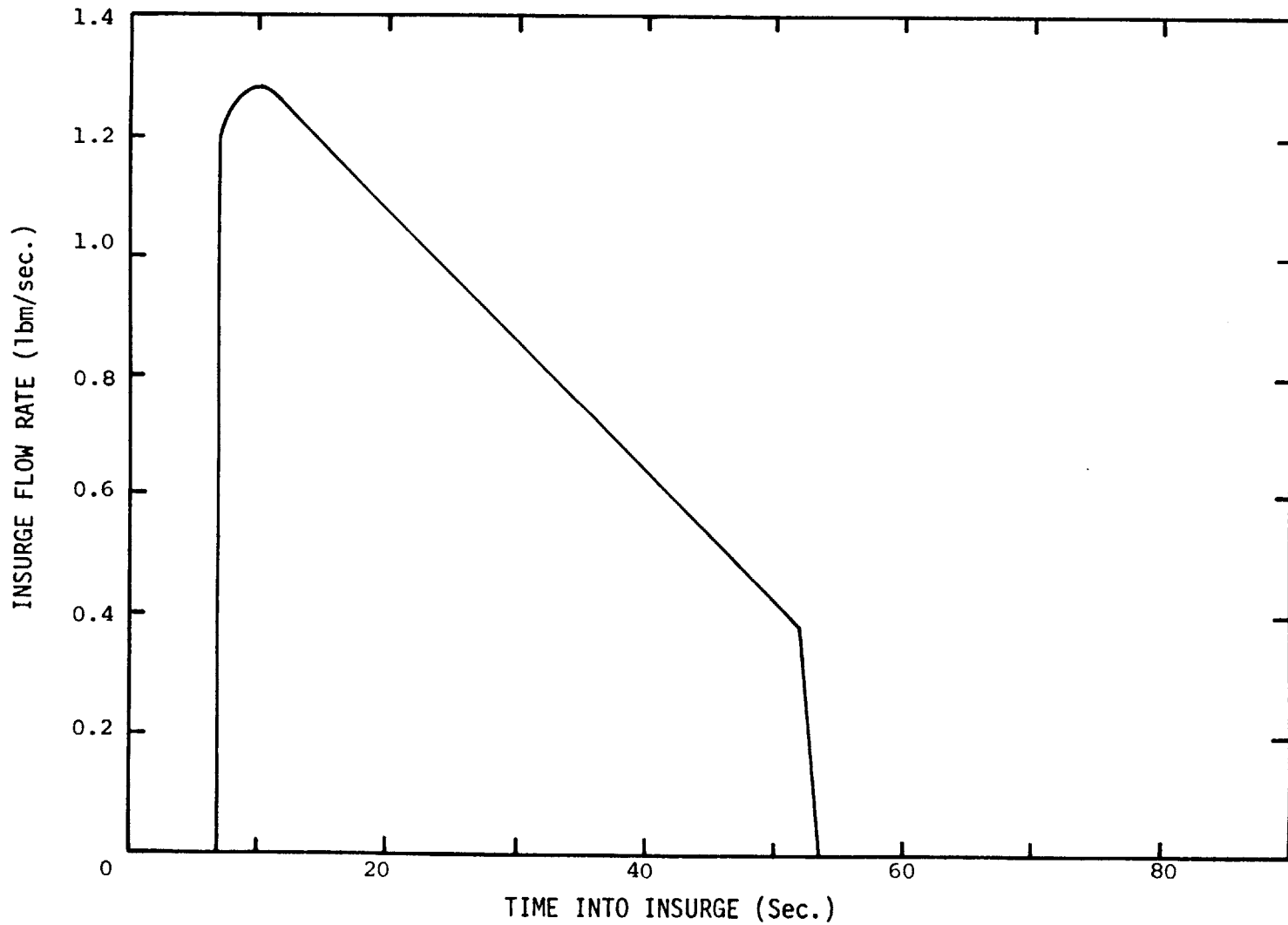
PREDICTION AND EXPERIMENTAL DATA OF PRESSURE RESPONSE
DURING INSURGE TRANSIENT

FIG. 20



PRESSURE RESPONSE OF A SCALED PRESSURIZER
TO AN EMPTY TANK INSURGE TRANSIENT

FIG. 21



MEASURED INSURGE FLOW RATE
FOR AN EMPTY TANK INSURGE TRANSIENT

FIG. 22

CHAPTER 6
CONCLUSIONS

An experimental study of the heat transfer at the vapor/liquid interface in a simulated PWR pressurizer has been performed. Four different sparger geometries have been tested, and the Stanton number scaling laws have been established.

The following conclusions are drawn based upon the experimental and analytical results:

- 1) The Stanton number for the water jets through the inlet sparger of a pressurizer is dependent upon the reference water level and the geometry of the sparger and the pressurizer vessel.
- 2) Despite the different shaped spargers, overall trends for each sparger geometry are similar.
- 3) Three distinct and different variations of interface heat transfer coefficients with water level exist. These regions are caused by changing insurge jet flow patterns with increasing water level.
- 4) Interface heat transfer in the pressurizer test vessel is significantly affected by the presence of non-condensable gases at the vapor/liquid interface.
- 5) As the water level in the pressurizer test vessel

increases, stable stratification of the bulk water is observed, and the heat transfer rate at the interface can be neglected.

- 6) The interface heat transfer coefficient is proportional to the velocity of the turbulent water jets in the inlet water pipe.

REFERENCES

1. Saedi, H.R. "Insurge Pressure Response and Heat Transfer for PWR Pressurizer" SM Thesis, Dept.of Mechanical Engineering, MIT, Nov. 1982.
2. Kim, S.N. "An Experimental and Analytical Model of a PWR Pressurizer during Transients" Ph.D. Thesis, Dept. of Nuclear Engineering, MIT, Jan. 1984.
3. Reynolds, O. "On the Extent and Action of the Heating Surface for Steam Boilers" Proc. Manchester Lit. Phil. Soc. 14, 7-12 (1874).
4. Tennekes, H. "A First Course in Turbulence" The MIT Press, Cambridge (1970).
5. Tritton, D.J. "Physical Fluid dynamics" Van Nos Reinhold (1977).
6. Leonard, M.T. "The Effects of a Non-Condensable Gas on Pressurizer Insurge Transients" SM Thesis, Dept. of Nuclear Engineering, MIT, Dec. 1983.
7. Collier, J.G. "Convective Boiling and Condensation" McGraw-Hill, (1971).

APPENDIX A

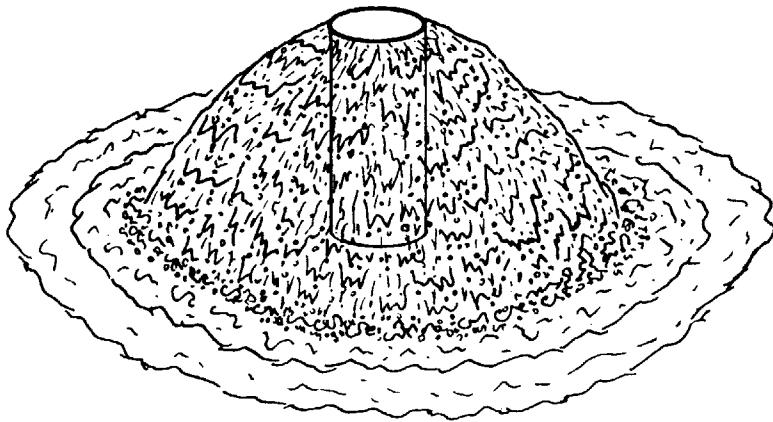
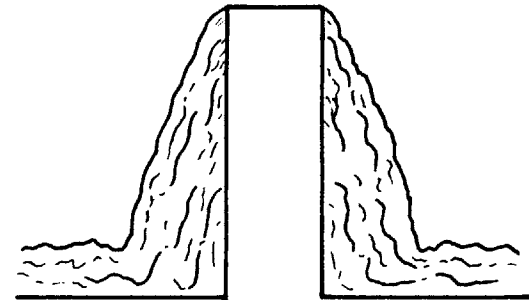
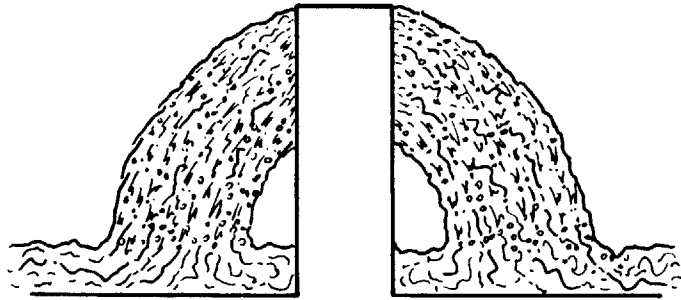
EXPERIMENTAL RESULTS FOR THE MILLSTONE 2 SPARGER MODEL

A.1 Flow Patterns

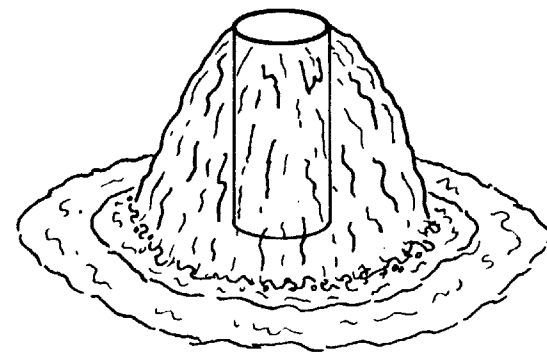
The model of the Millstone 2 sparger was connected to the 1.0 in. ID inlet water pipe, and the flat bottom test vessel was used during the experiments. The inlet water flow rate was varied from 2.2 gpm to 9.35 gpm and the water level ranged from 0.75 in. to 8.0 in. The inlet water temperature was maintained at a temperature of 75.0° F.

When the water level was less than the sparger height, 3.0 in., two different flow patterns for the baffled water jets were observed. As shown in Fig. A.1, for water flow rates greater than 6.6 gpm, the water sprayed through the holes above the water level and did not run down the side wall of the sparger. However, for water flow rates less than 5.5 gpm, water ran down along the side wall of the sparger. Accordingly, the condensation area of baffled water jets is much smaller than that for flow rates greater than 6.6 gpm. Water levels less than the sparger height, 3.0 in., are defined as Region 1.

As shown in Fig. A.2(a), when the water level was slightly greater than the sparger height, a hydraulic jump was observed around the edge of the sparger. The height of the hydraulic jump is dependent upon the momentum of baffled water jets, that is, this height increases with



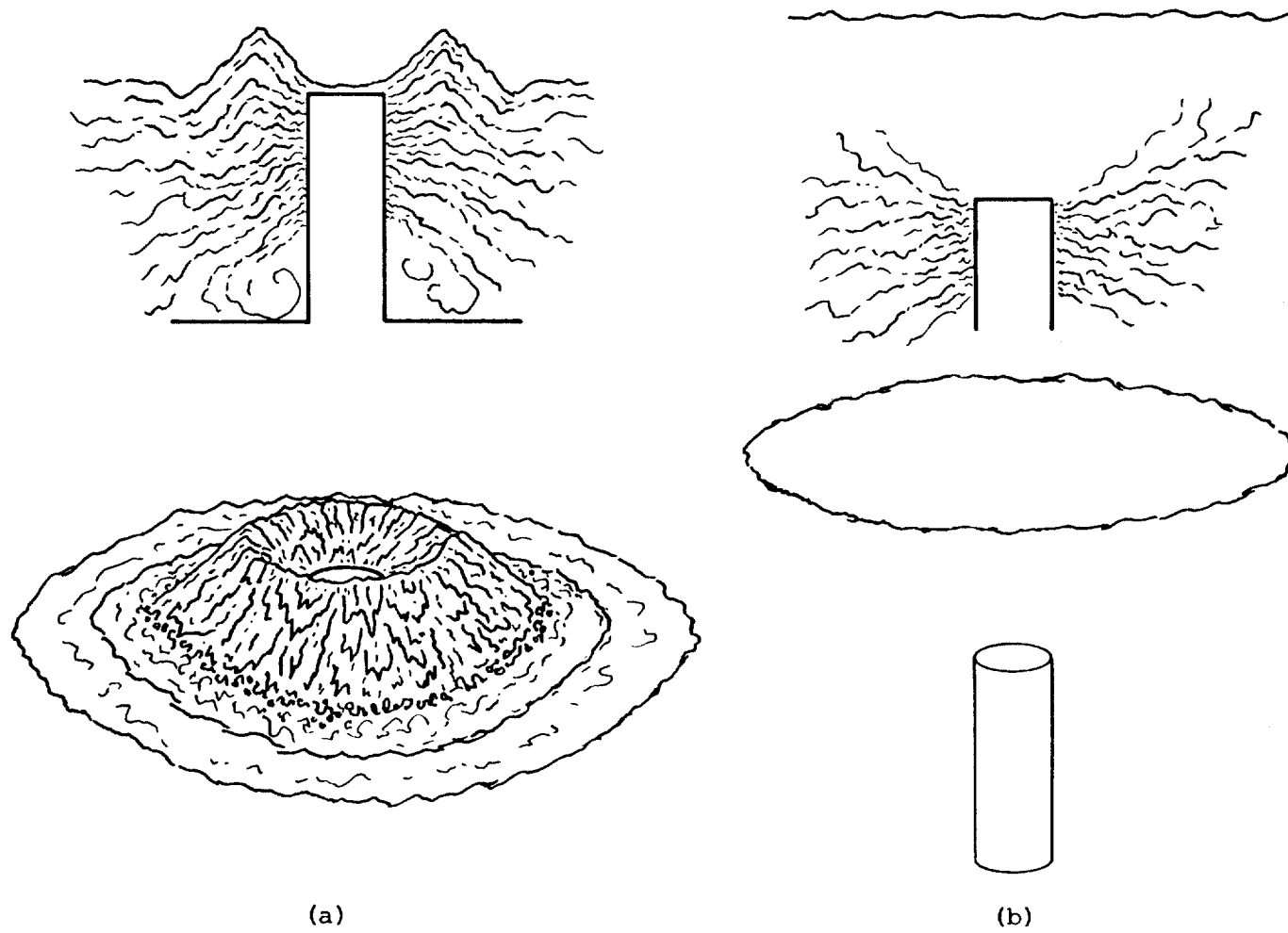
(a)



(b)

FLOW PATTERNS FOR MILLSTONE 2 SPARGER MODEL (REGION 1)

FIG. A.1



FLOW PATTERNS FOR MILLSTONE 2 SPARGER MODEL (REGIONS 2 & 3)

FIG. A.2

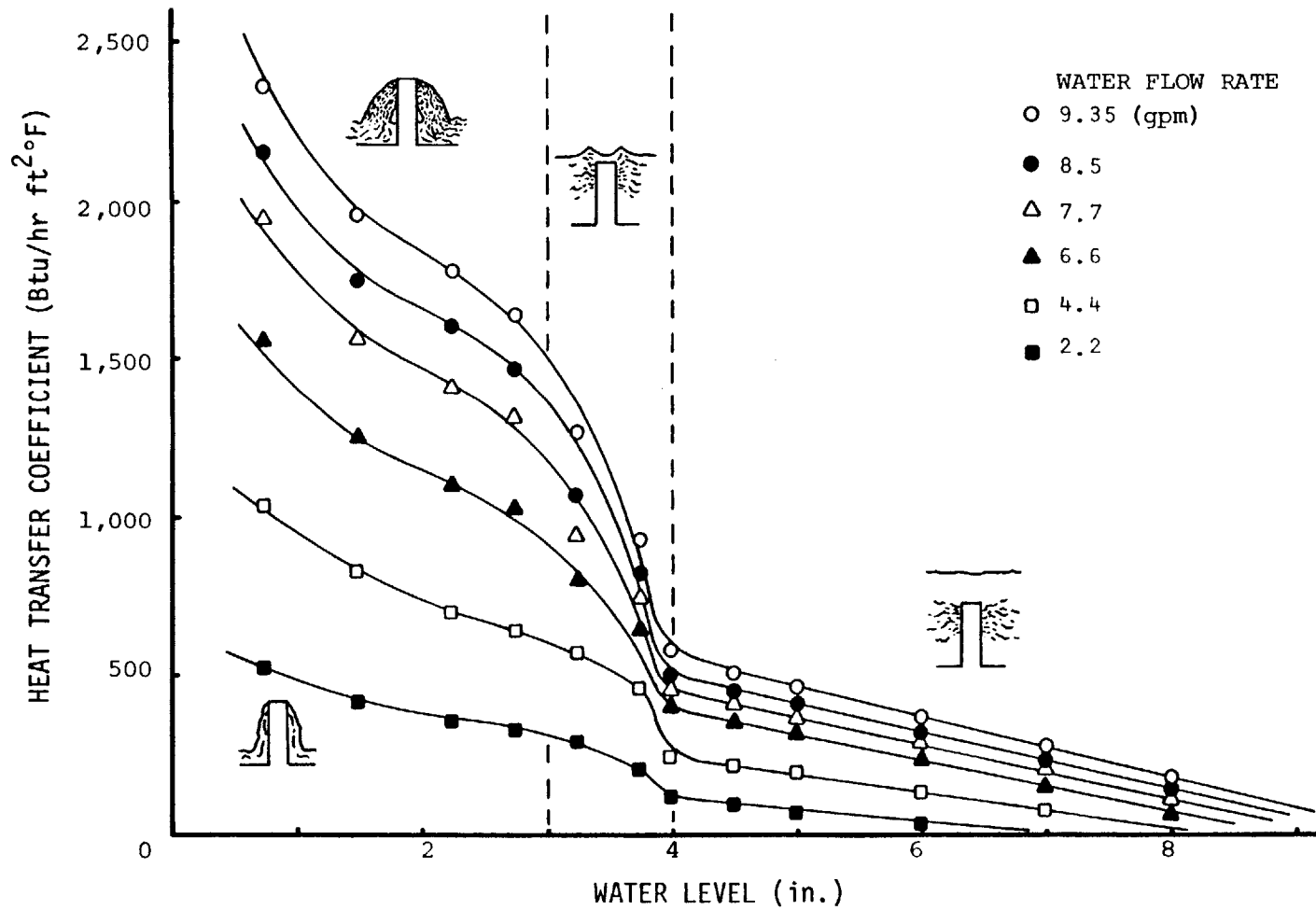
increasing water flow rate. As the water level reached around 4.0 in., the impingement, due to the hydraulic jump, disappeared suddenly and interface motion ceased. This transitional water level appears not to change for various water flow rates. Here, the region of water levels between the sparger height, 3.0 in., and the transitional water level, 4.0 in., is defined as Region 2.

Water levels above the transitional level are defined as Region 3. As the water level increased, in Region 3, water jets did not reach the interface, and no interface motion was observed.

A.2 Variation of Heat Transfer Coefficient with Water Level

The variation of heat transfer coefficient (h) with water level (L) and water flow rate is shown in Fig. A.3. As mentioned in Sect. A.1, in Region 1, the condensation area is larger than that of Regions 2 or 3. Hence, the heat transfer coefficients in Region 1 are higher than those in Regions 2 and 3. As the water level increases, due to the decrease in the condensation area and the interface agitation, the heat transfer coefficient in Region 1 decreases.

In Region 2, the heat transfer coefficient decreases severely with increasing water level. The slopes of the curves in Fig. A.3 are much steeper in Region 2 than in Regions 1 or 3.



VARIATION OF HEAT TRANSFER COEFFICIENT WITH WATER LEVEL AND WATER FLOW RATE (MILLSTONE 2 SPARGER MODEL)

FIG. A.3

In Region 3, h decreases linearly, and then approaches zero asymptotically with increasing water level. Also, the water level, where h approaches zero, appears to increase with increasing water flow rate. This can be explained by examining the conditions for stable stratification of the bulk water region. Details of stratification are described in Sect. 4.3.

A.3 Variation of Stanton Number with Reference Water Level

In order to non-dimensionalize the measured heat transfer coefficient in terms of other characteristic parameters, Stanton number (St) is defined as follows:

$$St = \frac{h}{G c_p}$$

Here, mass velocity, G , is obtained as

$$G = \frac{\dot{m}}{A}$$

where \dot{m} denotes the inlet water flow rate. For the Millstone 2 sparger model, the area A is defined by the total area of seven hundred and ninety-two tiny holes on the side wall of the sparger. The water level is non-dimensionalized as a reference water level (L/Z). Here, L denotes the water level, and Z denotes the sparger height.

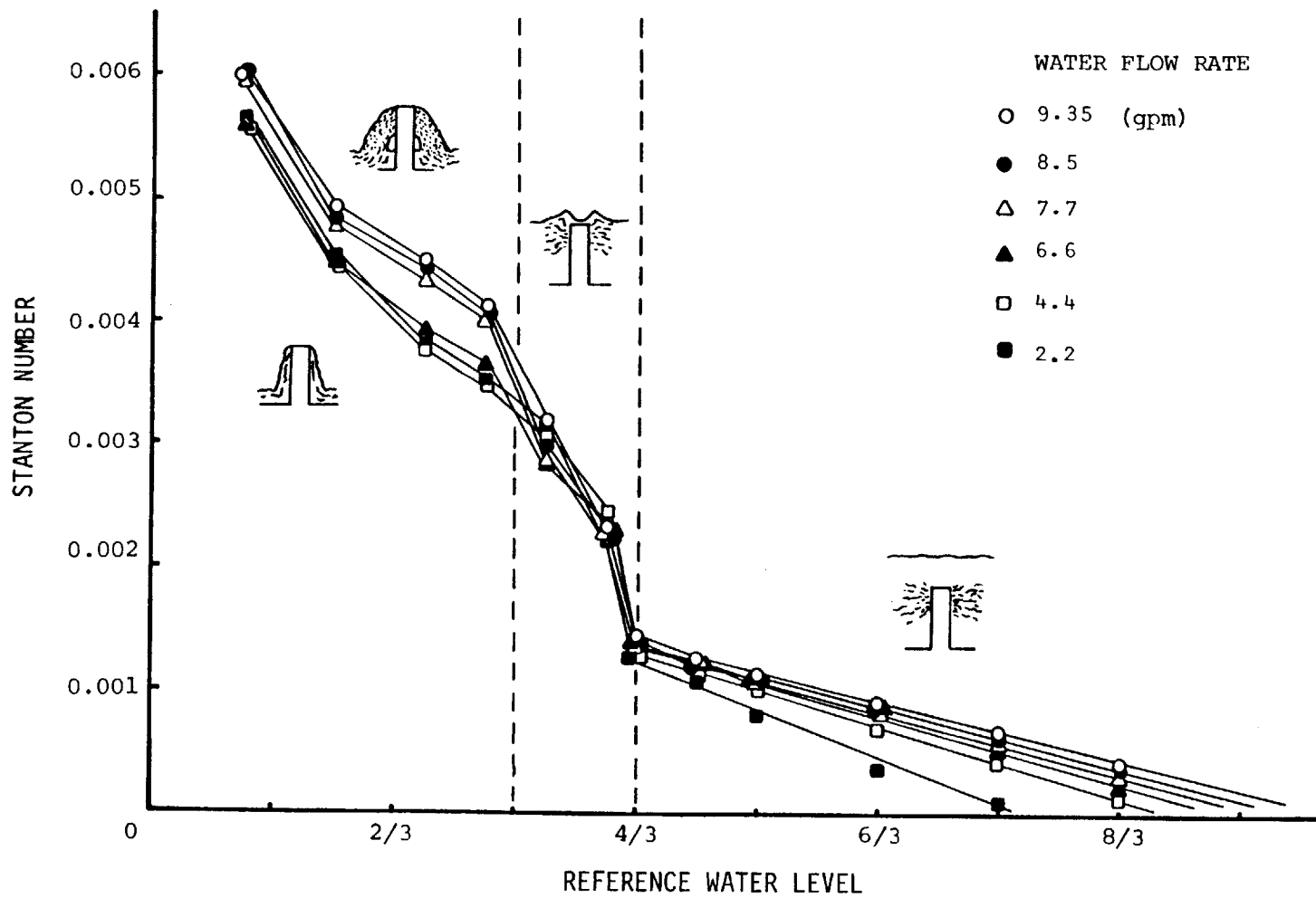
The variation of Stanton number (St) with a reference

water level (L/Z) and water flow rates over the range of 2.2 gpm to 9.35 gpm is shown in Fig. A.4. In Region 1, due to two different flow patterns of water jets, two different groups of the St curve are observed. The upper group of the St curve corresponds to water flow rates greater than 7.7 gpm, and the lower one corresponds to water flow rates less than 6.6 gpm. The variation of the St curves with a reference water level and water flow rate appears to be almost the same in Region 2. In Region 3, the St curves also coincide to some extent. However, as the reference water level increases, the St curves for the lower flow rates begin to deviate from the main St curve, and finally, approach zero.

For the same reference water level, as the water flow rate decreases, the Richardson number tends to increase, and therefore, the Stanton number for the higher flow rates is higher than that for the lower flow rates. Hence, each St curve can not coincide with increasing reference water level. Furthermore, the reference water level, where the St curve approaches zero, appears to increase with increasing water flow rate.

A.4 Variation of Heat Transfer Coefficient with Reynolds Number

The variation of heat transfer coefficient (h) with the Reynolds number (Re) in the inlet water pipe is shown in

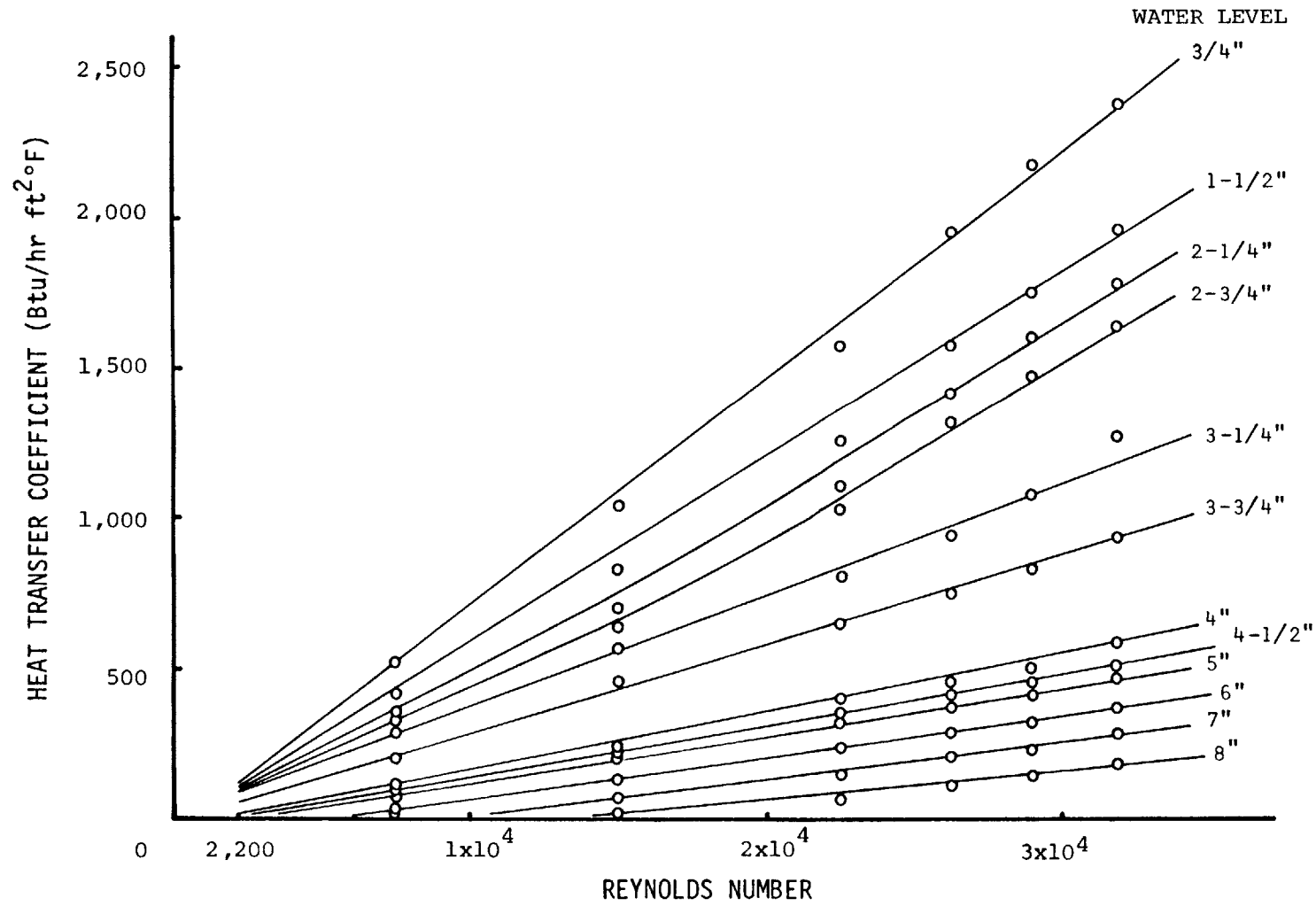


VARIATION OF STANTON NUMBER WITH REFERENCE WATER LEVEL AND WATER FLOW RATE (MILLSTONE 2 SPARGER MODEL)

FIG. A.4

Fig. A.5. A linear increase in the heat transfer coefficient with increasing Reynolds number is observed over all three regions. In Fig. A.5, the Reynolds number can be substituted for the velocity of turbulent water jets or the water flow rate. The slope of the h curves in Fig. A.5 is equal to Stanton number, if h is plotted versus Gc_p , where G denotes the mass velocity for the water jets in the inlet pipe, and c_p denotes the specific heat of the inlet water.

Based upon these results, it is concluded that the interface heat transfer coefficient is proportional to the first power of the velocity of the turbulent water jets in the inlet water pipe.



VARIATION OF HEAT TRANSFER COEFFICIENT WITH REYNOLDS NUMBER
(MILLSTONE 2 SPARGER MODEL)

FIG. A.5

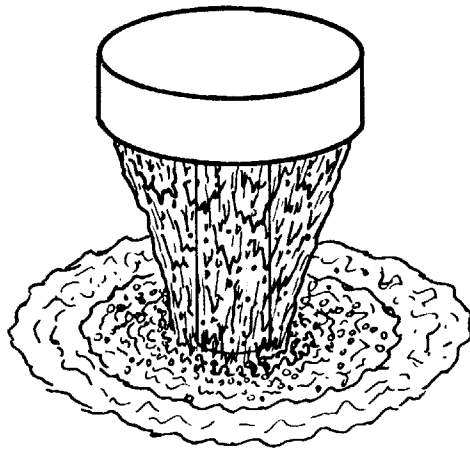
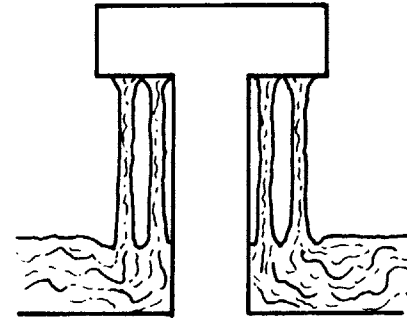
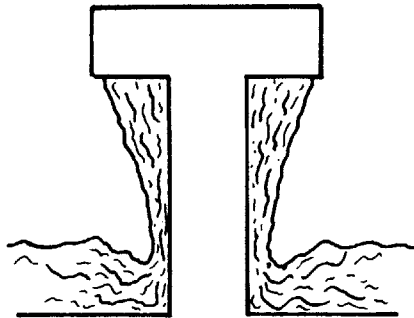
APPENDIX B

EXPERIMENTAL RESULTS FOR THE ROWE YANKEE SPARGER MODEL

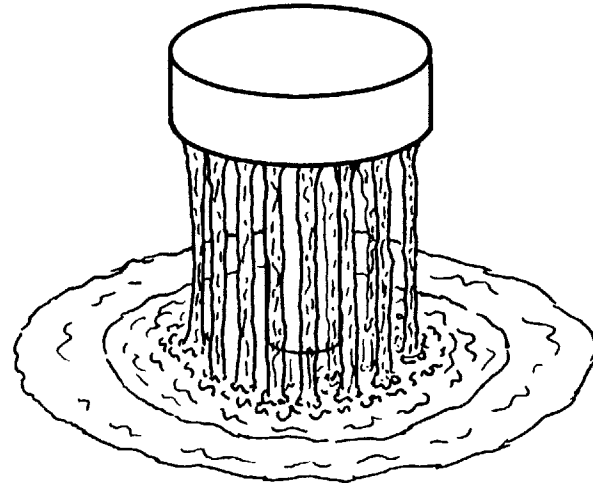
B.1 Flow Patterns

The inner diameter of the Yankee's pressurizer is smaller than that of the Millstone 2 and 3's pressurizer. During the experiments, in order to use the same flat bottom vessel, 8.25 in. ID and 17.0 in. in height, the 0.712 in. ID inlet water pipe was connected to the pool vessel bottom. The experiments were performed for water flow rates over the range of 1.7 gpm to 9.35 gpm. The water level ranged from 1.0 in. to 9.0 in., and the inlet water temperature was maintained at a temperature of 75.0^o F.

As shown in Fig. B.1, when the water level is less than 3.0 in., two different flow patterns for the baffled water jets were observed. For a water flow rate of 1.7 gpm, the water jets fell down perpendicular to the interface (Fig. B.1(b)). Due to the geometry of the sparger cap, water jets fell down and toward the center axis of the sparger for water flow rates greater than 2.0 gpm, and many bubbles were observed at the interface. As the water level increased from 3.0 in. to 3.25 in., interface motion ceased, and bubbles disappeared. Here, water levels less than 3.0 in. are defined as Region 1, and the region of water levels between 3.0 in. and 3.25 in. is defined as Region 2.



(a)



(b)

FLOW PATTERNS FOR ROWE YANKEE SPARGER MODEL (REGION 1)

FIG. B.1

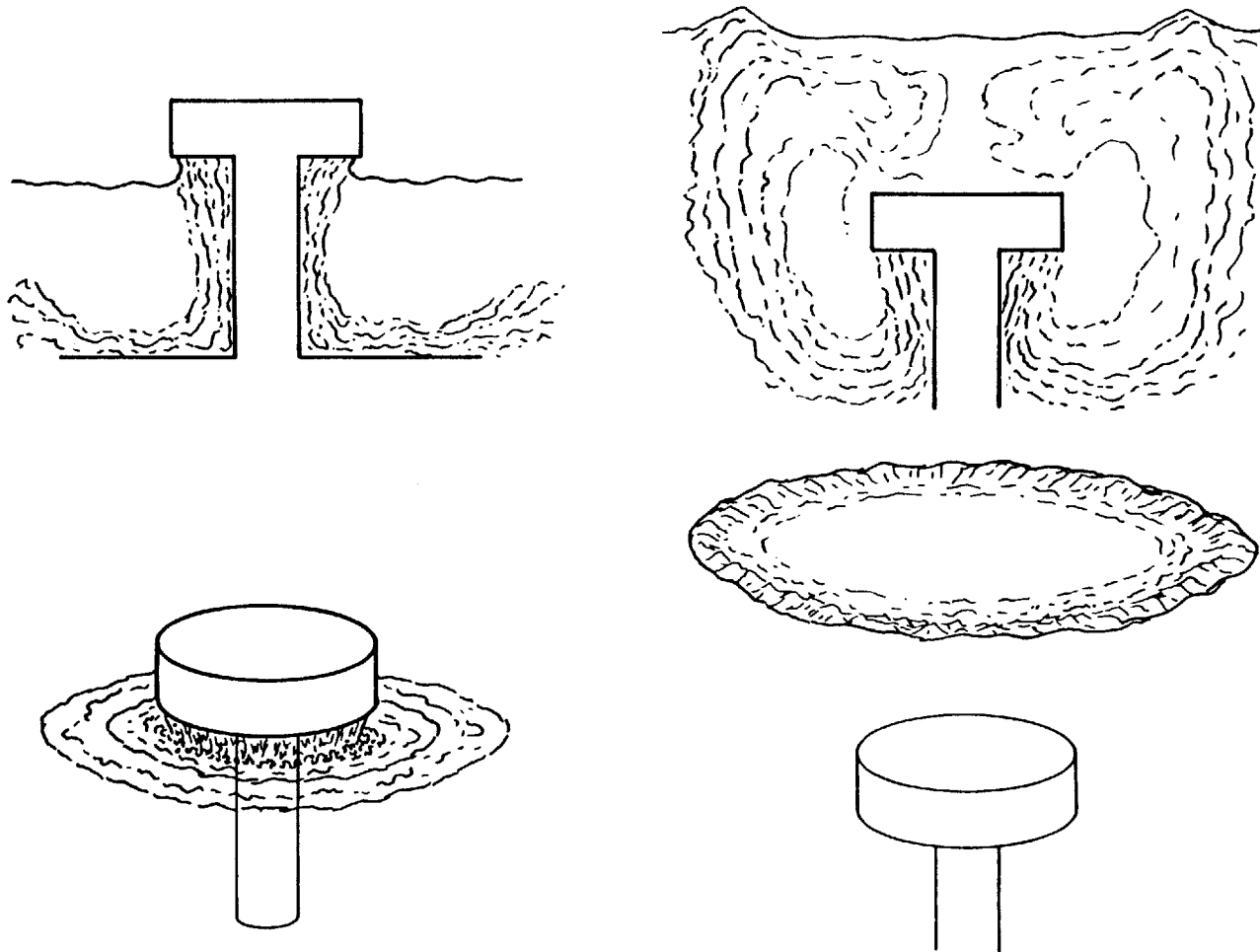
As shown in Fig. B.2, since the injected direction of the water jets for the Rowe Yankee sparger model is different than that for the other sparger models, different flow patterns of water jets were observed. Water jets hit the test vessel bottom and climbed along the vessel wall which agitated the interface near the test vessel wall. No interface motion was observed as the impingement of water jets disappeared with increasing water level. Here, water levels above 3.25 in. are defined as Region 3.

B.2 Variation of Heat Transfer Coefficient with Water Level

The variation of heat transfer coefficient (h) with water level (L) and water flow rate is shown in Fig. B.3. As mentioned in Sect. B.1, in Region 1, the interface is severely agitated, and the condensation area is larger than that of Regions 2 or 3. Hence, the heat transfer coefficient in Region 1 is much higher than that in Regions 2 and 3.

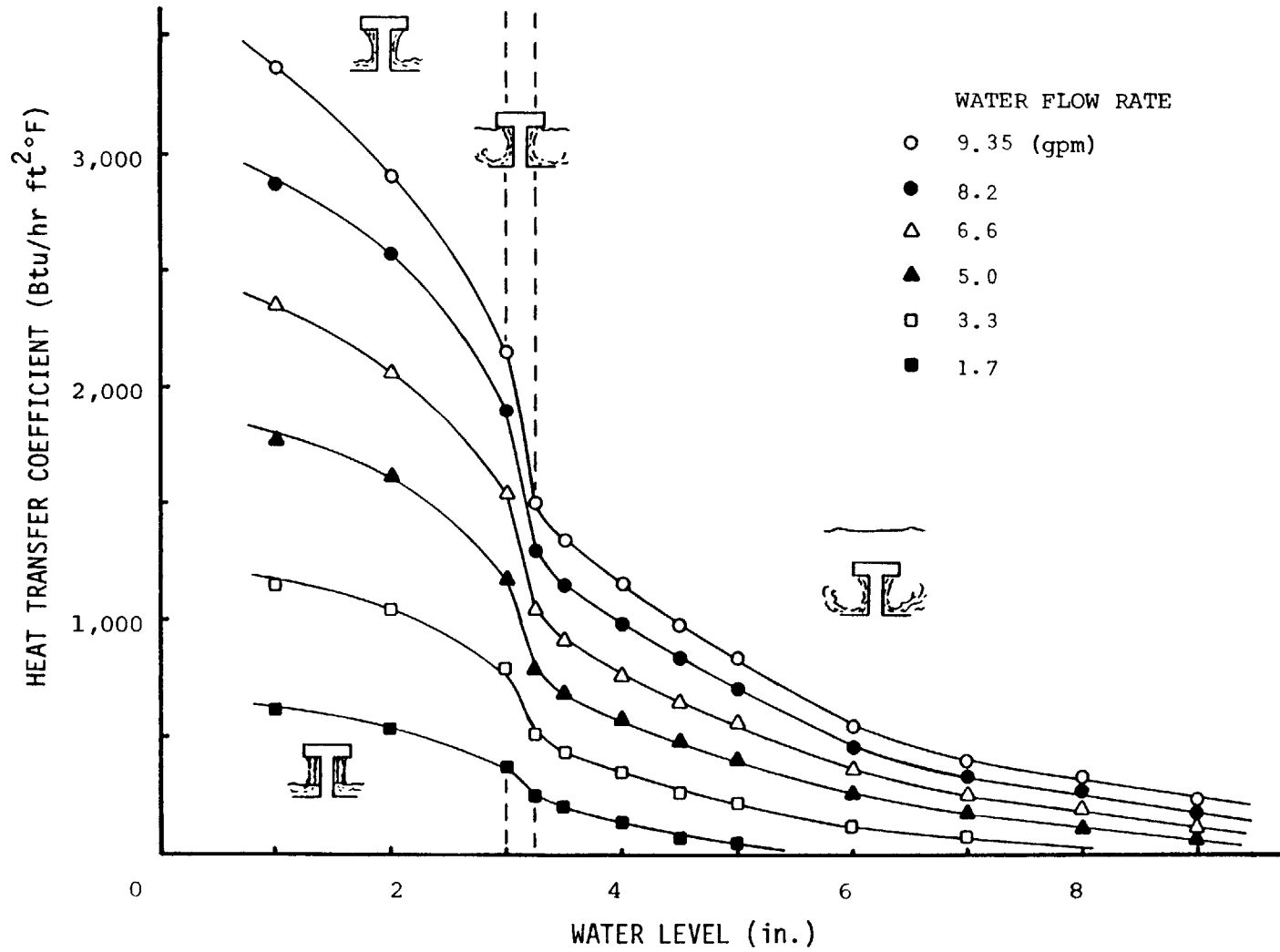
In Region 1, a decrease in h with increasing water level is observed. Especially, h appears to decrease rapidly with increasing water level in Region 2.

In Region 3, h decreases gradually with increasing water level. Furthermore, as water level increases, a linear decrease in h is observed, and finally, h approaches zero asymptotically. The trends in Region 3 is very similar to those of the TMI 2 sparger model and the Millstone 2



FLOW PATTERNS FOR ROWE YANKEE SPARGER MODEL (REGIONS 2 & 3)

FIG. B.2



VARIATION OF HEAT TRANSFER COEFFICIENT WITH WATER LEVEL AND WATER FLOW RATE (ROWE YANKEE SPARGER MODEL)

FIG. B.3

sparger model.

B.3 Variation of Stanton Number with Reference Water Level

The measured heat transfer coefficient (h) is non-dimensionalized as a Stanton number (St).

$$St = \frac{h}{G c_p}$$

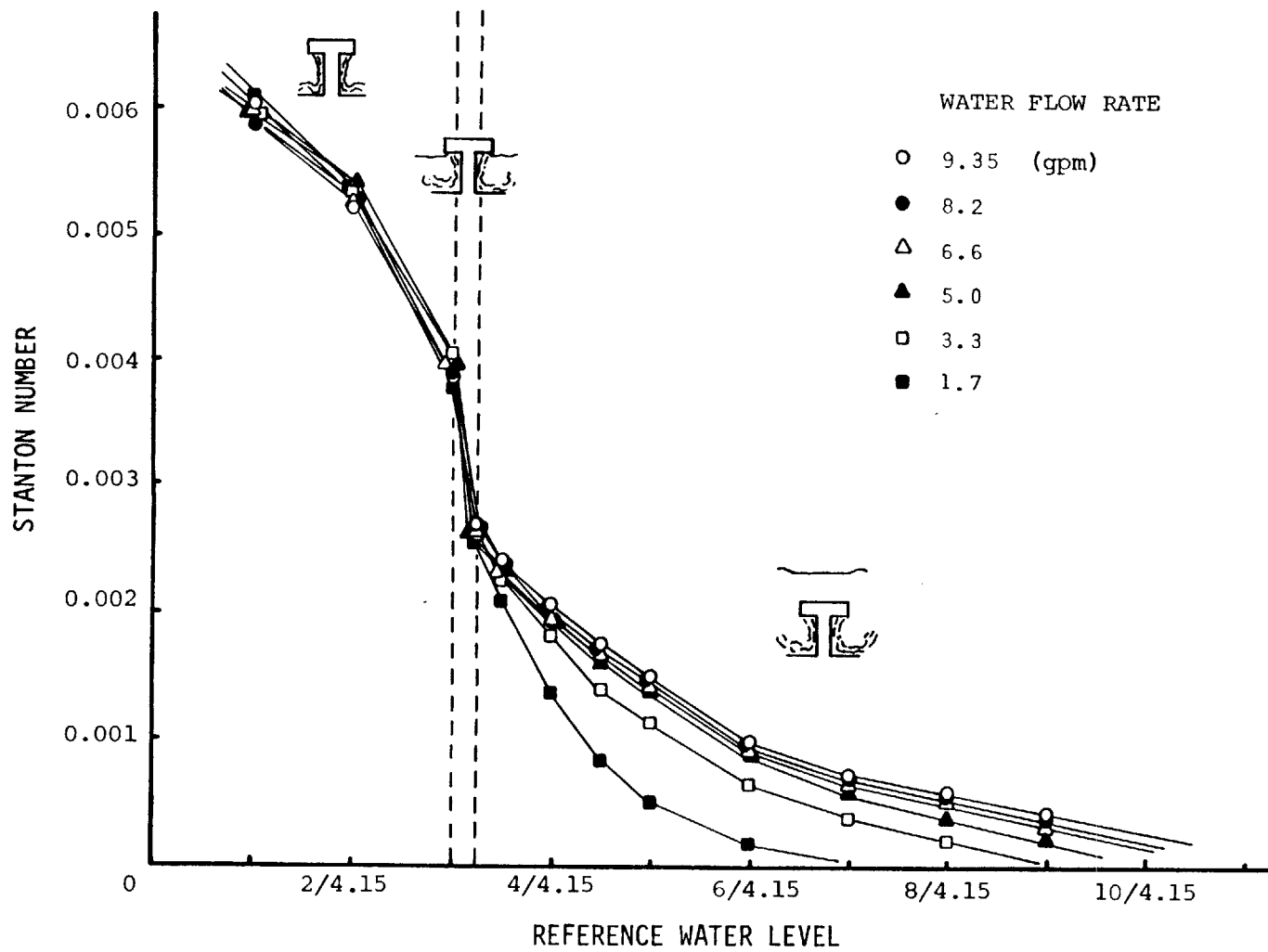
Here, mass velocity, G, is obtained as follows:

$$G = \frac{\dot{m}}{A}$$

where \dot{m} is the inlet water flow rate.

For the Rowe Yankee sparger model, the area A is defined by the total area of twenty holes on the under-side of the cylindrical cap. The water level (L) is non-dimensionalized as a reference water level (L/Z), where L is the water level and Z is the sparger height.

As shown in Fig. B.4, in Regions 1 and 2, the variation of Stanton number with reference water level coincides. In Region 3, as the reference water level increases, the St curves for the lower flow rates begin to deviate from the main St curve, and finally, approach zero. This trend of the St curve in Region 3 is similar to that for the TMI 2 sparger model and the Millstone 2 sparger model.

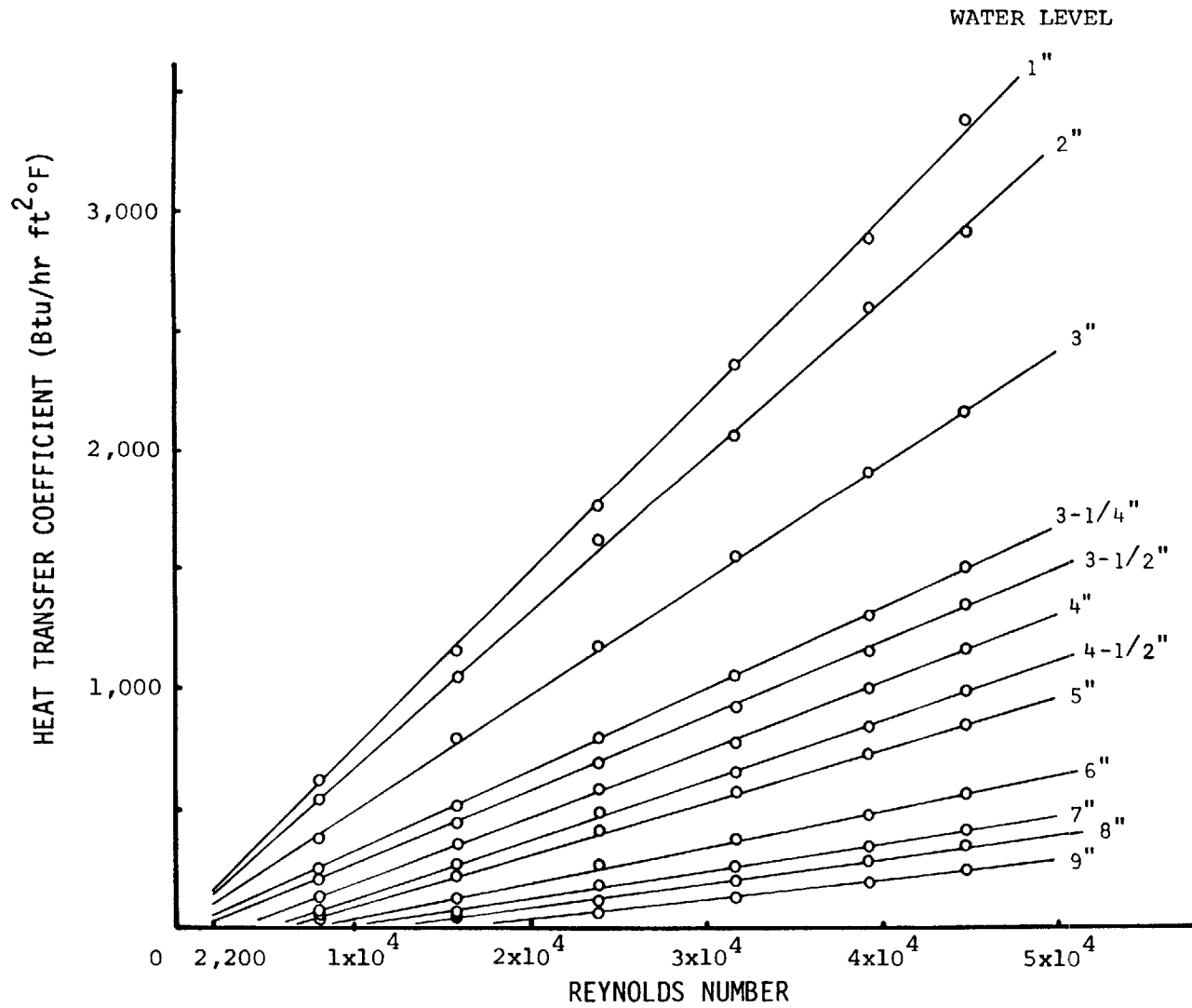


VARIATION OF STANTON NUMBER WITH REFERENCE WATER LEVEL AND WATER FLOW RATE (ROWE YANKEE SPARGER MODEL)

FIG. B.4

B.4 Variation of Heat Transfer Coefficient with Reynolds Number

Fig. B.5 shows the variation of heat transfer coefficient (h) with the Reynolds number (Re) in the inlet water pipe. A linear increase in the heat transfer coefficient with increasing Reynolds number is observed over all three regions. Fig. B.5 shows that the interface heat transfer coefficient is proportional to the first power of the inlet water velocity.



VARIATION OF HEAT TRANSFER COEFFICIENT WITH REYNOLDS NUMBER
(ROWE YANKEE SPARGER MODEL)

FIG. B.5

APPENDIX C

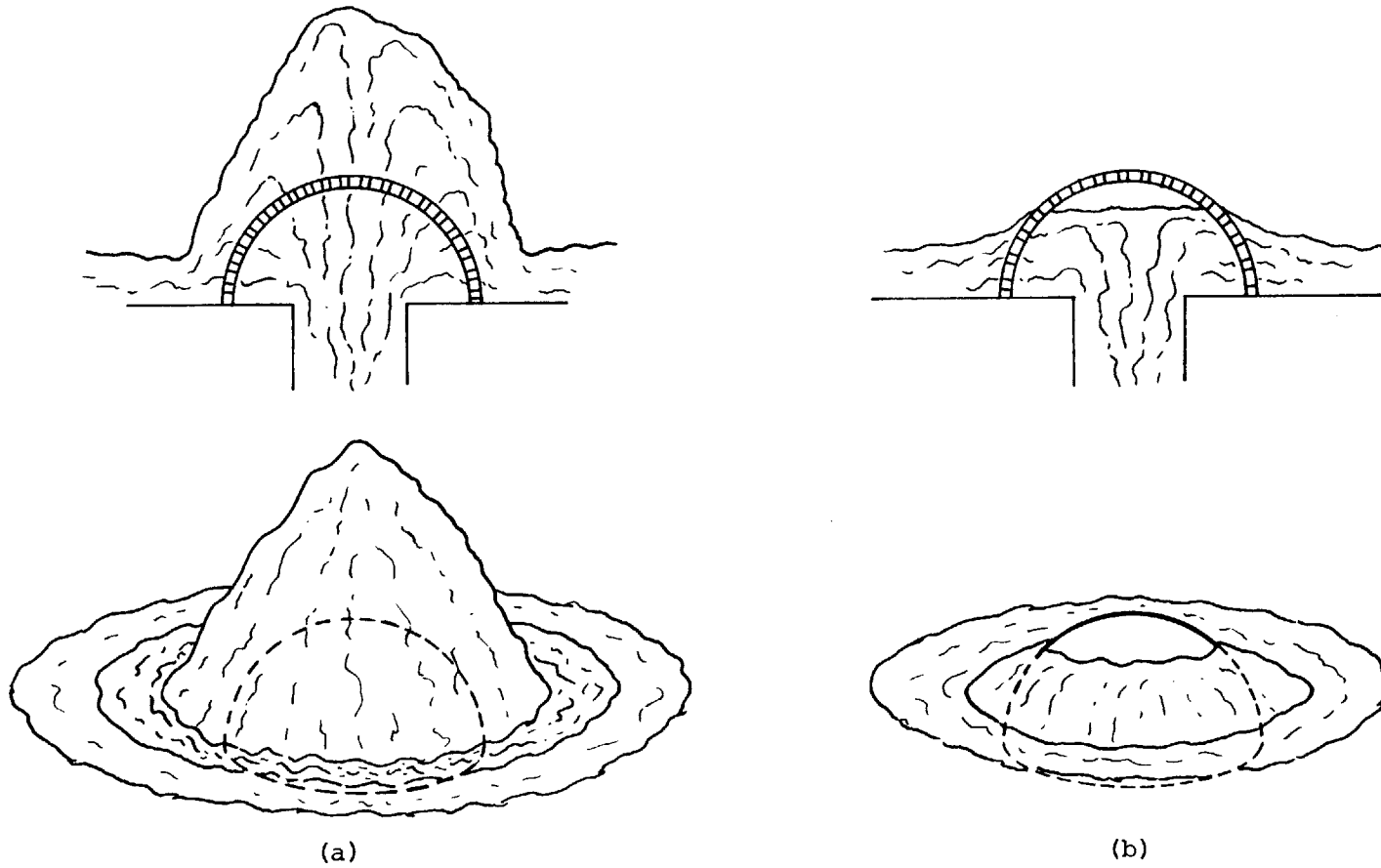
EXPERIMENTAL RESULTS FOR THE MILLSTONE 3 SPARGER MODEL

C.1 Flow Patterns

The model of the Millstone 3 sparger was connected to the 1.0 in. ID inlet water pipe, and the hemispherical bottom test vessel was used during the experiments. The inlet water flow rate was varied from 1.7 gpm to 9.35 gpm and the water level ranged from 0.75 in. to 9.0 in. The inlet water temperature was maintained at a temperature of 75.0° F.

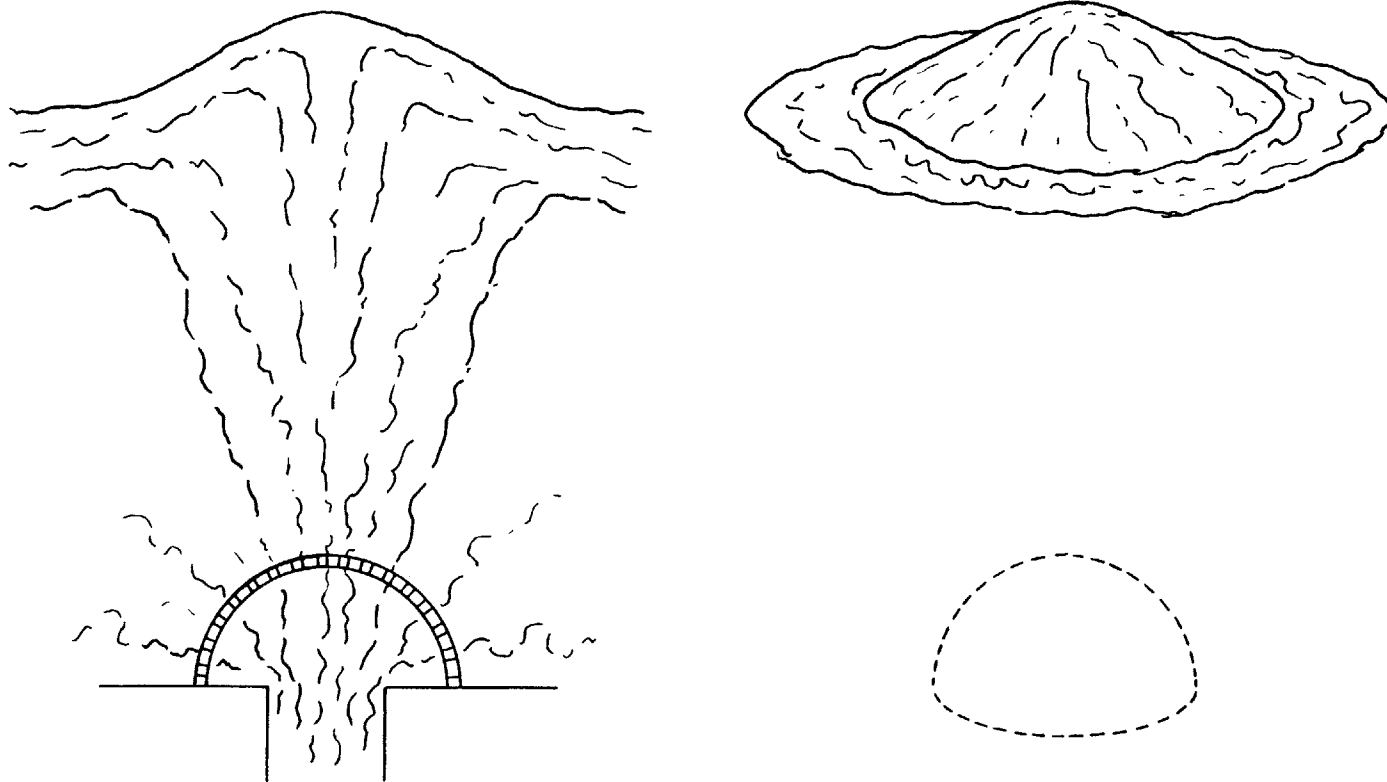
The observed flow pattern for the baffled water jets for flow rates greater than 2.0 gpm and water levels below the sparger height, 1.0 in., is shown in Fig. C.1 (a). For the same water level, but flow rates less than 2.0 gpm, the flow pattern is shown in Fig. C.1 (b). Water levels less than the sparger height, 1.0 in., are defined as Region 1.

Fig. C.2 shows the flow patterns for water levels greater than the sparger height. Water levels greater than the sparger height, 1.0 in., are defined as Region 2. As shown in Fig. C.2, since the injected direction of water jets for the Millstone 3 sparger model is upward, the water jets behave as if they are unbaffled. That is, due to little momentum dissipation by the sparger, the water jets easily reach the interface and the flow patterns do not change significantly as the water level increases.



FLOW PATTERNS FOR MILLSTONE 3 SPARGER MODEL (REGION 1)

FIG. C.1



FLOW PATTERNS FOR MILLSTONE 3 SPARGER MODEL (REGION 2)

FIG. C.2

C.2 Variation of Heat Transfer Coefficient with Water Level

The variation of heat transfer coefficient (h) with water level (L) and water flow rate is shown in Fig. C.3. In Region 1, the heat transfer coefficient decreases rapidly with increasing water level.

In Region 2, h continues to decrease rapidly up to 2.0 in. water level. However, for water levels between 2.0 in. and 9.0 in., h remains relatively constant and is much higher than that for the other sparger models. This results from little change in water jet's ability to break through the interface over this region.

Region 3, where stable stratification is normally observed, is expected above 9.0 in. water level. The design of the pool vessel restricted the maximum water level at which experiments could be performed to approximately 9.0 in.

C.3 Variation of Stanton Number with Reference Water Level

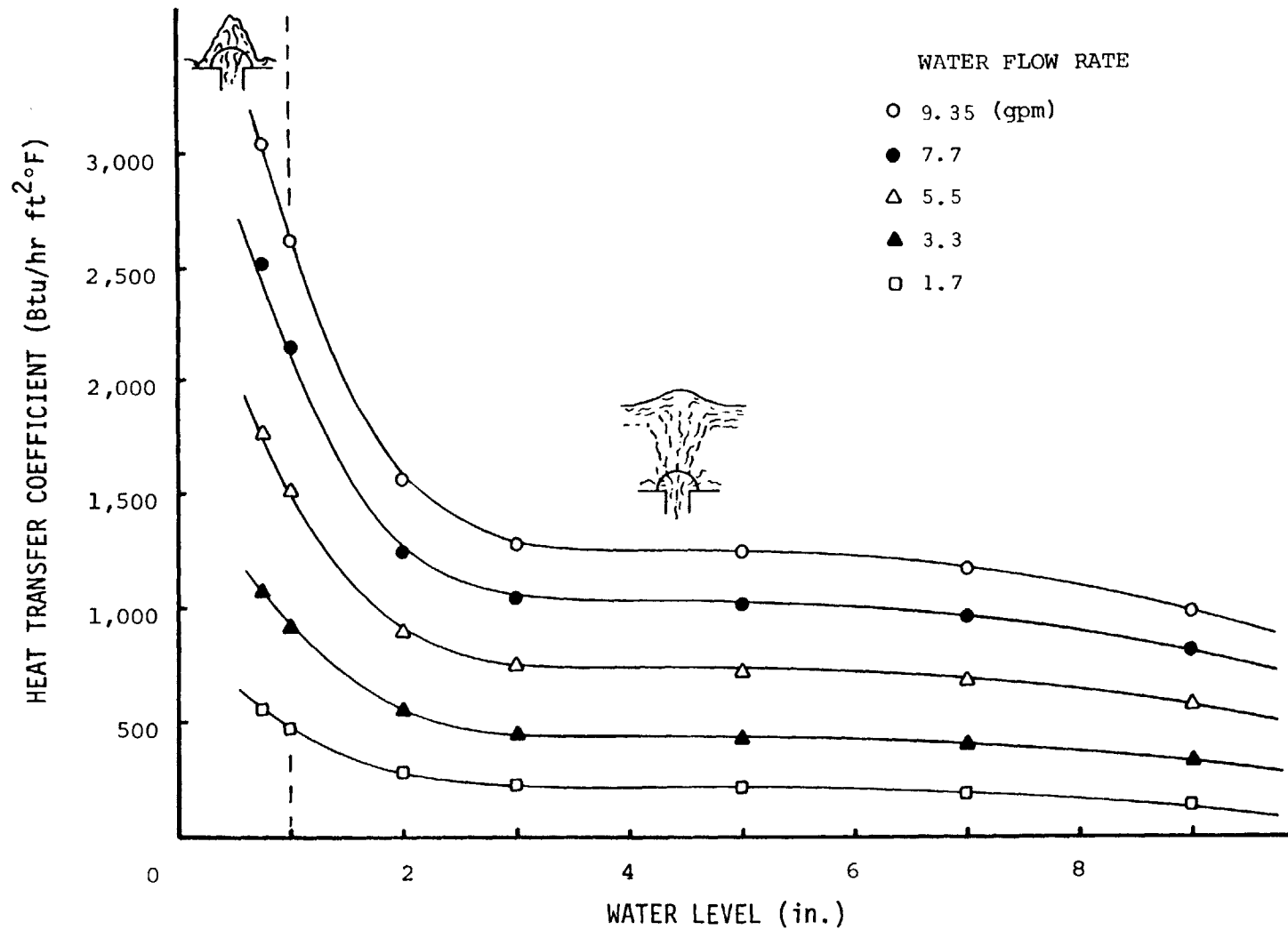
The measured heat transfer coefficient (h) is non-dimensionalized as a Stanton number (St).

$$St = \frac{h}{G c_p}$$

Here, mass velocity, G , is obtained as

$$G = \frac{\dot{m}}{A}$$

where \dot{m} denotes the inlet water flow rate. For the



VARIATION OF HEAT TRANSFER COEFFICIENT WITH WATER LEVEL AND WATER FLOW RATE (MILLSTONE 3 SPARGER MODEL)

FIG. C.3

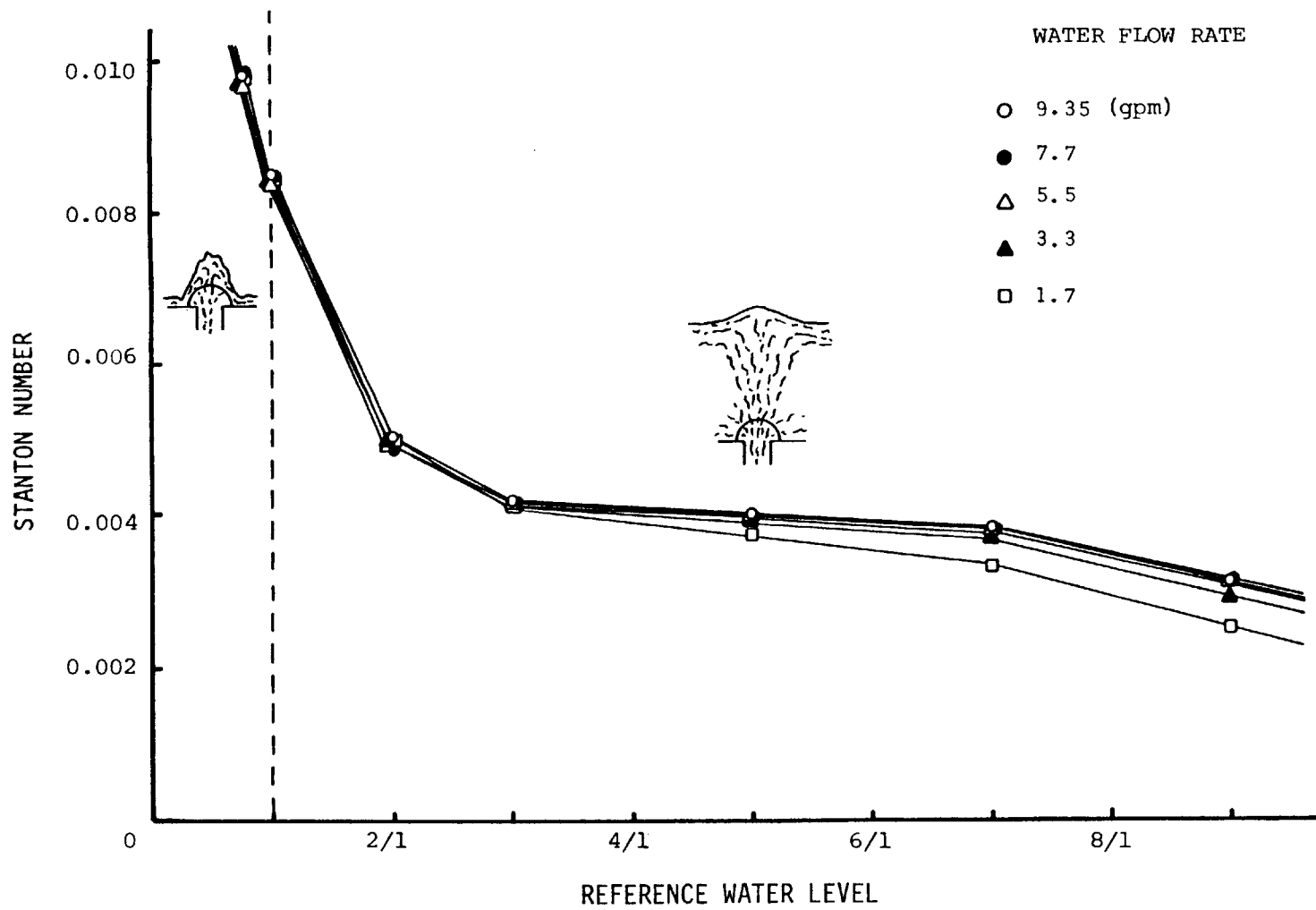
Millstone 3 sparger model, the area A is defined by the total area of four hundred and forty-eight tiny holes in the sparger. The water level is non-dimensionalized as a reference water level (L/Z). Here, L denotes the water level, and Z denotes the sparger height.

The variation of Stanton number (St) with a reference water level (L/Z) and water flow rates over the range of 1.7 gpm to 9.35 gpm is shown in Fig. C.4. Over all regions, the variation of Stanton number with reference water level, for all flow rates, coincides. The trend of the St curve in Region 2 is different than that for the other sparger models, due to the upward direction of the injected water jets; namely, the Stanton number does not decrease rapidly, but remains relatively constant over a significant range of reference water levels.

C.4 Variation of Heat Transfer Coefficient with Reynolds Number

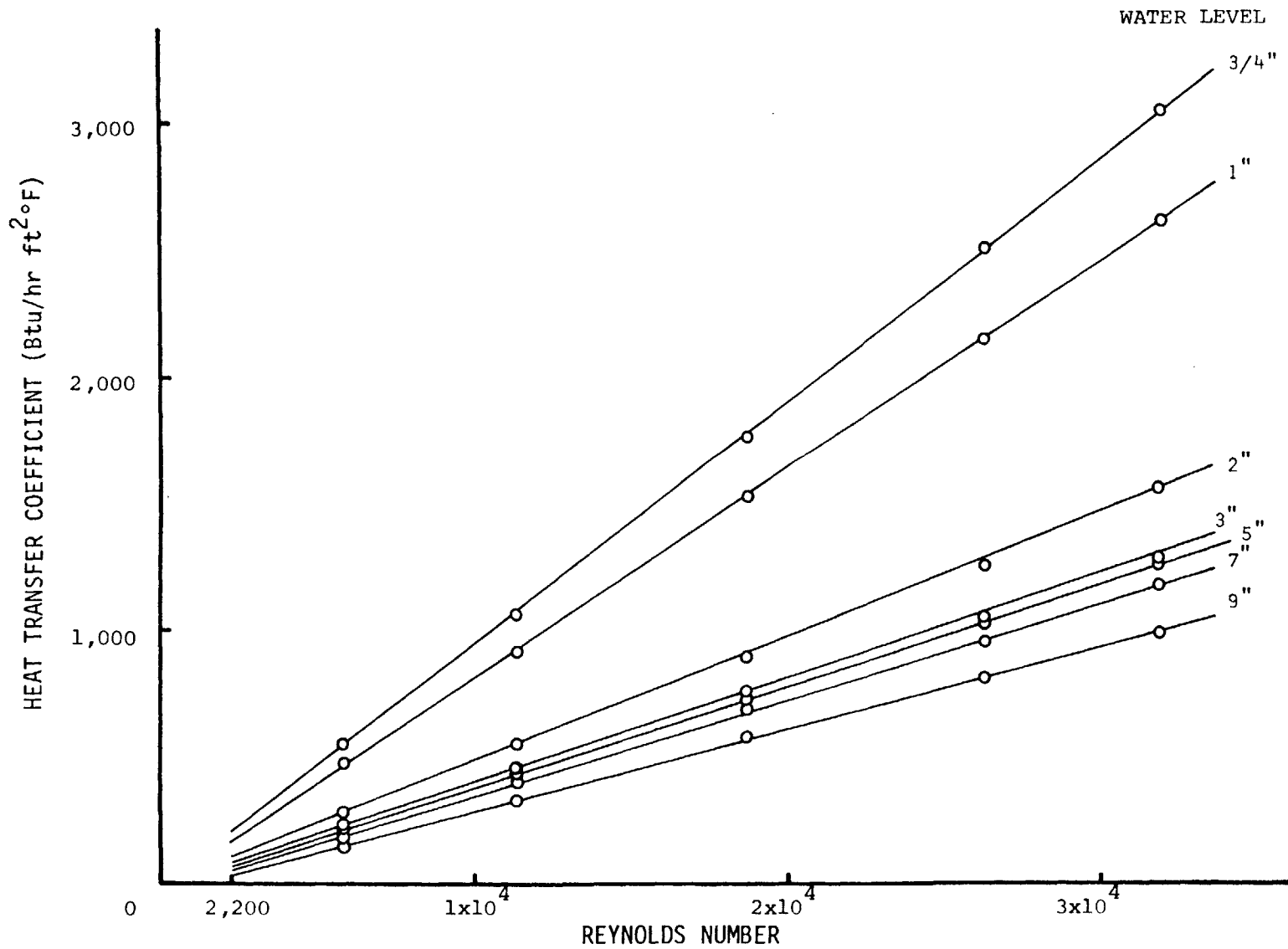
The variation of heat transfer coefficient (h) with the Reynolds number (Re) in the inlet water pipe is shown in Fig. C.5. The heat transfer coefficients increase linearly with increasing Reynolds number over all regions.

Based upon the experimentally determined heat transfer coefficients at the interface, it is concluded that the interface heat transfer coefficient is proportional to the first power of the velocity of the turbulent water jets in the inlet water pipe.



VARIATION OF STANTON NUMBER WITH REFERENCE WATER LEVEL
AND WATER FLOW RATE (MILLSTONE 3 SPARGER MODEL)

FIG. C.4



VARIATION OF HEAT TRANSFER COEFFICIENT WITH REYNOLDS NUMBER
(MILLSTONE 3 SPARGER MODEL)

FIG. C.5

APPENDIX D
SCALING LAWS

Based upon the Stanton number (St) versus reference water level (L/Z) diagrams for the Millstone 2 sparger model, the Rowe Yankee sparger model, and the Millstone 3 sparger model (Fig. A.4, B.4, and C.4), the simplified St vs. L/Z diagrams are obtained as shown in Fig. D.1, D.2, and D.3. Despite the slightly different St curves in Regions 1 and 2 in Fig. A.4, B.4, and C.4, these curves are collectively considered as one straight line.

The deviation of the St curves in Region 3, due to the stable stratification, is bounded by the two St curves shown in Fig. D.1 & D.2. In Tables II, III & IV, an empirical fit for the Stanton numbers for the three regions are expressed as a function of the reference water level (L/Z). For the Millstone 2 and Rowe Yankee sparger models, the deviation of the St curves in Region 3 for water flow rates over the range of 1.7 gpm to 9.35 gpm is modeled by a variable slope, m .

TABLE II

CORRELATION OF STANTON NUMBER AS A FUNCTION OF
REFERENCE WATER LEVEL (MILLSTONE 2 SPARGER MODEL)

Region 1 $(0 < \frac{L}{Z} \leq 1.0)$

$$St = St \left(\frac{L}{Z} \right) = -0.0027 \frac{L}{Z} + 0.0062$$

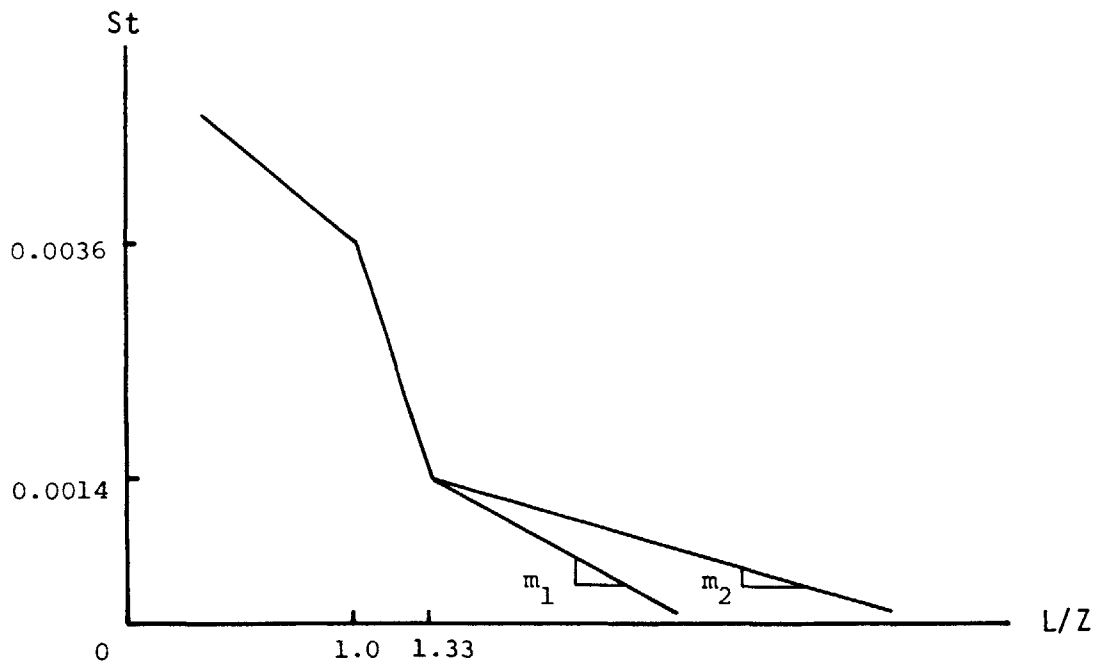
Region 2 $(1.0 \leq \frac{L}{Z} \leq 1.33)$

$$St = St \left(\frac{L}{Z} \right) = -0.0066 \frac{L}{Z} + 0.0102$$

Region 3 $(\frac{L}{Z} \geq 1.33)$

$$St = St \left(\frac{L}{Z} \right) = m \left(\frac{L}{Z} - 1.33 \right) + 0.0014$$

$$\text{where } -0.0014 \leq m \leq -0.00071$$



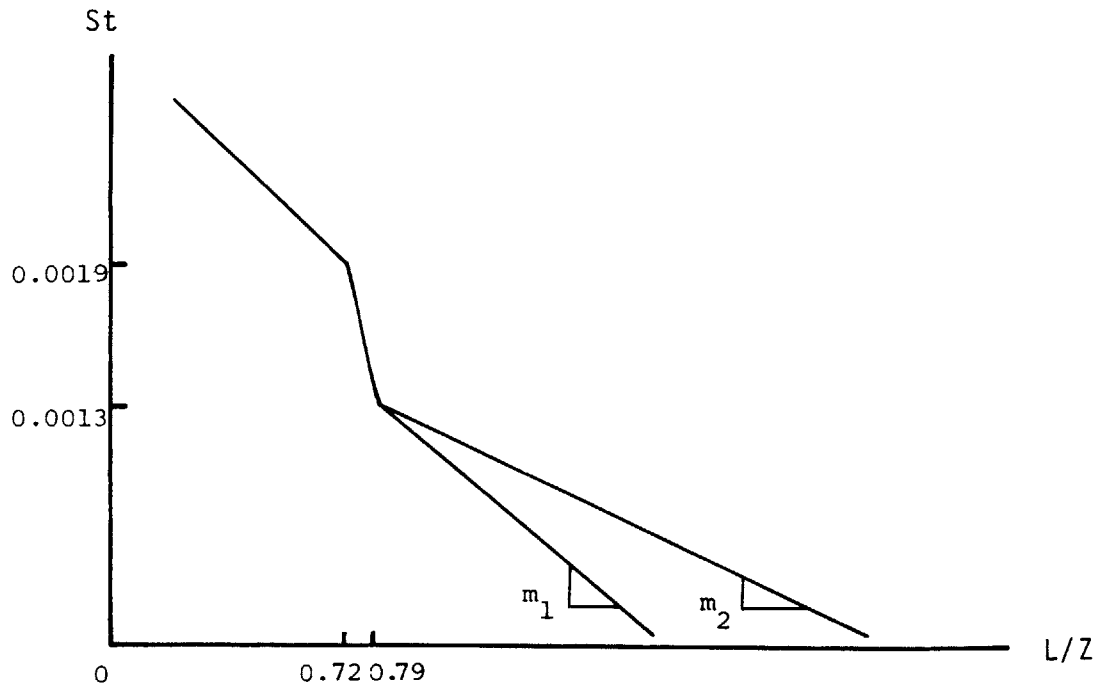
SIMPLIFIED St vs. L/Z DIAGRAM (MILLSTONE 2 SPARGER MODEL)

FIG. D.1

TABLE III

CORRELATION OF STANTON NUMBER AS A FUNCTION OF
REFERENCE WATER LEVEL (ROWE YANKEE SPARGER MODEL)

Region 1	$(0 < \frac{L}{Z} \leq 0.72)$
	$St = St(\frac{L}{Z}) = -0.0026 \frac{L}{Z} + 0.0038$
Region 2	$(0.72 \leq \frac{L}{Z} \leq 0.79)$
	$St = St(\frac{L}{Z}) = -0.0104 \frac{L}{Z} + 0.0095$
Region 3	$(\frac{L}{Z} \geq 0.79)$
	$St = St(\frac{L}{Z}) = m(\frac{L}{Z} - 0.79) + 0.00132$
	where $-0.0020 \leq m \leq -0.00079$



SIMPLIFIED St vs. L/Z DIAGRAM (ROWE YANKEE SPARGER MODEL)

FIG. D.2

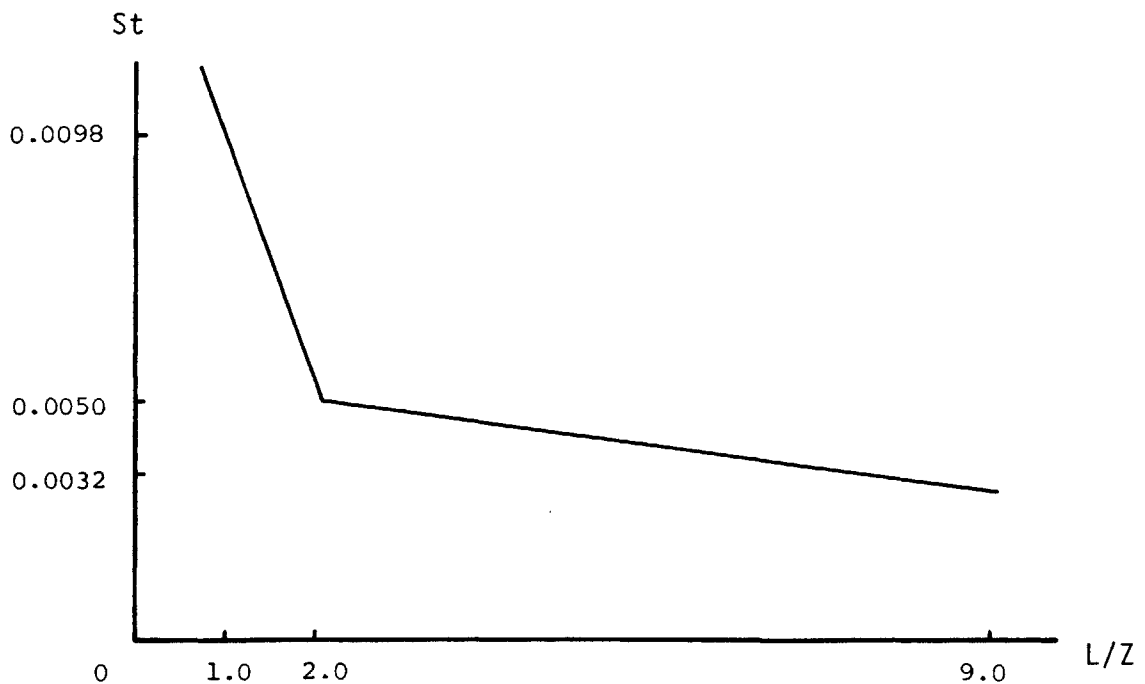
TABLE IV

CORRELATION OF STANTON NUMBER AS A FUNCTION OF
REFERENCE WATER LEVEL (MILLSTONE 3 SPARGER MODEL)

Region 1 $(0 < \frac{L}{Z} \leq 1.0)$
 $St = St(\frac{L}{Z}) = -0.0048 \frac{L}{Z} + 0.0146$

Region 2 $(1.0 \leq \frac{L}{Z} \leq 2.0)$
 $St = St(\frac{L}{Z}) = -0.0048 \frac{L}{Z} + 0.0146$

$(2.0 \leq \frac{L}{Z} \leq 9.0)$
 $St = St(\frac{L}{Z}) = -0.00026 \frac{L}{Z} + 0.0055$



SIMPLIFIED St vs. L/Z DIAGRAM (MILLSTONE 3 SPARGER MODEL)

FIG. D.3

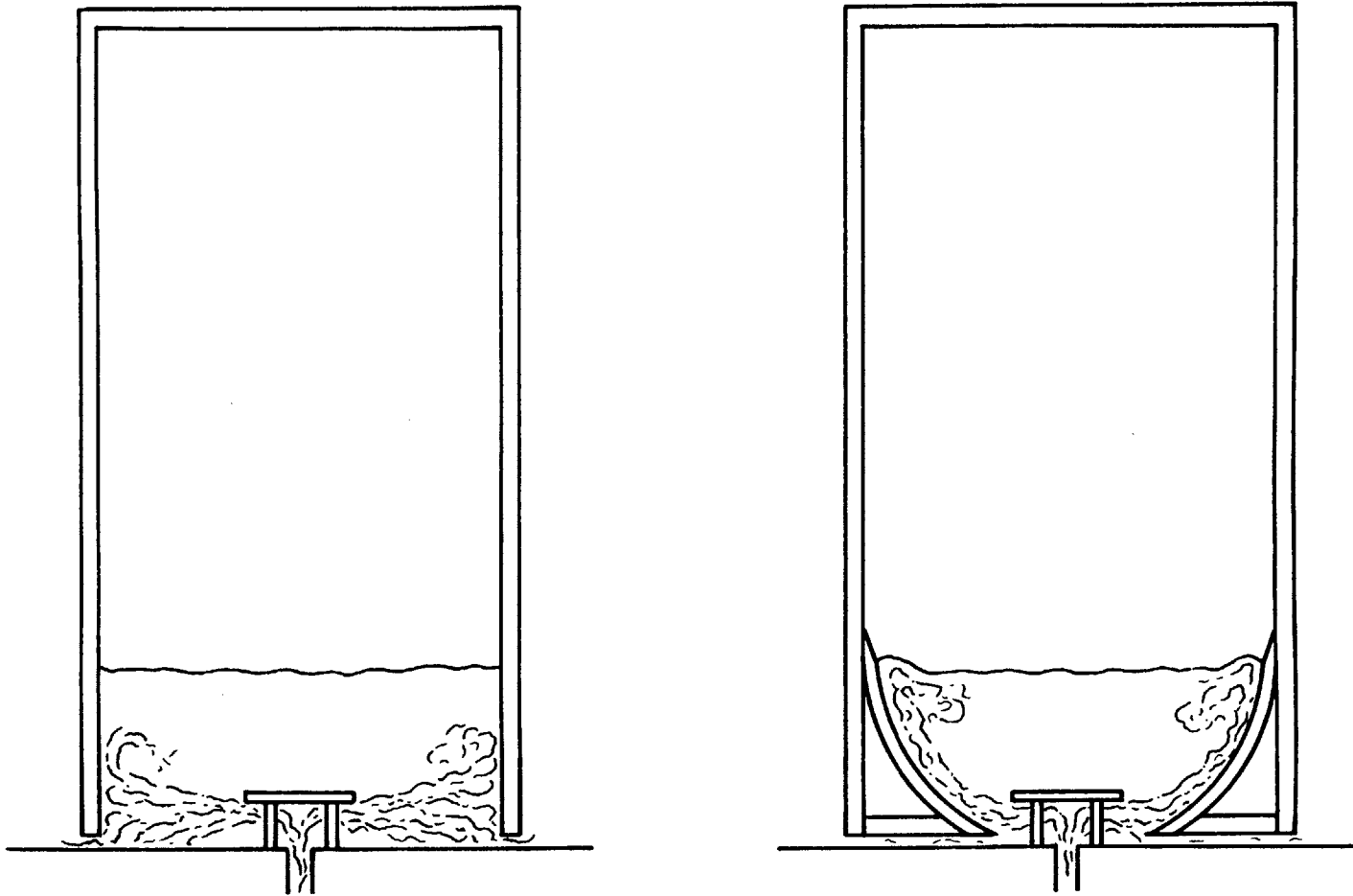
APPENDIX E

EXPERIMENTAL RESULTS FOR THE ROUND BOTTOM TEST VESSEL

Most of the experiments were performed by using the flat bottom test vessel. However, as shown in Appendix L, the actual pressurizer has a hemispherical bottom. Hence, the experiments with the round bottom test vessel were also performed, and the results for the round bottom vessel were compared with those for the flat bottom vessel.

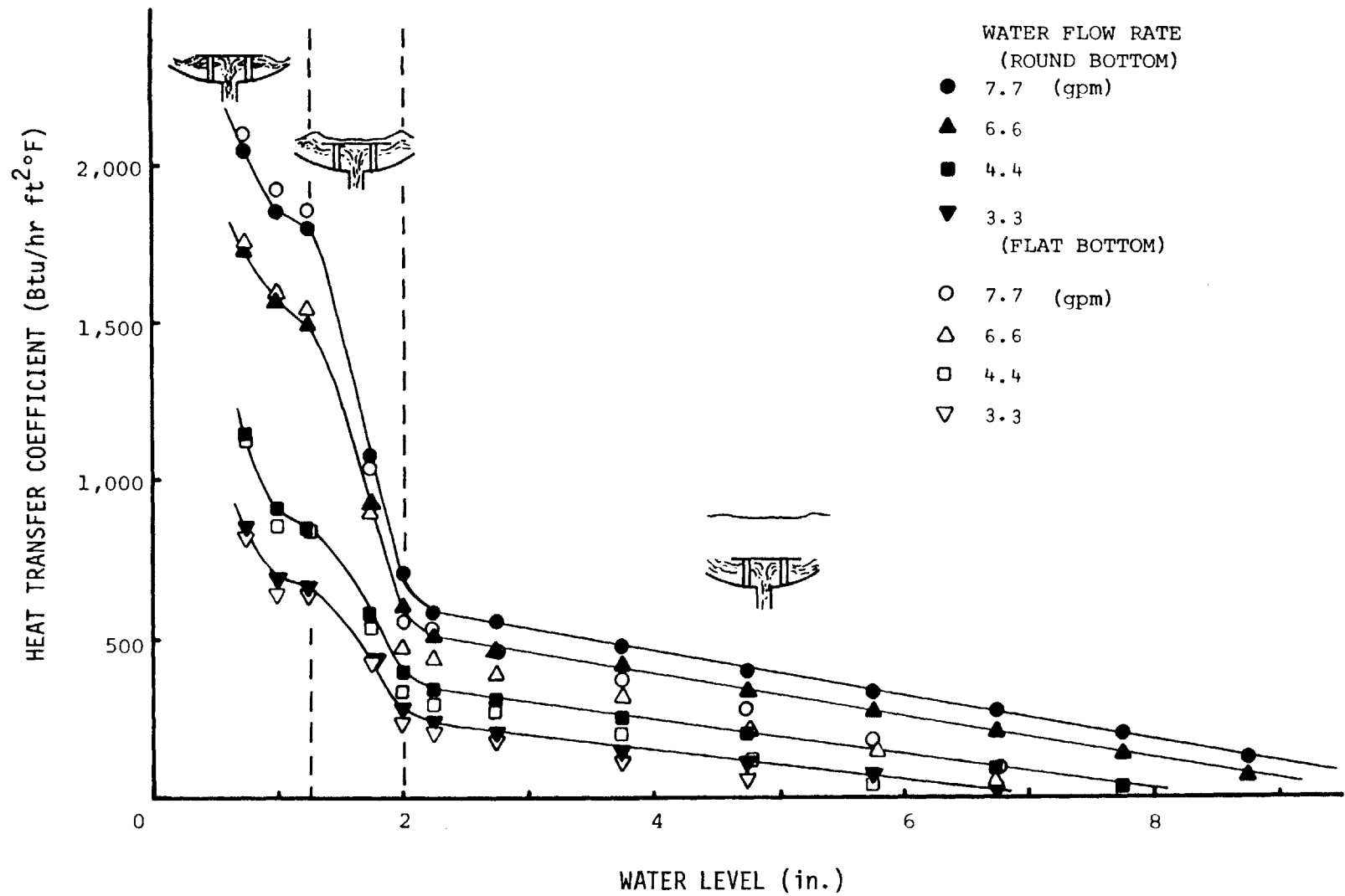
Flow patterns of baffled water jets for two different shaped vessels are shown in Fig. E.1. In the flat bottom test vessel, baffled water jets reach the side wall of the test vessel, and the momentum of water jets is dissipated. Accordingly, baffled water jets are difficult to reach the interface. However, in the round bottom test vessel, due to the smoothly curved bottom, baffled water jets climb along the round bottom, and reach the interface more easily. Hence, it is observed that the interface near the side wall is more agitated than that for the flat bottom vessel.

The variations of the heat transfer coefficients for two different test vessels with water level and water flow rate are shown in Fig. E.2. In Regions 1 and 2, the heat transfer coefficient for each test vessel appears to be the same. In Region 3, the heat transfer coefficient for the round bottom vessel is slightly higher than that for the flat bottom vessel. However, the absolute value of the heat



FLOW PATTERNS OF WATER JETS FOR DIFFERENT SHAPED VESSEL BOTTOMS

FIG. E.1



VARIATION OF HEAT TRANSFER COEFFICIENT WITH VESSEL BOTTOM GEOMETRY

FIG. E.2

transfer coefficient in Region 3 is comparatively smaller than that in Regions 1 and 2, and therefore, the small difference of the heat transfer coefficient in Region 3 is negligible. Hence, it is concluded that the results for the flat bottom vessel are similar to those for the round bottom vessel.

APPENDIX F
EFFECTS OF DIFFERENT SUBCOOLING

Most of the experiments were performed at a temperature of 75.0° F. In order to evaluate the effects of the different inlet water temperature on the interface heat transfer coefficients, the experiments with the flat bottom vessel were performed at a temperature of 150.0° F. The water flow rate varied from 4.4 gpm to 8.5 gpm.

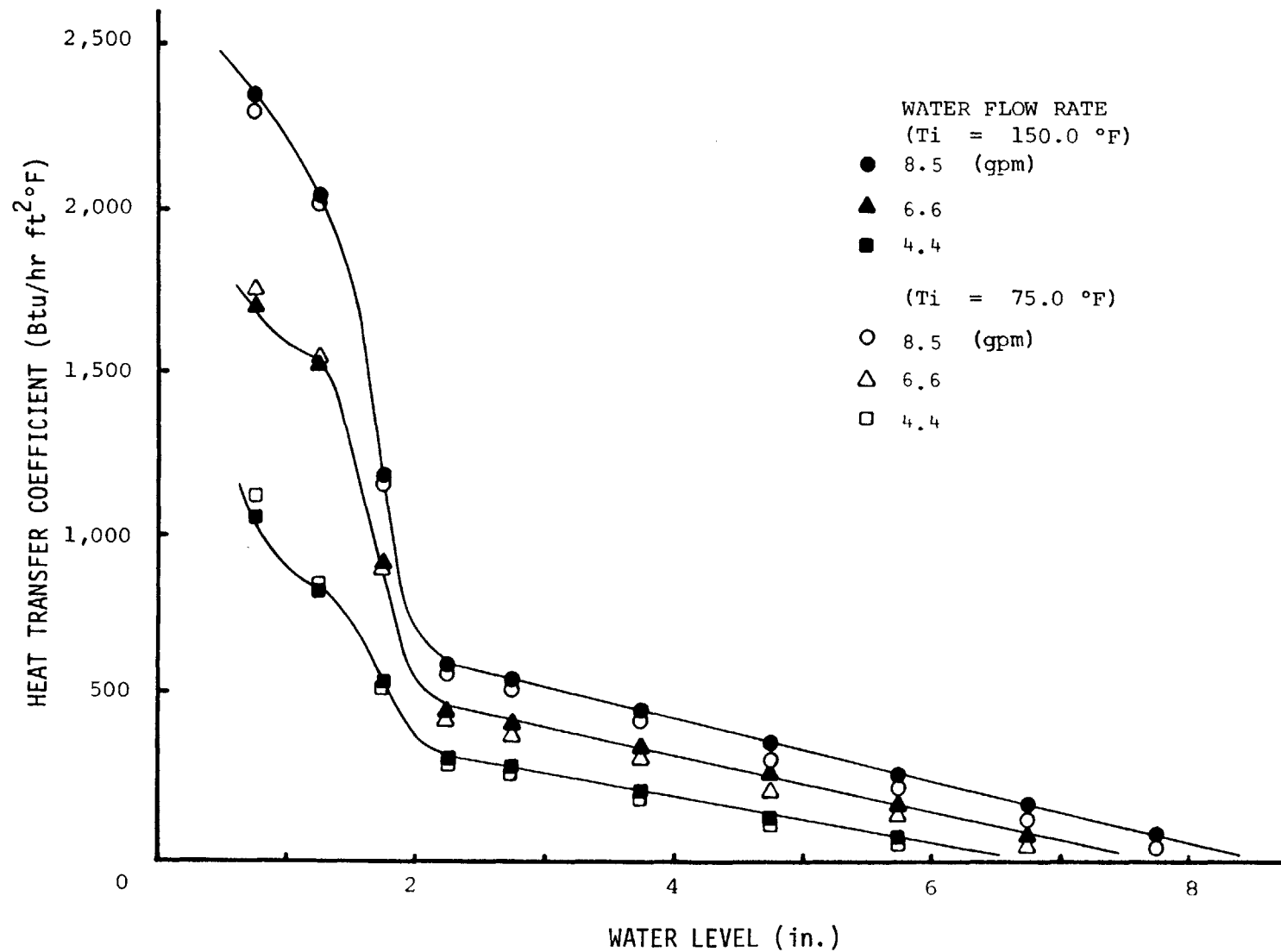
The heat transfer coefficients for the inlet water temperatures of 75.0° F and 150.0° F are plotted versus water level in Fig. F.1. In Regions 1 and 2, the heat transfer coefficients for each subcooling appear to be almost the same. However, in Region 3, the heat transfer coefficient for the inlet water temperature of 150.0° F is 3-15 % higher than that for 75.0° F. This can be explained by the change in the Richardson number with different subcooling. As subcooling decreases, the Richardson number tends to decrease, and the turbulence of baffled water jets is less suppressed by negative buoyancy forces. Accordingly, water jets would mix more easily with the upper water layer, and the interface heat transfer rate increases.

Based upon these results, the following conclusions are drawn:

- i) In Regions 1 and 2, there is little change in the heat transfer coefficient for different

subcooling.

- ii) In Region 3, as subcooling decreases, the interface heat transfer coefficient increases slightly.

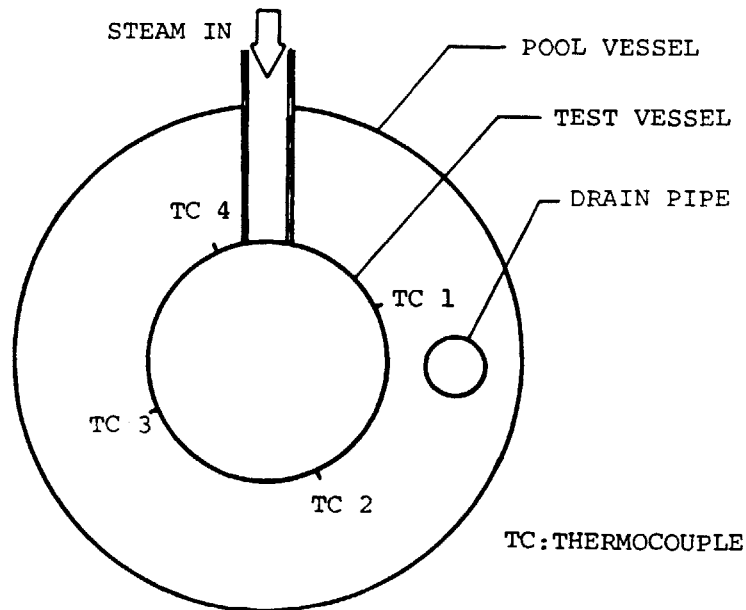


VARIATION OF HEAT TRANSFER COEFFICIENT WITH INLET WATER SUBCOOLING

FIG. F.1

APPENDIX G
 COMPARISON OF MEASURED OUTLET WATER TEMPERATURES
 FOR EACH THERMOCOUPLE LOCATION

In order to compare the uniformity of the outlet water temperature around the circumference of the test vessel, temperatures were measured at four different locations. The experiments were performed with the hemispherical bottom vessel and for an inlet water temperature of 74.0° F. The inlet water flow rate ranged from 1.7 gpm to 9.35 gpm and the water level ranged from 1.5 in. to 8.0 in. Fig. G.1 shows each thermocouple location around the test vessel. The outlet water temperatures for each thermocouple location are tabulated in Table XV.



CIRCUMFERENTIAL LOCATIONS OF THERMOCOUPLES

FIG. G.1

APPENDIX H
CALIBRATION OF WATER FLOW METER

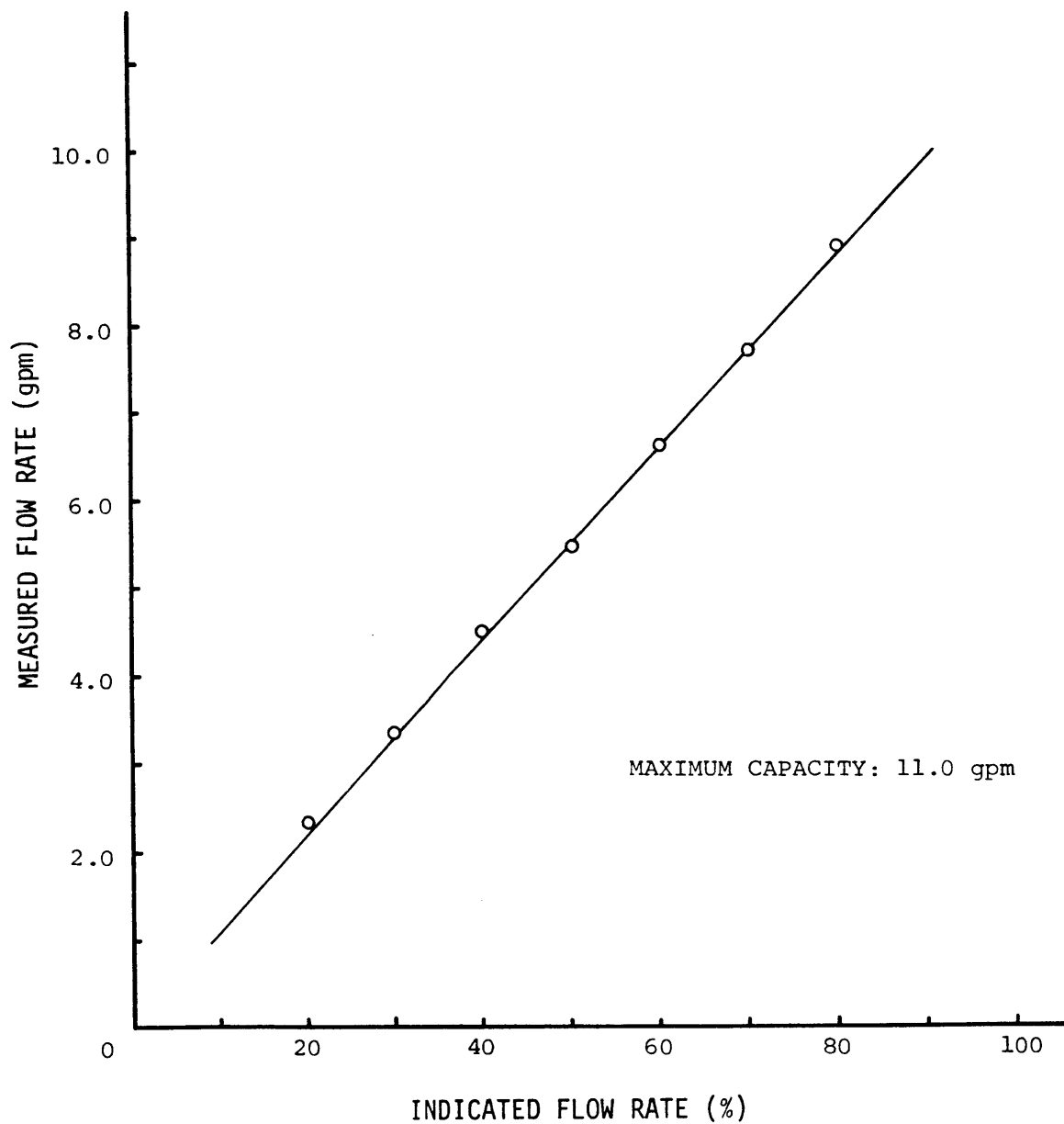


FIG. H.1

APPENDIX I

DATA TABLE

TABLE V

HEAT TRANSFER COEFFICIENT VS. WATER LEVEL AND WATER FLOW RATE
(TMI 2 SPARGER MODEL)

Water Level (in.) \ Water Flow Rate (gpm)	$\frac{3}{4}$	1	$1\frac{1}{4}$	$1\frac{1}{2}$	$1\frac{3}{4}$	2	$2\frac{1}{4}$	$2\frac{3}{4}$	$3\frac{1}{4}$	$3\frac{3}{4}$	$4\frac{1}{4}$
9.35	2560	2360	2210	2000	1270	650	620	575	525	480	430
8.5	2300	2140	2030	----	1150	---	570	520	---	430	---
7.7	2100	1930	1860	1600	1020	530	505	470	430	370	320
6.6	1760	1600	1550	----	890	---	435	390	---	320	---
5.5	1500	1145	1150	950	715	380	365	330	285	255	205
4.4	1120	860	850	---	540	---	300	275	---	195	---
3.3	820	640	645	550	440	235	215	185	140	110	75
2.2	570	422	420	370	280	150	140	110	70	45	30

(h: Btu/hr ft²°F)

Water Level (in.)	$4\frac{3}{4}$	$5\frac{1}{4}$	$5\frac{3}{4}$	$6\frac{1}{4}$	$6\frac{3}{4}$	$7\frac{1}{4}$	$7\frac{3}{4}$
Water Flow Rate (gpm)							
9.35	370	320	260	210	170	120	70
8.5	320	---	225	---	135	---	45
7.7	265	230	180	130	100	50	0
6.6	220	---	145	---	50	0	0
5.5	160	120	85	45	0	0	0
4.4	115	---	50	0	0	0	0
3.3	45	15	0	0	0	0	0
2.2	10	0	0	0	0	0	0

(h: Btu/hr ft²°F)

TABLE VI

STANTON NUMBER VS. REFERENCE WATER LEVEL AND WATER FLOW RATE
(TMI 2 SPARGER MODEL) (St x 10⁴)

Water Level (in.) $\frac{3}{4}$	1	$1\frac{1}{4}$	$1\frac{1}{2}$	$1\frac{3}{4}$	2	$2\frac{1}{4}$	$2\frac{3}{4}$	$3\frac{1}{4}$	$3\frac{3}{4}$	$4\frac{1}{4}$	
Water Flow Rate (gpm)											
9.35	449	414	388	351	217	114	109	101	92	84	75
8.5	444	413	392	---	222	---	110	100	--	83	--
7.7	447	411	396	341	217	113	107	100	91	79	68
6.6	437	398	385	---	221	---	109	97	--	80	--
5.5	447	341	343	283	213	113	109	98	85	75	61
4.4	418	321	317	---	200	---	112	102	--	72	--
3.3	408	318	320	273	219	117	107	92	69	54	37
2.2	425	315	313	277	209	112	104	82	52	33	22

Water Level (in.)	(St x 10 ⁴)						
	4 $\frac{3}{4}$	5 $\frac{1}{4}$	5 $\frac{3}{4}$	6 $\frac{1}{4}$	6 $\frac{3}{4}$	7 $\frac{1}{4}$	7 $\frac{3}{4}$
9.35	65	56	46	37	30	21	12
8.5	62	--	43	--	26	--	8
7.7	56	49	38	28	21	10	0
6.6	54	--	36	--	12	0	0
5.5	48	36	24	13	0	0	0
4.4	43	--	18	0	0	0	0
3.3	22	8	0	0	0	0	0
2.2	5	0	0	0	0	0	0

TABLE VII

HEAT TRANSFER COEFFICIENT VS. WATER LEVEL AND WATER FLOW RATE
(MILLSTONE 2 SPARGER MODEL)

Water Level (in.)	$\frac{3}{4}$	$1\frac{1}{2}$	$2\frac{1}{4}$	$2\frac{3}{4}$	$3\frac{1}{4}$	$3\frac{3}{4}$	4	$4\frac{1}{2}$	5	6	7	8
Water Flow Rate (gpm)												
9.35	2375	1960	1780	1640	1265	930	580	510	465	370	280	180
8.5	2170	1750	1600	1470	1070	825	500	450	410	320	230	145
7.7	1950	1570	1410	1310	935	745	455	410	370	290	205	115
6.6	1565	1250	1100	1025	800	645	400	355	320	240	150	65
4.4	1040	825	700	640	570	460	245	220	200	135	80	0
2.2	525	420	360	330	295	205	120	100	75	35	0	0

(h: Btu/hr ft²°F)

TABLE VIII

STANTON NUMBER VS. REFERENCE WATER LEVEL AND WATER FLOW RATE
 (MILLSTONE 2 SPARGER MODEL) (St x 10⁵)

Water Level (in.)	$\frac{3}{4}$	$1\frac{1}{2}$	$2\frac{1}{4}$	$2\frac{3}{4}$	$3\frac{1}{4}$	$3\frac{3}{4}$	4	$4\frac{1}{2}$	5	6	7	8
9.35	600	495	450	415	320	235	146	129	117	93	70	45
8.5	604	486	444	408	297	229	139	125	114	89	64	40
7.7	598	482	433	402	287	228	139	126	113	89	63	35
6.6	560	447	393	367	286	231	143	127	114	86	53	23
4.4	558	443	376	343	306	247	131	118	107	72	43	0
2.2	564	451	386	354	317	221	129	109	82	40	0	0

TABLE IX

HEAT TRANSFER COEFFICIENT VS. WATER LEVEL AND WATER FLOW RATE
(ROWE YANKEE SPARGER MODEL)

Water Level (in.)	1	2	3	$3\frac{1}{4}$	$3\frac{1}{2}$	4	$4\frac{1}{2}$	5	6	7	8	9
9.35	3370	2910	2160	1500	1345	1157	980	845	557	410	340	242
8.2	2880	2585	1900	1295	1150	990	840	720	470	345	277	192
6.6	2355	2065	1550	1050	920	770	655	568	375	267	202	127
5.0	1770	1612	1175	795	695	580	490	410	270	180	120	69
3.3	1160	1050	797	520	445	360	275	223	131	78	45	0
1.7	621	546	380	260	212	140	85	53	20	0	0	0

(h: Btu/hr ft²°F)

TABLE X

STANTON NUMBER VS. REFERENCE WATER LEVEL AND WATER FLOW RATE
 (ROWE YANKEE SPARGER MODEL) (St x 10⁵)

Water Level (in.)	1	2	3	3 $\frac{1}{4}$	3 $\frac{1}{2}$	4	4 $\frac{1}{2}$	5	6	7	8	9
Water Flow Rate (gpm)												
9.35	303	262	194	135	121	104	88	76	50	37	30	22
8.2	295	265	195	133	118	101	86	74	48	35	28	19
6.6	300	263	197	134	117	98	83	72	48	34	26	16
5.0	298	271	197	134	117	97	82	69	45	30	20	11
3.3	296	268	203	132	113	92	70	57	33	20	11	0
1.7	307	270	188	128	105	69	42	26	10	0	0	0

TABLE XI
HEAT TRANSFER COEFFICIENT VS. WATER LEVEL AND WATER FLOW RATE
(MILLSTONE 3 SPARGER MODEL)

Water Level (in.)	$\frac{3}{4}$	1	2	3	5	7	9
9.35	3042	2620	1560	1281	1240	1172	980
7.7	2513	2150	1243	1044	1011	957	810
5.5	1760	1514	893	750	720	680	574
3.3	1069	914	547	448	426	400	326
1.7	553	474	282	230	211	186	140

(h: Btu/hr ft²°F)

TABLE XII

STANTON NUMBER VS. REFERENCE WATER LEVEL AND WATER FLOW RATE
(MILLSTONE 3 SPARGER MODEL) (St x 10⁵)

Water Level (in.)	$\frac{3}{4}$	1	2	3	5	7	9
9.35	981	845	503	413	400	378	316
7.7	984	842	487	409	396	374	317
5.5	965	830	490	411	395	373	315
3.3	976	835	500	409	389	366	298
1.7	980	840	500	407	375	330	248

TABLE XIII

HEAT TRANSFER COEFFICIENTS FOR ROUND AND FLAT BOTTOM VESSELS
(TMI 2 SPARGER MODEL)

Water Level (in.)		Water Flow Rate (gpm)									
		$\frac{3}{4}$	1	$1\frac{1}{4}$	$1\frac{3}{4}$	2	$2\frac{1}{4}$	$2\frac{3}{4}$	$3\frac{3}{4}$	$4\frac{3}{4}$	$5\frac{3}{4}$
7.7	Round Bottom	2050	1860	1800	1080	705	585	560	475	400	330
	Flat Bottom	2100	1930	1860	1020	530	505	470	370	265	180
6.6	Round Bottom	1730	1580	1500	930	605	510	465	420	340	275
	Flat Bottom	1760	1600	1550	890	---	435	390	320	220	145
4.4	Round Bottom	1150	915	855	580	400	345	310	255	205	145
	Flat Bottom	1120	860	850	540	---	300	275	195	115	50
3.3	Round Bottom	850	695	670	450	280	240	205	145	110	65
	Flat Bottom	820	640	645	440	235	215	185	110	45	0

(h: Btu/hr ft²°F)

TABLE XIV

HEAT TRANSFER COEFFICIENTS FOR DIFFERENT INLET WATER SUBCOOLING
(TMI 2 SPARGER MODEL)

Water Level (in.)		$\frac{3}{4}$	$1\frac{1}{4}$	$1\frac{3}{4}$	$2\frac{1}{4}$	$2\frac{3}{4}$	$3\frac{3}{4}$	$4\frac{3}{4}$	$5\frac{3}{4}$	$6\frac{3}{4}$	$7\frac{3}{4}$
Water Flow Rate (gpm)											
	8.5	150°F	2350	2050	1180	595	560	470	365	270	180
75°F		2300	2030	1150	570	520	430	320	225	135	45
6.6	150°F	1700	1530	910	455	425	355	270	185	75	0
	75°F	1760	1550	890	435	390	320	220	145	50	0
4.4	150°F	1050	830	555	310	295	220	135	70	0	0
	75°F	1120	860	540	300	275	195	115	50	0	0

(h: Btu/hr ft²°F)

Water Level (in.)	$6\frac{3}{4}$	$7\frac{3}{4}$	$8\frac{3}{4}$
Water Flow Rate (gpm)			
7.7 Round Bottom	270	200	125
Flat Bottom	100	10	0
6.6 Round Bottom	205	140	75
Flat Bottom	50	0	0
4.4 Round Bottom	90	35	0
Flat Bottom	0	0	0
3.3 Round Bottom	20	0	0
Flat Bottom	0	0	0

(h: Btu/hr ft²°F)

TABLE XV
CIRCUMFERENTIAL VARIATION OF OUTLET WATER TEMPERATURES

Water Level (in.)	Thermocouple Location		TC 1	TC 2	TC 3	TC 4
	Water Flow Rate (gpm)					
1.5	9.35		79.4	80.9	80.5	79.6
	6.6		78.5	80.3	80.0	78.7
	4.4		78.3	80.0	80.7	79.4
	1.7		81.0	81.7	82.0	81.6
4.0	9.35		82.1	81.7	80.7	81.3
	6.6		81.8	81.1	80.7	81.2
	4.4		80.0	80.0	79.7	80.1
	1.7		76.2	76.1	76.0	76.1
8.0	9.35		79.0	79.1	78.9	79.1
	6.6		77.7	77.5	77.3	77.5
	4.4		76.2	76.1	76.0	76.1
	1.7		75.5	75.5	75.3	75.4

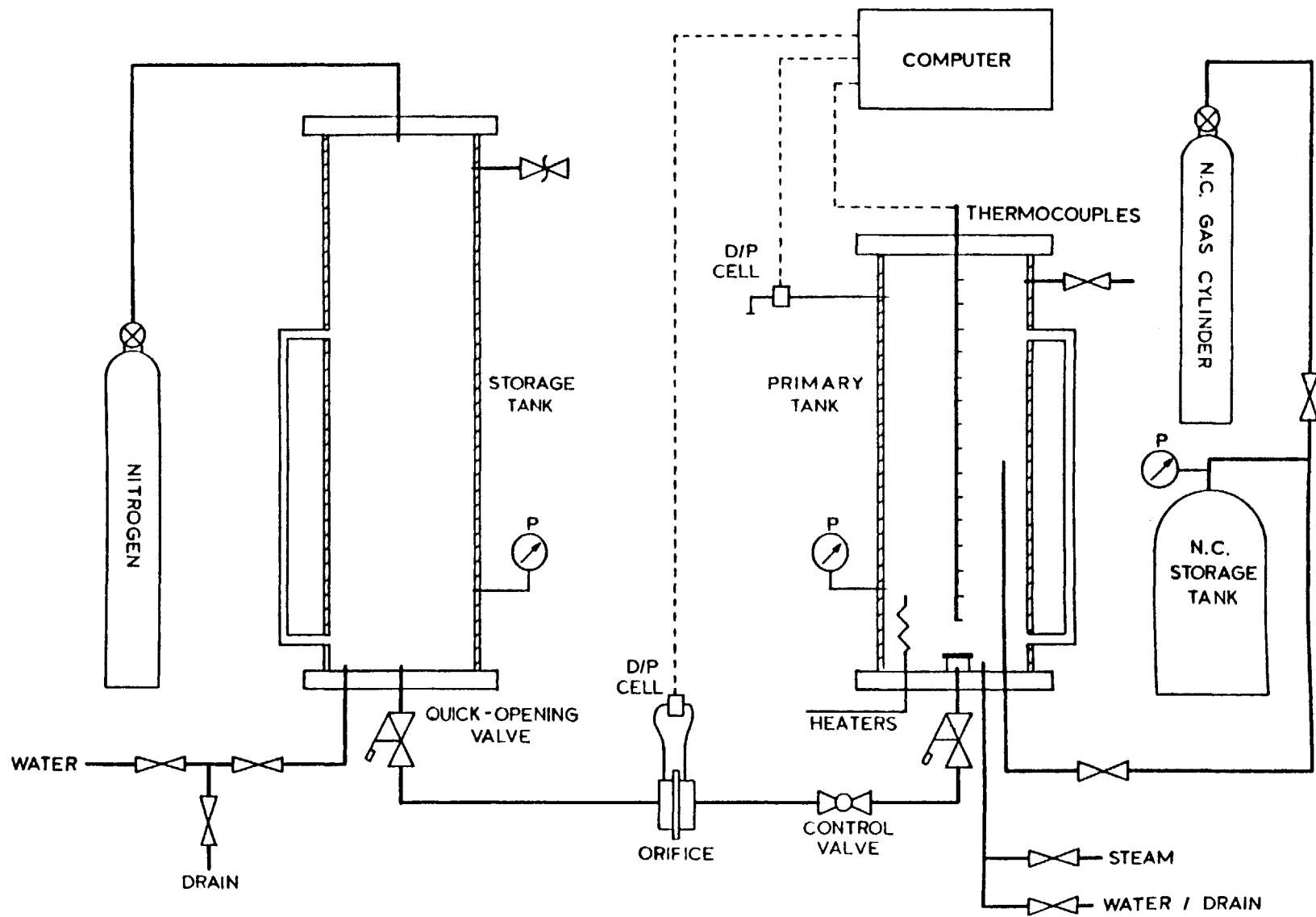
(Temperature: °F)

** Inlet Water Temperature = 74.0 °F

APPENDIX J
DESCRIPTION OF A SCALED PRESSURIZER APPARATUS
AND EXPERIMENTAL PROCEDURES

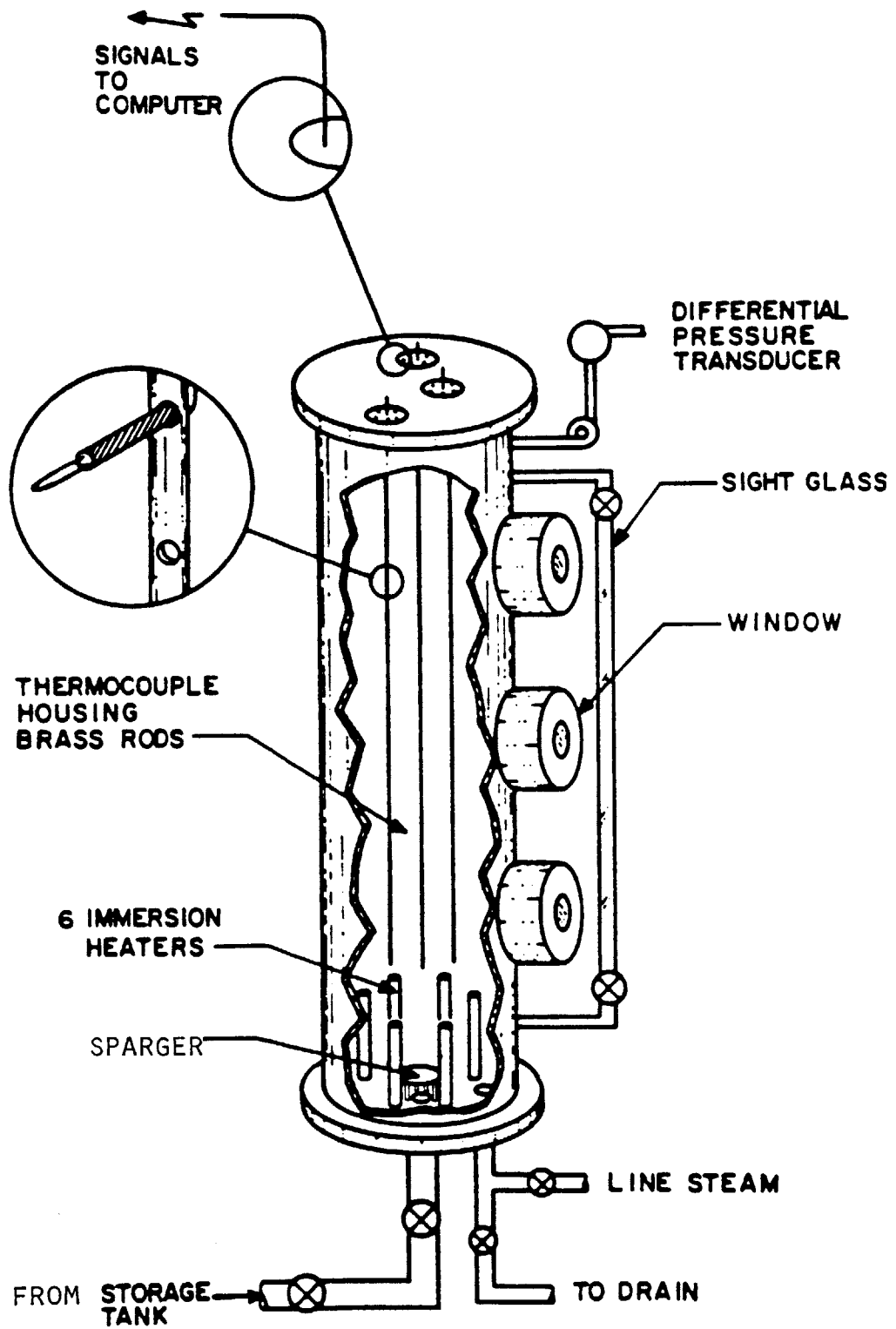
Fig. J.1 & J.2 show Kim's [2] experimental apparatus. The system consists of two stainless steel tanks, an insurge line with flow control, service lines, a gas injection system and a data acquisition system. One of the steel tanks (primary tank) models the pressurizer volume and the other (storage tank) serves as a reservoir for cold injection water.

The primary tank is instrumented with thermocouples along the full length of the center of the fluid volume, a visual pressure gage, and a pressure transducer. Along with a pressure transducer in the surge line (measuring flow rate), the pressure and temperature signals from the primary tank are scanned and recorded by a microcomputer. The primary tank is 8.0 in. ID, 45.0 in. in height, and 1/3 in. thick. It is insulated to keep heat loss at a minimum, and equipped with an external gage glass to accurately measure the initial liquid level. The primary tank is also equipped with immersion heaters capable of approximately 9.0 Kw total power. The sparger at the inlet pipe of the primary tank is made of a 3.0 in. diameter and 1/8 in. thick stainless steel disk, and welded to the bottom flange by four legs, 1-1/4" x 1/8" x 1/8" (Fig. J.2).



SCHEMATIC DIAGRAM OF A SCALED PRESSURIZER APPARATUS

FIG. J. 1



SCHMATIC DIAGRAM OF A SCALED PRESSURIZER VESSEL
(MIT TEST VESSEL)

FIG. J.2

The storage tank is 8.0 in. ID, 57.0 In. in height, and 1/3 in. thick. The storage tank is filled with approximately 70.0^o F water to a level also measured with an external gage glass. This tank is pressurized with nitrogen and maintained at an approximately constant pressure during the transient.

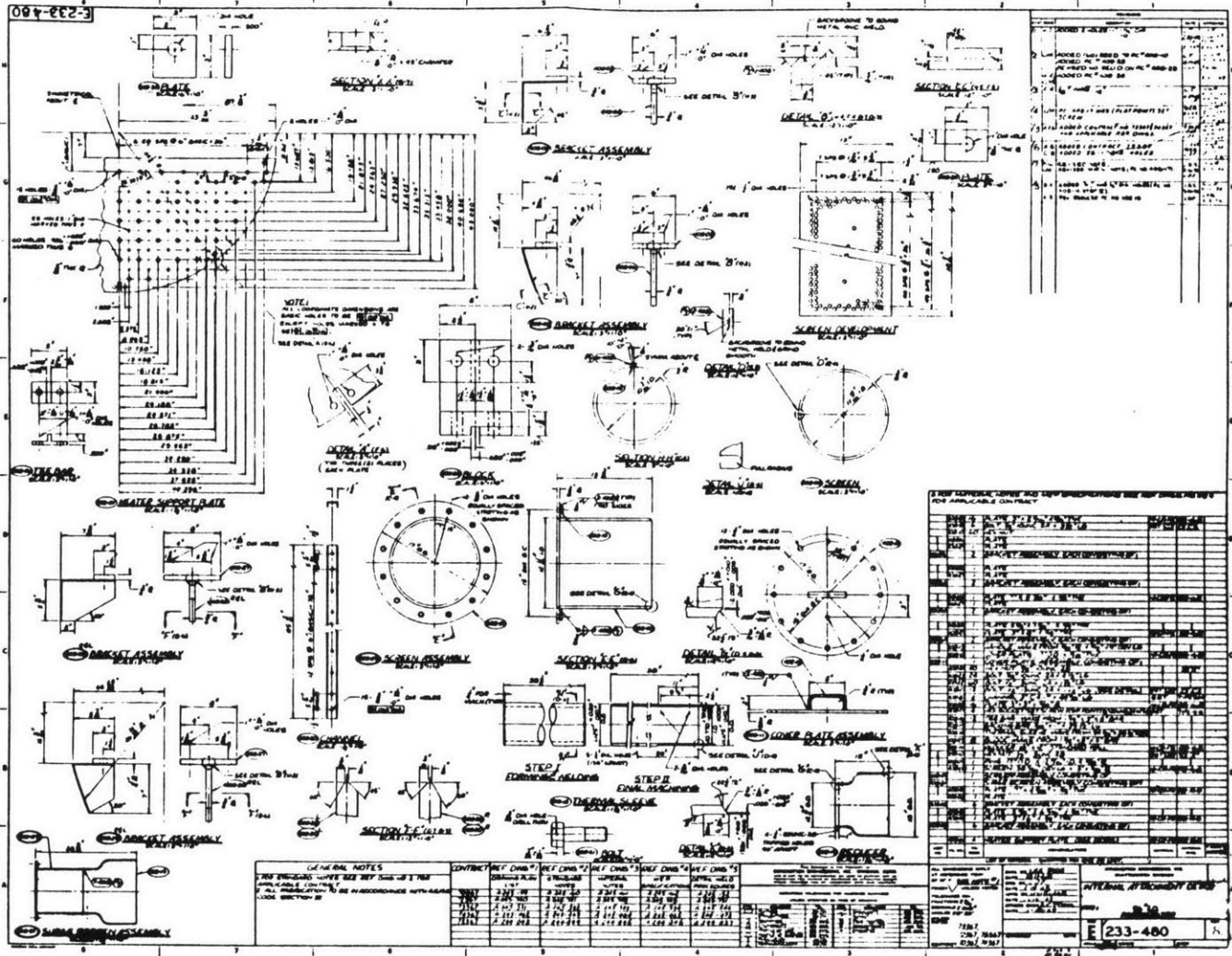
The experimental procedures for the insurge transient into the empty tank are described as follows:

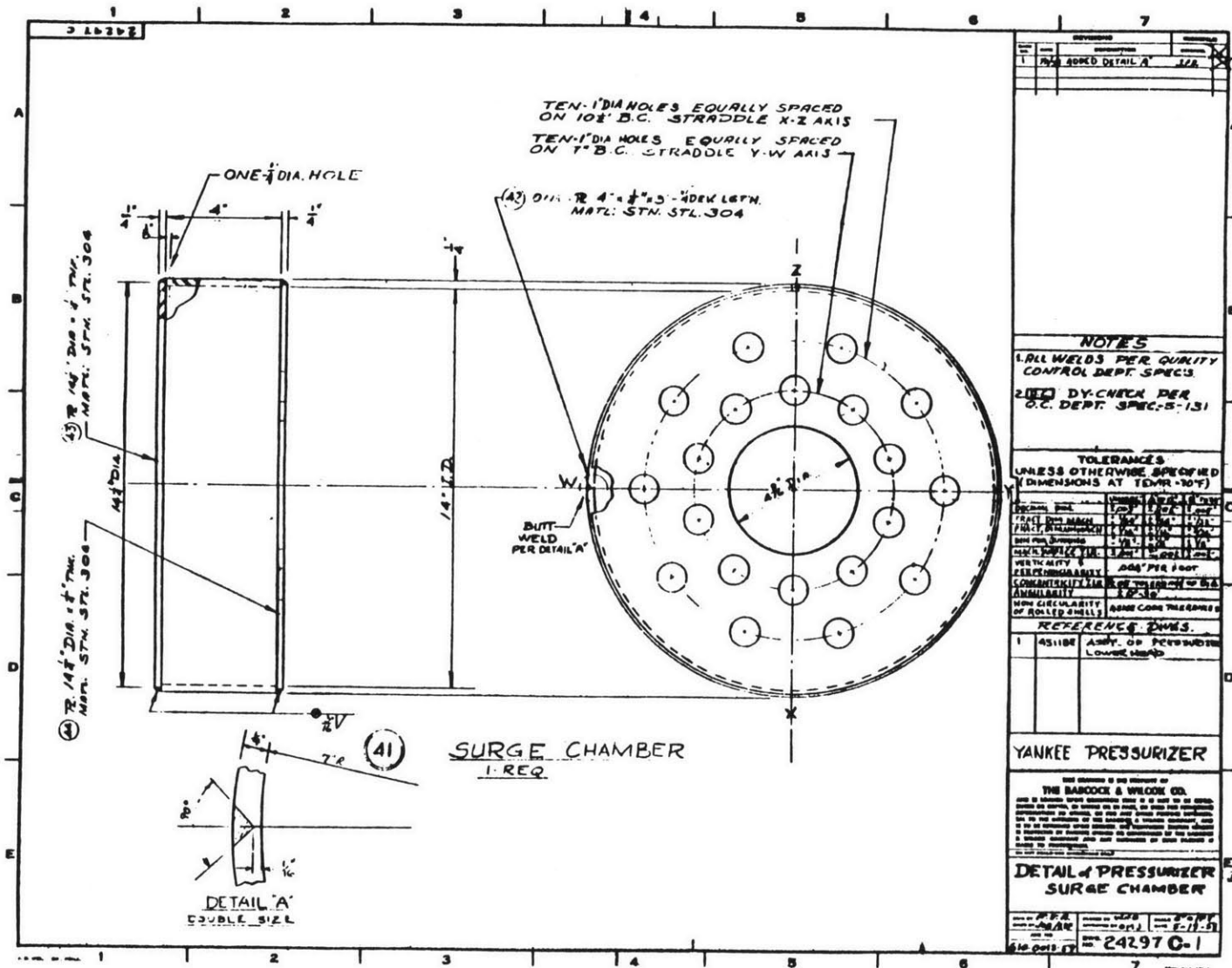
- i) Fill the primary tank with cold water up to the 10.0 in. elevation (high enough to submerge the heaters).
- ii) Boil the water with the electrical heaters while the non-condensable gas is venting.
- iii) While the water is boiling, set up the computer to take data.
- iv) Fill the storage tank with cold water and pressurize it to about 20.0 psia higher than the initial pressure of the primary tank.
- v) When the desired primary tank pressure is obtained (approximately 130.0 psia), reduce the heat input and achieve a steady state.
- vi) Turn the heaters off and drain out all of the water (one should be careful not to drain the steam unnecessarily).
- vii) Wait a few seconds to restore equilibrium.
- viii) As the data acquisition system begins recording

data, open the surge line isolation valves to initiate the insurge transient.

- ix) When the water level reaches the desired final value, close the valves to terminate the transient. Data acquisition is continued after the insurge is terminated to measure the transient decay of pressure.

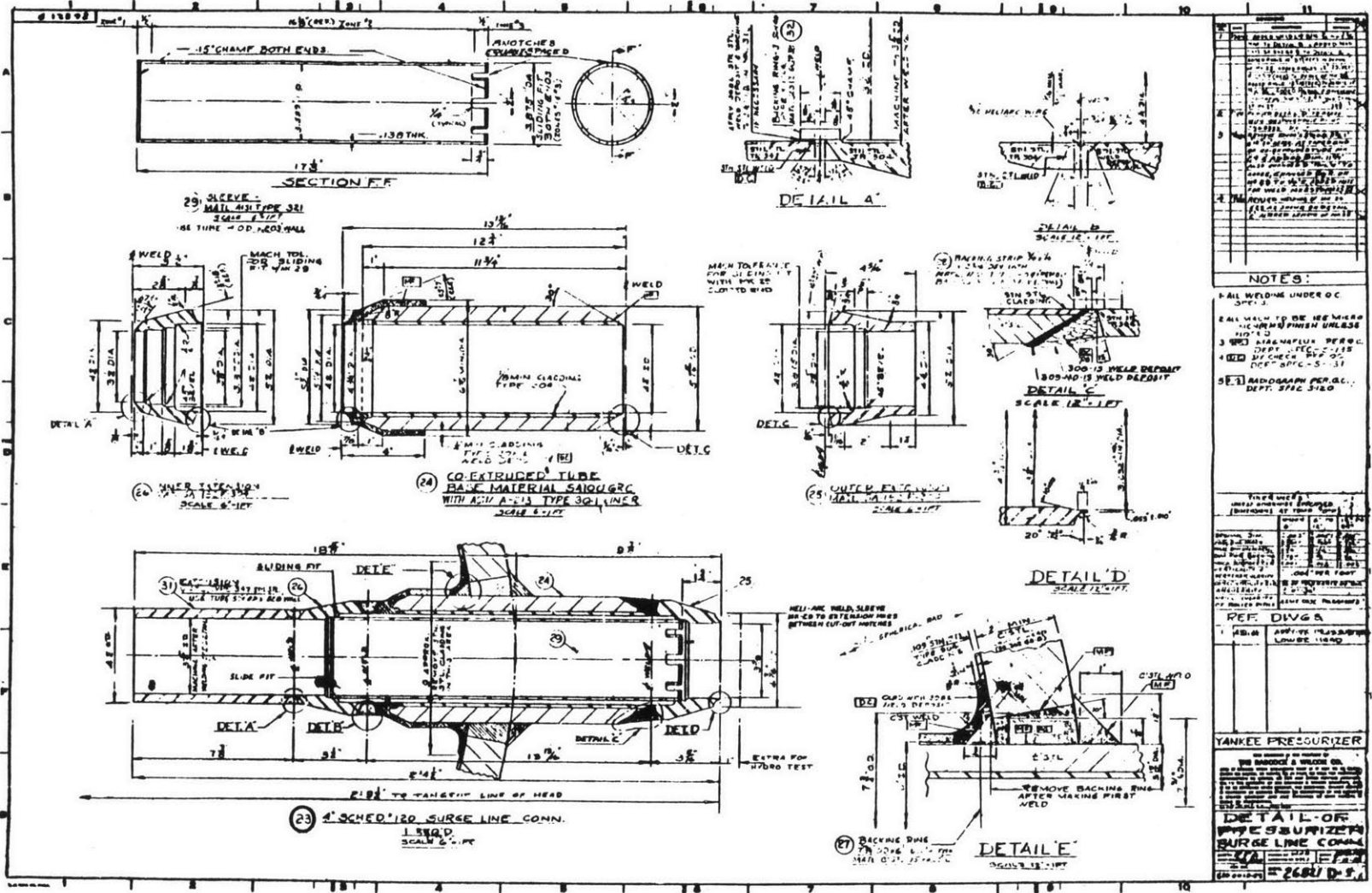
APPENDIX K





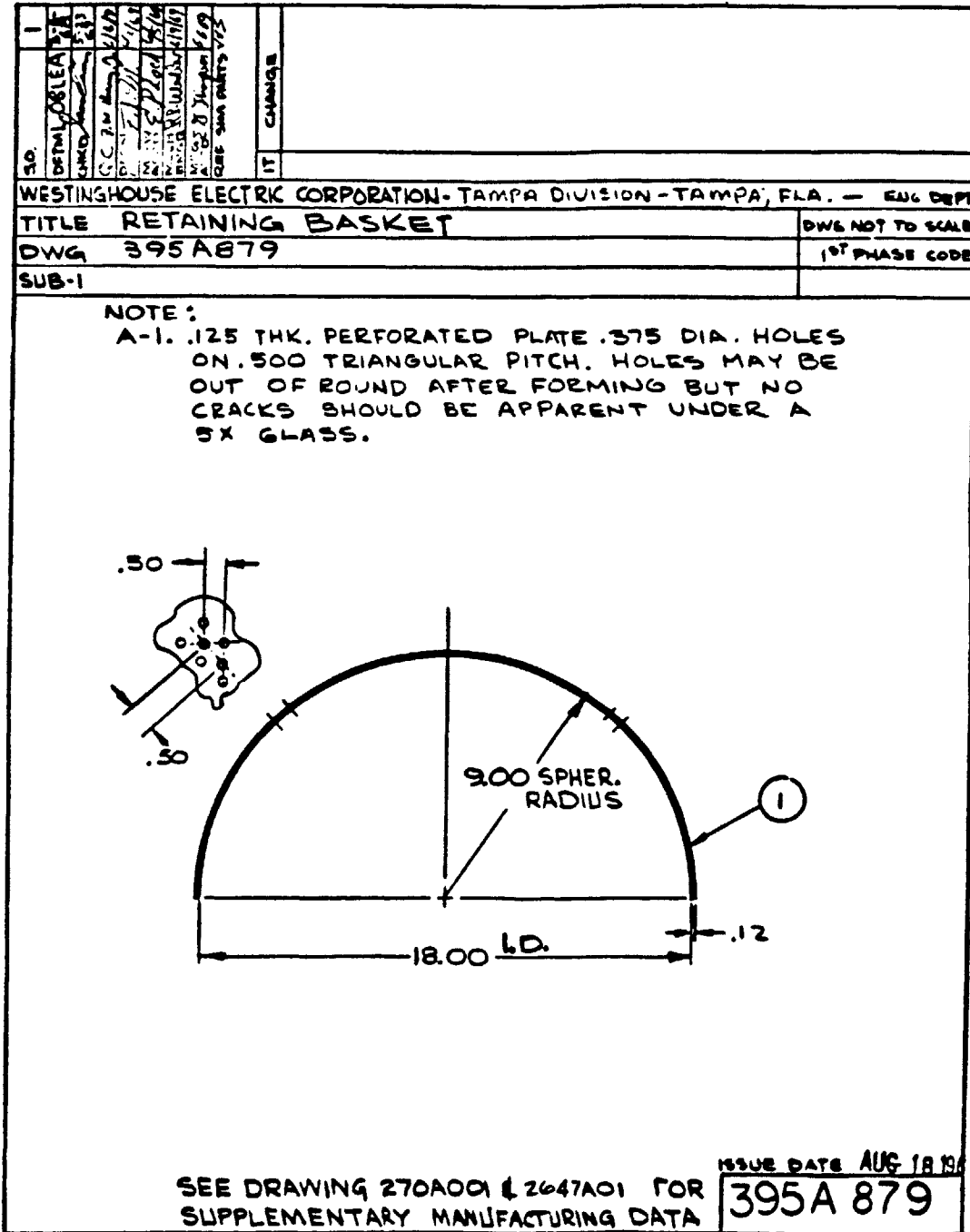
DETAILS OF ROWE YANKEE SPARGER (SURGE CHAMBER)

FIG. K.2 (a)



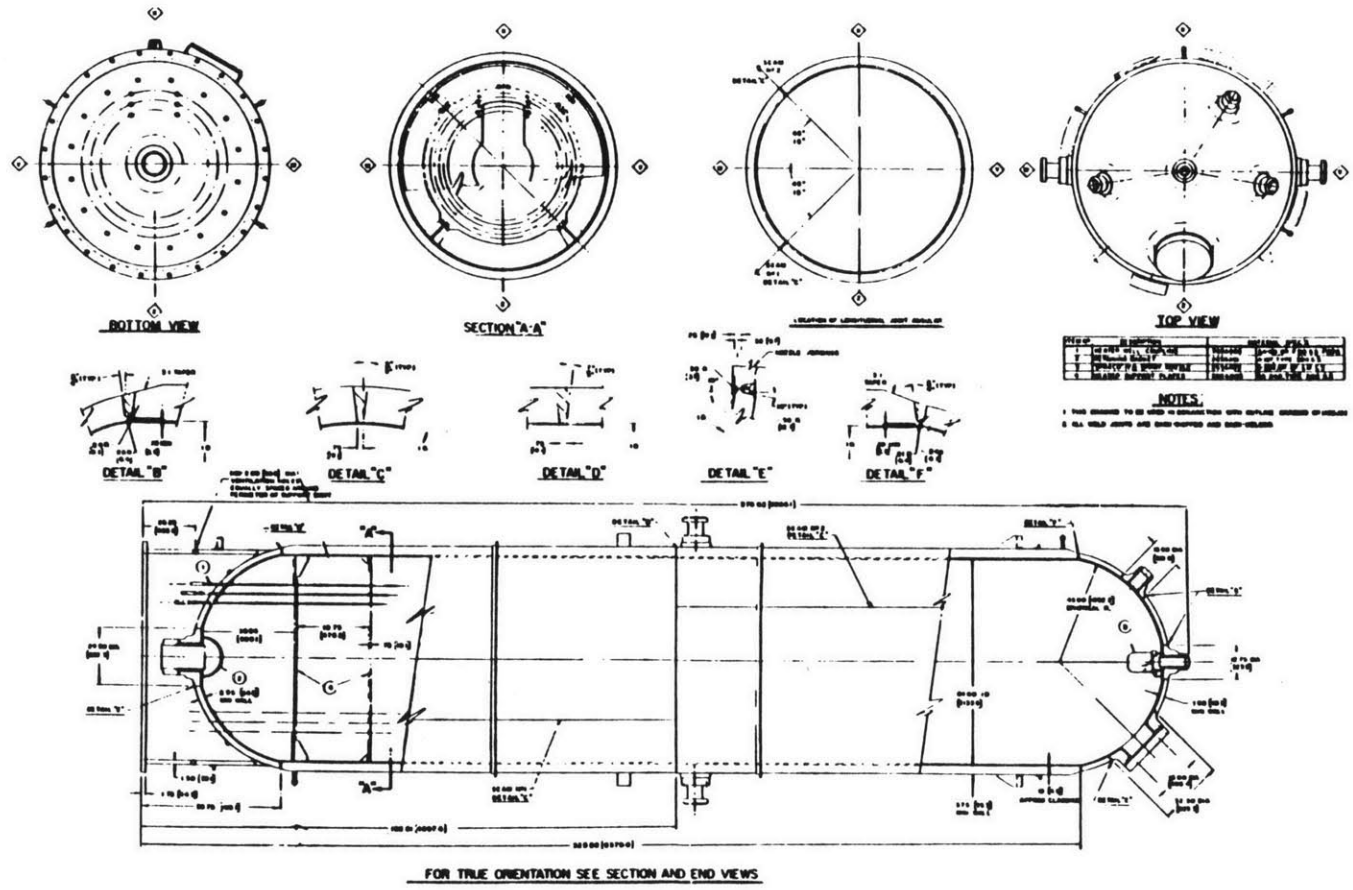
DETAILS OF ROWE YANKEE SPARGER (SURGE LINE)

FIG. K.2 (b)



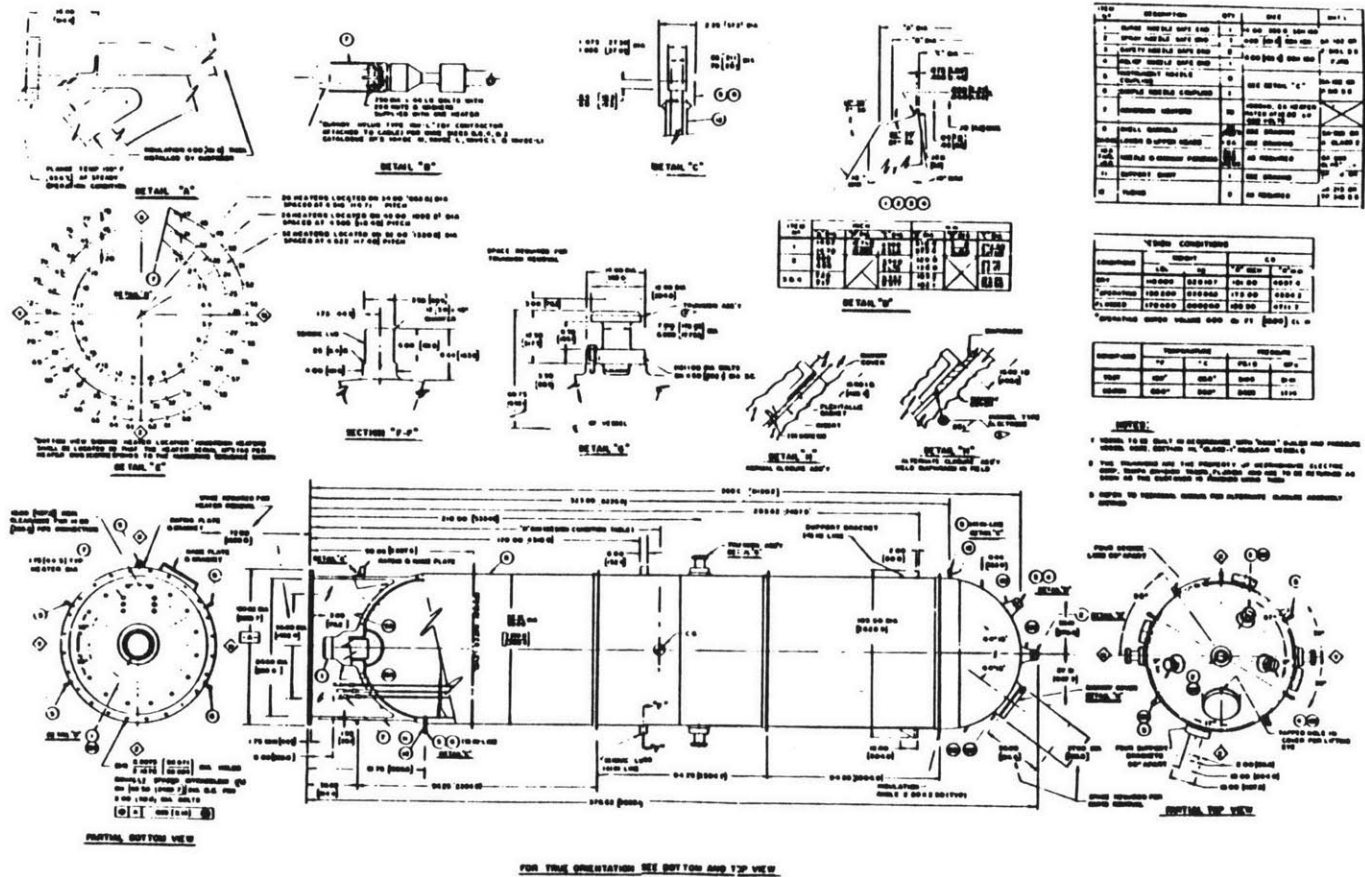
DETAILS OF MILLSTONE 3 SPARGER

FIG. K.3



DETAILS OF WESTINGHOUSE PRESSURIZER

FIG. L.1



ITEM	DESCRIPTION	QTY	UNIT	REF.
1	HEATER ASSEMBLY	1	EA	1000
2	HEATER ELEMENT	1	EA	1000
3	HEATER ELEMENT	1	EA	1000
4	HEATER ELEMENT	1	EA	1000
5	HEATER ELEMENT	1	EA	1000
6	HEATER ELEMENT	1	EA	1000
7	HEATER ELEMENT	1	EA	1000
8	HEATER ELEMENT	1	EA	1000
9	HEATER ELEMENT	1	EA	1000
10	HEATER ELEMENT	1	EA	1000
11	HEATER ELEMENT	1	EA	1000
12	HEATER ELEMENT	1	EA	1000

TEMPERATURE			
TEMPERATURE	°F	°C	PSIG
MAXIMUM	300	150	1500
NORMAL	200	100	1000
MINIMUM	100	50	500

- NOTES:**
1. REFER TO THE DRAWING FOR DIMENSIONS AND MATERIAL SPECIFICATIONS.
 2. THE DRAWING IS FOR INFORMATION ONLY. IT IS NOT TO BE USED FOR FABRICATION.
 3. REFER TO THE DRAWING FOR DIMENSIONS AND MATERIAL SPECIFICATIONS.

DETAILS OF WESTINGHOUSE PRESSURIZER
FIG. L.2

